PTB mitteilungen 2 2020

Metrology in Medicine

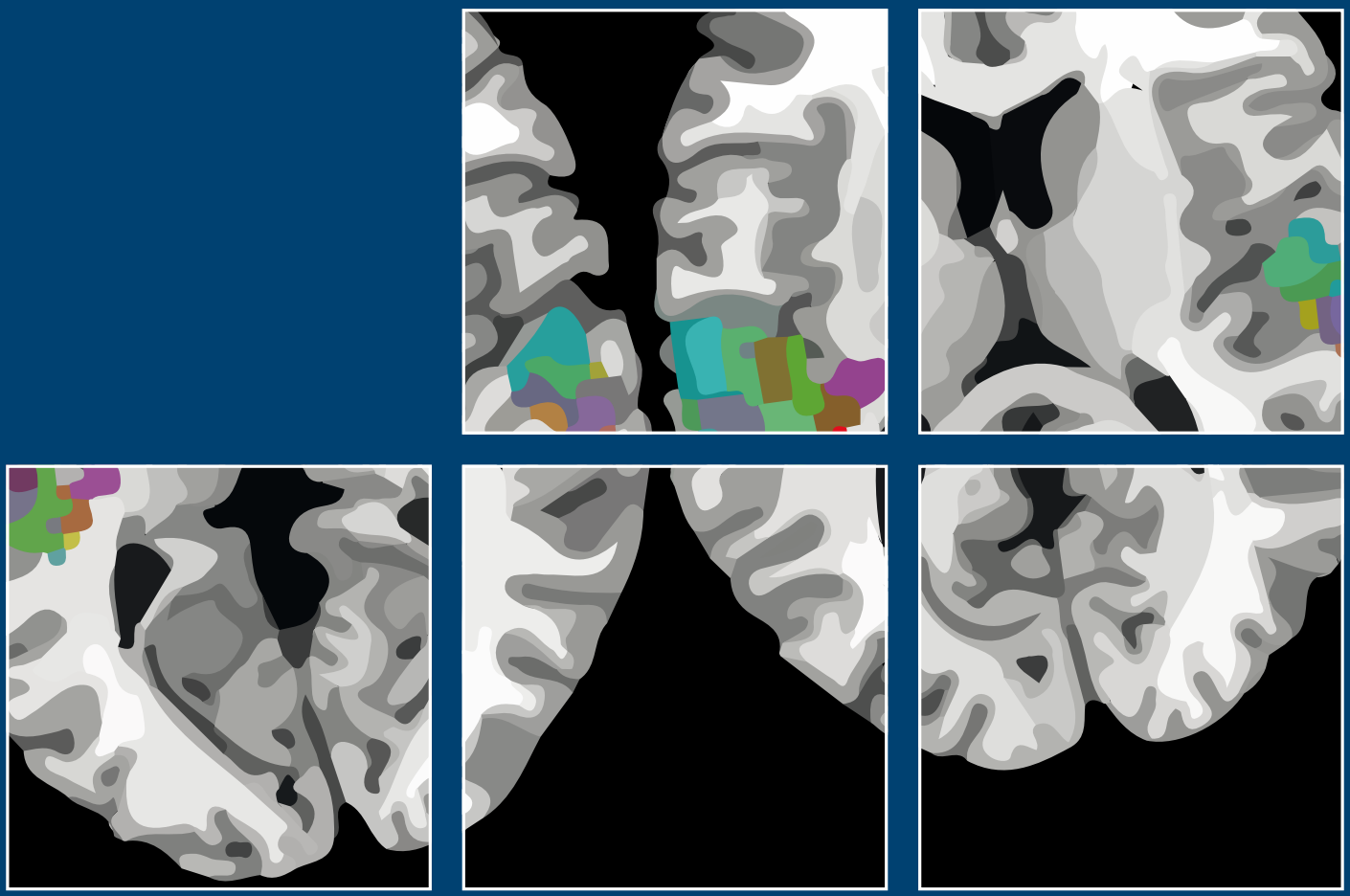

Physikalisch-Technische Bundesanstalt ■ Braunschweig and Berlin National Metrology Institute

PTB mitteilungen

Special Journal for the Economy and Science Official
Information Bulletin of the Physikalisch-Technische Bundesanstalt
Braunschweig and Berlin

Volume 130, No. 2, June 2020

Metrology in Medicine

Cover picture:
Infrasound: Regions of brain activity (color overlay) obtained by fMRI using sound stimuli with different frequencies (see article M. Bug et al.)

Contents

Metrology in Medicine

- Editorial: Metrology in Medicine . . . 03
  Tobias Schaeffter, Ulrike Ankerhold, Bernd Güttler, Christian Koch, Jörn Stenger
- Metrology for Medical Acoustics and Audiology . . . 07
  Marion Bug, Elisa Burke, Thomas Fedtke, Christian Koch
- New Sensors for Biosignal Detection . . . 15
  Rainer Körber, Victor Lebedev, Thomas Middelmann, Jens Voigt, Tilmann Sander
- Electrolytes in Human Serum – Two Decades of SI Traceability . . . 23
  Olaf Rienitz, Karin Röhker, Carola Pape, Silvia Ulbrich, Ursula Schulz, Jessica Towara, Volker Görlitz, Reinhard Jährling, Anita Röthke, Detlef Schiel, Rainer Stosch
- Assuring SI Traceable Measurement Results in Germany for Organic, Peptide and Protein Biomarkers. . . . 31
  Gavin O'Connor, André Henrion, Claudia Swart, Cristian Arsene, Rüdiger Ohlendorf, Christine Brauckmann, Claudia Frank, Rainer Stosch and Bernd Güttler
- Quantitative Magnetic Resonance Imaging . . . 43
  Christoph Kolbitsch, Sebastian Schmitter, Tobias Schaeffter
- Metrology for RF Safety in Magnetic Resonance Imaging . . . 51
  Frank Seifert
- Dosimetry in Medical X-ray Imaging . . . 61
  Ludwig Büermann
- Image Quality Assessment for CT and Mammography . . . 71
  Mathias Anton, Tobias Kretz, Marcel Reginatto, Clemens Elster

PTB-Innovationen

- Ausgesuchte Technologieangebote und Erfolgsgeschichten . . . 79

Metrology in Medicine

Tobias Schaeffter[1], Ulrike Ankerhold[2], Bernd Güttler[3], Christian Koch[4], Jörn Stenger[5]

Healthcare is one of the major European challenges and a strategic cornerstone in almost all EU R&D programs. In the upcoming decades healthcare will remain a top priority politically as well as socio-economically, and its importance will even be intensified due to demographic change and increasing costs. This has been highlighted by the World Health Organization (WHO), European policy drivers and foresight studies with significant effort through research and technology development. The overall aim is to provide an early patient-specific diagnosis and to select the optimal individual therapy, thus making the healthcare system more efficient. This approach is based on the knowledge that individual biological predisposition, as well as lifestyle and the environmental factors, have an influence on the individual health. With this a new concept of stratified or personalized medicine has been established.

Modern medicine strongly depends on physical measurements and biochemical analysis techniques and requires the interdisciplinary interactions between physical and biomedical sciences to advance healthcare. Over the last decades new disciplines, such as medical physics, biomedical engineering or bioinformatics have been established with a strong research base in Europe. In particular, in Germany the medical technology industry and academic sector has been highly innovative and dynamic and builds the basis of the growing healthcare industry sector worldwide.

Metrology plays a key role in this context. Precise measurement methods, reliable quality assurance, and comparable data are the basis of modern medicine and used to determine multiparametric measures. This information is used to make patient-specific decisions during the different phases of the care cycle, i.e. during prevention, diagnostics, therapy and follow-up. For example, highly sensitive and quality assured measurement methods are needed to detect diseases at an early stage. Objective parameter, also called biomarkers, allow the prediction of the therapy success as well as possible side effects. Biomarkers play particularly an important role in evidence-based medicine, where new therapeutic approaches were assessed by independent organizations in Germany (www.iqwig.de) and worldwide (www.cochrane.org).

Metrology provides the methods for the approval of new medical products and for their quality assurance in clinical routine. In the context of stratified and individualised medicine objective decisions need to be taken in the care cycle. Since the majority of unnecessary health care costs arise from ineffective therapies, the best therapy has to be taken for the individual patient at the right time by taking all available data in consideration. In the future, an even stronger "digital integration" of multiparametric measurement data will become necessary. Ensuring the comparability of the measurement data together with their accuracy and precision is of fundamental importance in this context. However, accuracy and comparability cannot be guaranteed in many cases due to differences of applied measurement techniques. Metrology addresses this challenge by organizing and evaluating inter-comparisons to identify the reasons for differences and to improve the data. In the long term, tools to assure reliable data must become integral part of digital health databases.

Metrology in medicine is a relatively young and complex field, which requires interdisciplinary approaches developed in an extensive exchange with medical users, basic scientists and industrial developers. This has been supported by health-related projects within the European metrology research programs iMERA-Plus, EMRP and EMPIR. The programs have significantly improved the metrological capability in Europe by

[1] Prof. Dr.Tobias Schaeffter, Steering Committee "Metrology in Medicine", Division „Medical Physics and Metrological IT", PTB Berlin, ORCID: https://orcid.org/0000-0003-1310-2631, email: tobias.schaeffter@ptb.de

[2] Dr. Ulrike Ankerhold, Steering Committee "Metrology in Medicine", Department "Dosimetry for Radiation Therapy and Diagnostic Radiology", PTB Braunschweig, email: ulrike.ankerhold@ptb.de

[3] Dr. Bernd Güttler, Steering Committee "Metrology in Medicine", Division "Chemical Physics and Explosion Protection", PTB Braunschweig, ORCID: https://orcid.org/0000-0001-8293-2773, email: bernd.guettler@ptb.de

[4] Dr. Christian Koch, Steering Committee "Metrology in Medicine", Department "Sound", PTB Braunschweig, email: christian.koch@ptb.de

[5] Dr. Jörn Stenger, Steering Committee "Metrology in Medicine", Member of the Presidential Board, PTB Braunschweig, email: joern.stenger@ptb.de

combining expertise and resources from different national metrology institutes and designated institutes. Over the years, PTB has focused on those application areas with strong metrological needs ranging from medical temperature, blood pressure and hearing measurements to quantitative imaging techniques, diagnostic radiology, radiotherapy and laboratory medicine.

This issue of the "*PTB-Mitteilungen*" gives an overview of some of the activities in metrology for medicine at PTB.

The prevention of hearing loss plays an important role for wellbeing of an elderly population. In the article "Metrology for medical acoustics and audiology" it is shown that comprehensive hearing assessment requires quantitative measurements with traceability. This includes the distribution of reference data for audiology as well as developing novel methods for assessment of so-called transient stimuli. In addition, research is under way that deals with current topics as the measurement and perception of infrasound. This is a highly topical subject, since unconscious noise is caused by many environmental factors and can affect the quality of life of people whereas the overall effect on health is unknown. Starting point was to show whether infrasound can be perceived through hearing. This is highly demanding and requires the detection of small activities in the human brain. In addition to functional magnetic resonance imaging (fMRI) also quantum interference devices can be used to detect such neural biosignals in the brain with high temporal resolution. The PTB works on a new class of optical quantum sensors, which are presented in the article "New sensors for biosignal detection".

In the area of diagnosis, laboratory medicine builds the bases for many clinical decisions nowadays and reliable measurement methods at the level of DNA, electrolytes, proteins and up to the cellular level are an essential prerequisite for many biomedical applications. Hence, the development and application of metrology in clinical biochemistry has become highly dynamic with a growing industry involvement. For example, the accurate measurements of electrolytes in human serum, a biomarker for several diseases, is fundamental. In the article "Electrolytes in human serum – two decades of SI-traceability" the long-term effort to develop primary methods for SI-traceable determination of such ions is described. Over the years, the Consultative Committee for Amount of Substance (CCQM) of the International Committee of Weights and Measures (CIPM) has organized different key comparisons and as a consequence, PTB holds eighteen serum-related Calibration and Measurement Capability (CMC) claims in the Key Comparison Data Base (KCDB). There is significant effort to expand these activities in clinical chemistry to more complex substances, such as nucleic acids or proteins. New approaches to define reference methods and standardization for protein analysis are summarized in the article "Assuring SI traceable measurement results in Germany for organic, peptide and protein biomarkers" showing the international effort to address the measurement challenges in this important area of medicine.

Modern clinical diagnosis is also highly based on medical imaging with more than 5 billion imaging investigations each year. Despite this tremendous technical progress, a major obstacle in medical imaging is the lack of reproducibility and comparibility. One reason for this is that current image information is non-quantitative, since no intrinsic tissue properties are displayed. Worldwide initiatives such as the Quantitative Imaging Biomarkers Alliance (QIBA) and European Imaging Biomarkers Alliance (EIBALL) aim at making medical imaging a more quantitative science. The article "Quantitative magnetic resonance imaging" provides results of recent developments at PTB allowing the accurate measurement of biophysical parameters for an objective assessment of pathologies. Quantitative MRI does not depend on hardware or measurement related parameters, making it much easier to combine data from multiple hospitals in multi-centre studies and thus allowing for the monitoring of disease progression or treatment outcome in larger trials.

Another important metrological aspect is the quality assurance in medical imaging to ensure the patient's safety. For instance, in magnetic resonance imaging tissue heating occurs due to the absorption of radiofrequency (RF) energy that is applied to the human body during the imaging process. This becomes a safety issue for patients with implants, which often need be excluded in the diagnosis of disease of assessment of treatments. At PTB the "Metrology for RF safety in magnetic resonance imaging" includes reference techniques for assessing RF-heating and new concepts for the safe use of high-frequency RF-fields are being developed.

In contrast to MRI, in medical X-ray imaging patients are exposed with X-radiation for diagnostic purposes, always with the approach to optimize ratio the image quality to applied dose ratio. To assure a high patient safety, traceable and reliable dose measurements are essential and of high importance. They are prescribed by law and regulations in the scope of regular quality assurance procedures and acceptance tests. In the field of medical X-ray imaging, PTB is responsible for the type approval of dosimeters and

provides for several dose quantities calibration of dosimeters for different X-ray imaging modalities. The article “Dosimetry in medical X-ray imaging” gives an overview about this field with the quality assurance concepts and instruments, the high number of dose quantities for the different X-ray imaging modalities and the international standardisation activities. A new research field is the personalized dosimetry for computed tomography with the goal to establish a general procedure for patient-specific dose estimates based on the effective dose due to the CT scan.

In medical X-ray imaging the applied dose and the image quality is strongly correlated. Therefore a tradeoff between the image quality and possible risks to the patient has to be found. Unfortunately, new X-ray based imaging systems such as computed tomography (CT) make use of iterative non-linear reconstruction algorithms that hamper the application of established image quality measures that assume linearity and shift-invariance of the imaging system. Recently PTB started research in “Image quality assessment for CT and mammography”, which may be viewed as being in between medical research and classical metrology. In particular results from task-specific image quality assessment using mathematical model observers are shown in the respective article. One of the goals is to include uncertainty evaluation in the mathematical model observers in line with current standards in metrology. Another aim of this research is to apply modern techniques of data analysis, including deep learning, to improve image quality assessments.

These are examples of the various activities within PTB in the field Metrology for Medicine. Since health is one of the major challenges in an ageing society, the demands for metrology are continuously growing to support improved, robust, reliable and more comparable clinical measurements. In future, metrology will expand from measurement systems towards data analysis tools and provide fundamental reference data, benchmark tests allowing the comparison of algorithms and to prevent wrong medical decisions made by new tools of artificial intelligence.

Metrology for Medical Acoustics and Audiology

Marion Bug[1], Elisa Burke[2], Thomas Fedtke[3], Christian Koch[4]

Abstract

Hearing plays an important role in shaping human life with high social and individual quality and comfortable wellbeing. Diagnosis, assessment and conservation of hearing is a key factor and plays an important role in health care also with respect to an increasingly elderly population. Considering a simultaneously rising anticipation of wellbeing by many individuals in European countries, meeting the requirements of quality of all processes involved represents a challenge for the heath care system of a country.

A comprehensive hearing assessment requires sophisticated measurements of a variety of variables. To ensure reliability and high or at least sufficient selectivity and specificity of a diagnosis, all measurements, but most importantly any quantitative measurements, should be underpinned by a quality management process to realise traceability to appropriate standards and references for all measurements. In this publication a short overview about PTB contributions to the metrological underpinning in the field of medical acoustics and audiology is presented. This includes the determination and distribution of important reference data describing the status of hearing. Novel methods will be developed as, for example the processing of transient stimuli which are preferentially applied in objective audiological techniques. Many activities are made in relation to the medical device regulation which currently became effective. In addition, research work is under way dealing with current topics as the measurement and perception of infrasound.

1. Introduction

Hearing is one of our most versatile senses. From an evolutionary perspective hearing is important for survival by detecting noise and inevitable for realising speech as the basic element of communication. In modern civilization, acquired hearing disorders are often a reason for social isolation and life in industrialized societies can have negative effect on hearing due to daily high exposure to noise. Bearing in mind natural degradation of hearing ability while growing older, hearing conservation is an important issue and plays an increasing role in health care also with respect to the increasing elderly population. This process is highly individual, and the necessary objective and subjective hearing assessment is a logical element in individualised medicine.

A comprehensive hearing assessment is based on quantitative data to describe the individual hearing state of a person. This requires sophisticated measurements of a variety of variables, reflecting the hearing status. To ensure reliability and high or at least sufficient selectivity and specificity of a diagnosis, all measurements, but most importantly any quantitative measurements, should be underpinned by a quality management process to realise traceability to appropriate standards and references for all measurements.

Reference values are fundamental to allow the comparison of individually obtained data with well-known values to settle a diagnosis. Hearing threshold levels or speech intelligibility scores are typical examples and PTB provides such data for audiometric transducers. These data are often the origin for an international standardisation procedure. Once determined, those reference hearing threshold levels need to be transferred from the standard laboratory at PTB to the individual audiometer, which is realised by transfer devices, such as ear simulators and artificial mastoids for bone conduction systems. Methods were specifically developed to define the hearing threshold values by means of the transfer devices, and they are recorded in international regulations. The values applied for calibration of

[1] Dr. Marion Bug, Department "Sound", PTB Braunschweig, email: marion.bug@ptb.de

[2] Elisa Burke, current address: elisa@burkegermany.de

[3] Dr. Thomas Fedtke, Department "Sound", PTB Braunschweig, email: thomas.fedtke@ptb.de

[4] Dr. Christian Koch, Department "Sound", PTB Braunschweig, email: christian.koch@ptb.de

audiometers are based on reference equivalent hearing threshold levels and are recorded and finally provided to any user by international standards for different types of audiometric transducers. The applied methods are, however, in question for transient signals. In addition, no appropriate transfer device exists for neonates and children and PTB has been active in a consortium to develop a new ear simulator family and to improve the testing methodology.

For all devices mentioned so far, a quality management system is established in Germany as it is claimed by the Medical Device Directive [1] which is currently being replaced by the Medical Device Regulation [2]. Annual checks are mandatory for devices with measuring function and they follow clearly defined rules [3]. PTB is responsible for the maintenance of the guidelines for these metrological verifications [4] and can carry out several of the required tests itself.

Although significant improvements were achieved, noise is still a major environmental health problem with increasing impact on the wellbeing of European citizens. Both, the World Health Organisation (WHO) in its guidelines from 2018 [5] and the European Environment Agency (EEA) in its report of 2014 [6] describe noise as a "growing environmental concern" (citation from [6]). This includes also noise emitted with frequencies at or beyond the borders of the human hearing range. It is essential to understand the way of perception in order to assess these emerging noise contributions. This knowledge will also scientifically underpin the discussion about the impact on humans controversially led in the public. PTB contributes to this highly topical issue by providing test and validation of new noise measurement devices and methods. In addition, dedicated studies on details of the perception and processing of noise by humans are performed.

In this publication a short overview about PTB contributions to the field of medical acoustics and audiology is presented. Section 2 describes how important reference data are provided including a novel processing of transient stimuli (section 3). Section 4 explains the input into MDR and section 5 illuminates resent research work on perception of infrasound. Section 6 closes with a brief look into future challenges.

2. Reference data for audiology

Reference values for the human hearing ability are essential for any diagnosis, separating a pathological occurrence from normal hearing. Typical examples are reference equivalent hearing threshold sound pressure levels (RETSPL), which define the zero setting of an audiometer. In a hearing test, a possible hearing loss is always assessed with reference to this zero setting. The RETSPLs strongly depend on the conditions during their determination and, therefore, the preferred measurement conditions are standardized [7]. In the case of any change in those conditions or new setups for the stimulus, transducer type, coupling configuration, etc., a new determination of the related reference value is required. Among other parameters, PTB determines RETSPL values which are specific to audiological transducers and which are requested mainly by manufacturers of those transducers. Newly determined RETSPL values also contribute to updates of international standards, such as the ISO 389 series "Acoustics – Reference zero for the calibration of audiometric equipment". Until now, RETSPLs are determined by pure-tone audiometry. To illustrate the process of RETSPL determination, recent measurements for a newly designed type of headphone (RadioEar DD65v2) are presented hereafter.

The RadioEar DD65v2 is an ear-encompassing (circumaural) audiometric headphone. Equivalent hearing threshold sound pressure levels (ETSPL) were measured under the conditions given in ISO 3899 [7]. This standard regulates, for example, the maximum allowed background noise level, the conditions related to the test subjects, requirements on the audiometric equipment, the measurement procedures for the hearing threshold measurement as well as for the calibration of the audiometric equipment and, finally, the declaration of the data.

In the recent study, 25 otologically normal male and female test subjects between the ages of 18 and 25 years took part. Prior to the ETSPL measurements, the hearing ability of each test subject was determined with a clinically approved audiometer, which was operated by staff with audiological background. The ETSPL measurements were then performed by seating the test subject in the dedicated test room at PTB, a so-called anechoic chamber, which was specifically developed to achieve low background noise levels down to frequencies of (at least) 100 Hz. Hearing thresholds for pure sinusoidal test tones of 11 audiometric frequencies between 125 Hz and 8 kHz were determined by means of the so-called "bracketing method" according to ISO 8253-1 [8]. The measurement is fully automated to rule out any influence of the audiometrist. The hearing threshold measurement is repeated for each test subject individually and with the same headphone. After all measurements, the hearing threshold values of all test subjects are averaged for each pure-tone stimulus.

At this stage, only the relation between the (behavioural) mean hearing threshold of the group of test subjects and the signals (frequency and

voltage) applied to the headphone is known. This relation can be used for determining the ETSPL values by mounting the headphone onto a calibrated ear simulator (according to IEC 60318-1 [9]) for circumaural headphones, applying the signal with defined frequency and voltage and obtaining the respective sound pressure level developed in the ear simulator. These sound pressure levels represent those at the human ear drum.

Furthermore, a comprehensive measurement uncertainty budget for such reference data was established for the first time. This is not common, because usually uncertainty budgets were created for physical quantities. For behavioural parameters, as in this experiment, special strategies are required. Figure 1 shows the ETSPLs for the RadioEar DD65v2 headphone as mean values with a 95 % confidence interval. The frequency dependence of the data is due to the combination of the frequency characteristics of the ear and of the headphone: the highest sensitivity is at 2–3 kHz. Here, the sound pressure levels at the hearing threshold are the lowest, while they increase for lower and higher frequencies.

The calibration of audiometric equipment operated with a RadioEar DD65v2 headphone can now be performed and assessed by confirming that the difference between the sound pressure level measured with an IEC 60318-1 [9[ear simulator and the set hearing level is exactly the ETSPL value for the given pure tone.

3. Transient stimuli

Transient signals, such as clicks, tone bursts and chirps, are very important stimuli for objective audiometry based on auditory evoked (brain) potentials (AEP) or otoacoustic emissions (OAE). They evoke predominantly onset responses, which are strong and have characteristic properties and, thus, are valuable for diagnosis of hearing system and processes. They can provide both, objective measures that relate to the behavioural hearing threshold and information on a potential (dis-) function of several parts of the auditory system. Both outcomes can be part of a diagnostic process underwent during a patient investigation. Used for basic hearing screening of neonates and clinical investigation the brain response can be optimised by designing specialised stimuli, for example particular chirps [10, 11].

To transfer any reference value (section 2) determined to an audiometer, a device acoustically representing the human hearing system is required, and ear simulators (for earphones) as well as artificial mastoids (for bone conduction systems) are available reproducing the main acoustic properties ear or mastoid. For steady signals the magnitude of the sound is relatively easy to quantify, but for short-duration stimuli there are different ways this can be specified. The concept of expressing reference thresholds by means of peak-to-peak equivalent Reference Equivalent Threshold Sound Pressure Levels (peRETSPL) according to IEC 60545-3 is easy to implement, even with rather basic instrumentation. However, this concept frequently results in calibration values, which do not correlate at all with either the behavioural hearing thresholds or the spectral energy of the periodically repeated stimuli. In an alternative concept [12] a root-mean-square (RMS)-based approach was proposed for calibrating short-term stimuli by directly measuring the unweighted RMS sound pressure level (L_{Zeq}) of the short-term stimulus presented periodically at a given repetition rate. In the following, this measure is being referred to as LZ_{eq}ETSPL.

This procedure was applied for determining RMS-based LZ_{eq}ETSPL values, directly measured as the L_{Zeq} of the periodically repeated short-term stimuli by a Norsonic 840 real time analyzer for a RadioEar IP 30 insert earphone. As shown in Figure 2, excellent agreement was found between measured and estimated levels, with typical differences of 0.2 dB and a maximum deviation of 0.3 dB. The estimated levels were obtained by a procedure using predetermined transfer data for an individual ear simulator that allows the estimation from known peETSPL values obtained following the conventional definition. The concept for specifying equivalent hearing threshold levels by an RMS-based measure turned out to be well applicable for the RadioEar IP30 insert earphone in conjunction with a Norsonic RTA 840 analyzer (IEC 61672-1 Class 1) used for measuring the Z-weighted equivalent continuous sound pressure level of the periodically repeated short-term stimuli [13].

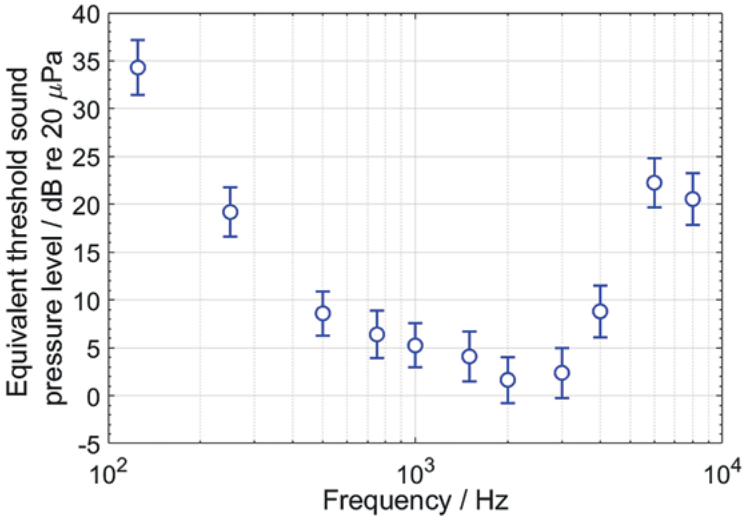

Figure 1:
Mean values of equivalent reference hearing threshold for pure tones for the RadioEar DD65v2 headphone.
The error bars represent the 95 % confidence interval.

In another study, measurements on selected test subjects were carried out to determine their individual hearing thresholds using the RadioEar IP30 insert earphone. The tests were made with steady tones, tone bursts and clicks. For the latter two, being short-duration stimuli, the magnitude of the sound was calculated using the currently established peak-level approach (peETSPL) and the proposed new approach (LZ_{eq}ETSPL). The results could show the applicability of the new method which allows are more realistic definition of hearing threshold.

4. Relevant work for Medical Device Regulation

Considering the facts given in previous two sections, it is obvious that correctly measured threshold data, their transfer to the individual audiometer at application site and, finally, the proper functioning of the device are essential for the quality of a diagnosis. This in turn is the basis for the success of any follow-up rehabilitation activities as providing and fitting a hearing aid or the supply of a cochlear implant (CI). Accuracy and reliability need to be maintained and since this issue represents a general interest of the society it is generally organised within the framework of EU regulation, i. e. the Medical Device Regulation (MDR). The increasing requirements on quality of hearing and the more and more ambitious individual expectations of disabled persons are the driver of a constantly growing market for hearing aids and cochlear implants. German manufacturers play a leading role and metrological support is a prerequisite for a future successful technical and economic development.

Audiometers are classified as medical devices with measuring function. Following EU regulation, in Germany the law requires annual tests of audiometers and a periodic calibration and / or a test of all devices which are used in the quality management process, with a period of three years, is mandatory. PTB holds the standards for these procedures and ear simulators are tested and mastoids are calibrated giving traceability for accredited laboratories or approved service providers that perform the on-site checks at hospitals or medical offices.

For the determination of peRETSPL values, i. e. the test of any audiometric system, standard sound measuring devices are required to determine the level of test stimuli. For application of these device for legal or administrative purposes PTB accomplishes conformity assessments in combination with its different tasks in legal metrology implementing the German law for measurement systems. This includes a comprehensive calibration service and a type approval procedure. Alternatively, they can be calibrated by accredited laboratories which, however, get traceability from PTB via the calibration service.

During the process of bringing a medical device to market, manufacturers need referenced or proven measurements to declare, for example, output parameters essential for functioning or safety issues. This holds also for other groups of devices as ultrasound machines. They are not classified as measuring devices but for the CE-mark a couple of traceable measurements must be submitted which strictly requires calibrated

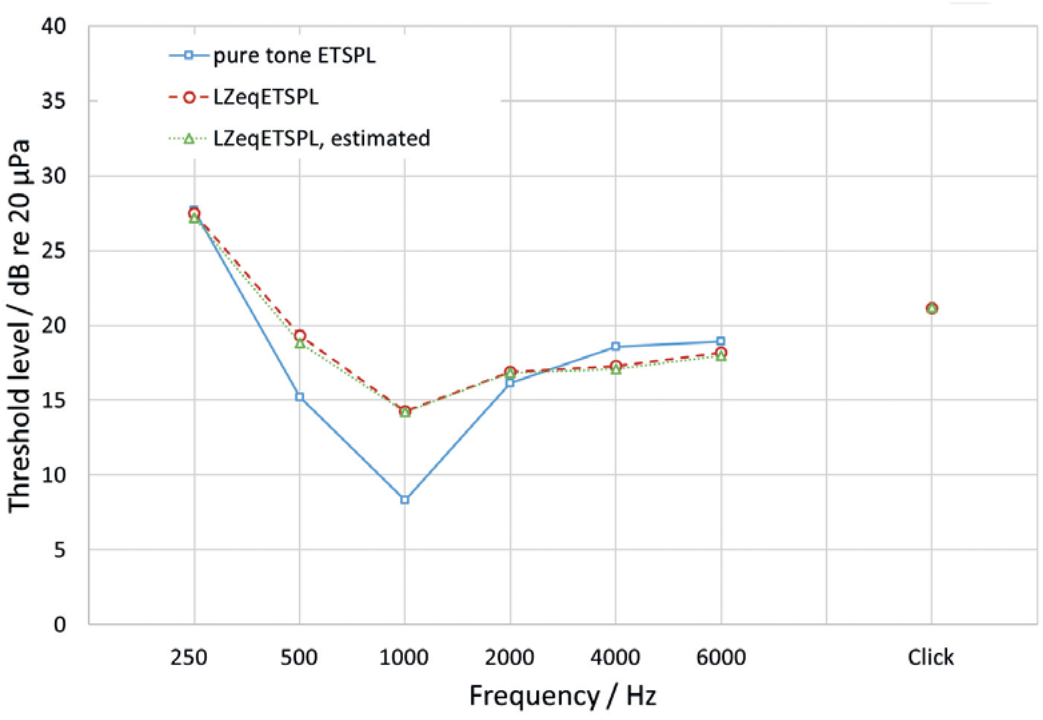

Figure 2: Measured LZeqETSPL compared to estimated LZeqETSPL (calculated from peETSPL) and pure-tone ETSPL, for the RadioEar IP30 insert earphone and an occluded-ear simulator according to IEC 60318-4 (2010), From [13].

measurement instrumentation and traceability is provided by PTB. In case of the ultrasound machines PTB provides a comprehensive calibration service for hydrophones and standard transducers which form the basis of required output power declarations and safety assessments.

5. Measurement and perception of infrasound

Noise is still a serious environmental factor influencing significantly the quality of life mainly in urban regions. During the last decades major effort has been carried out to collect comprehensive data about the noise load together with the impact on residents in European cities and countryside. This, however, does not hold for contributions with frequencies at the borders of the widely accepted hearing range between 16 Hz and 16 kHz. Perception of airborne ultrasound and, in particular, infrasound is controversially discussed, which is additionally stoked up by the fact that the perception mechanisms at both sides of the hearing frequency range are not well understood.

For the perception of infrasound various assumptions exist [14]. It seems to be unquestionable that infrasound enters the ear canal and can be transferred through the middle ear and finally enters the inner ear. Hearing sensations are stimulated, and hearing threshold could be measured in various laboratories including a study at PTB [15, 16]. This study also determined the loudness of infrasound and equal-loudness-contours were deduced. To obtain a more objective picture of the perception of infrasound a functional magnetic resonance imaging (fMRI) study was carried out. Playing infrasound stimuli to test persons while lying in an MRI-scanner produced significant brain activities in the auditory cortex as to be seen in Figure 3 (adapted from [14]). These results showed that the definition of the "hearing frequency range" is difficult because infrasound can be perceived if it is loud enough.

Since infrasound occurs rarely without accompanying audible sound components one possible mechanisms of perception of infrasound consists in its interaction with the audible noise. At infrasound frequencies, a best place (or an appropriate critical band) on the basilar membrane does no longer exist when the sound enters the cochlea and, thus the sound moves the basilar membrane as a whole. This leads to periodical changes in the basilar membrane position which influences the action of inner hairs cells processing the audible sound in the inner ear. The result is that humans detect a modulated signal [17, 18] which has a high mindfulness and may be interpreted as hearing infrasound by an exposed person.

To test this assumption further, the interaction between infrasound and audible sound was investigated in a study in two consecutive steps. First, the mutual influence on the hearing thresholds of the respective other sound type was determined [19]. One hypothesis was that the threshold for audible sound changes when simultaneously presented with infrasound due to the perceived modulation effect or a potential masking effect. Therefore, hearing threshold measurements were performed for infrasound

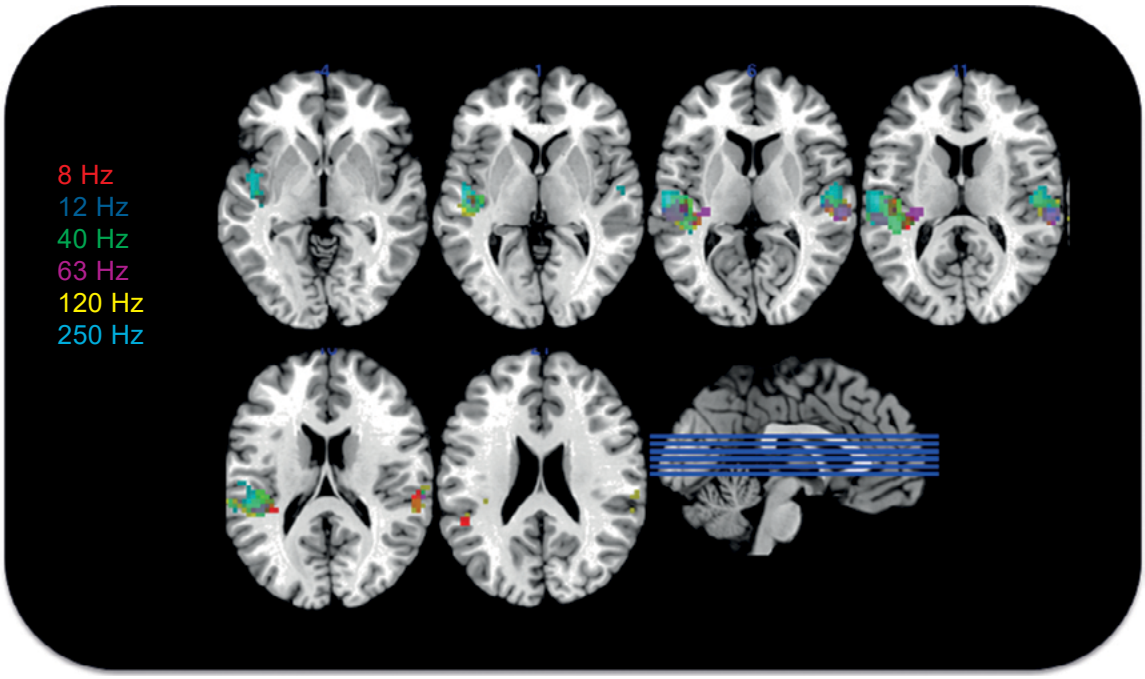

Figure 3:
Slices of the brain obtained from fMRI, 16 test persons; Stimuli: pure tones with a loudness of 20 phon, frequencies are colour coded, right ear, p<0.001, cluster size > 22.

and audible sound, separately and in presence of the respective other sound type as background noise. Thirteen test persons aged between 18 and 30 years with normal hearing participated in the study. The hearing threshold measurements were separated in three experiments: First, thresholds levels were determined for infrasound (pure tones at 5 and at 12 Hz) and audible sound (pure tones at 100 Hz and at 1000 Hz, and a band-limited pink noise 250–4000 Hz) in quiet. Then, threshold level measurements were conducted for infrasound in the presence of audible sound presented at 5 dB and at 50 dB above the individual threshold level. In the third experiment, threshold levels were determined for audible sound in the presence of infrasound presented at levels within 10 dB above and below the individual threshold level. Threshold shifts were calculated as the difference between the threshold level for infrasound and audible sound signals in quiet (reference value) and the threshold level for the same signals in the presence of a specific background noise. All threshold level measurements were repeated twice for each test person on separate days to gather robust hearing threshold data. We focussed on the perception of infrasound by means of the auditory system. Therefore, we used a specially developed insert earphone sound source system that delivered the sound directly to the ear canal of the test person [20].

Contrary to the initial hypothesis, it was found that thresholds for audible sound were not affected by infrasound. However, threshold levels for infrasound increased significantly when specific audio sound stimuli were presented at a sufficient level (see Figure 4, adapted from [19]). In other words, it is more difficult to detect infrasound in a noisy than in a quiet environment. For example, the average threshold increase for infrasound was around 5 dB caused by the band limited pink-noise stimulus as background noise at a level of 50 dB above the individual threshold. The reason for this increase of the thresholds for infrasound is not yet clear. One possible hypothesis is that the response to infrasound might by suppressed by audible sound on a physiological level [21]. An alternative explanation is that the attention of the listener might be shifted towards the perception of audio sound when the listener is exposed to a combination of infrasound and audible sound. The findings of this study may indicate that infrasound might even be perceived as less annoying in a noisy than in a quiet environment.

A second hypothesis is that, because very high sound pressure levels are accompanied with hearing infrasound, nonlinear processes in the middle and inner ear have the potential to generate spectral components of noise at new, and particularly higher frequencies than that of the infrasound stimulus. These contributions have the potential to be heard.

In order to investigate whether non-linear processes within the ear play a role in infrasound perception, a sound reproduction system was developed that can generate sufficiently high sound pressure levels and, at the same time, has distortion component levels well below the threshold in quiet at these frequencies. A low-noise ear-canal microphone was incorporated into the system that monitors the sound in the ear and detects possible distortions, which is not affected by the high infrasound pressure levels in the ear canal.

Figure 5 shows a photograph of the sound reproduction system. It includes two RadioEar DD45 (RadioEar, USA) audiometric earphone transducers, which were mounted in air-sealed

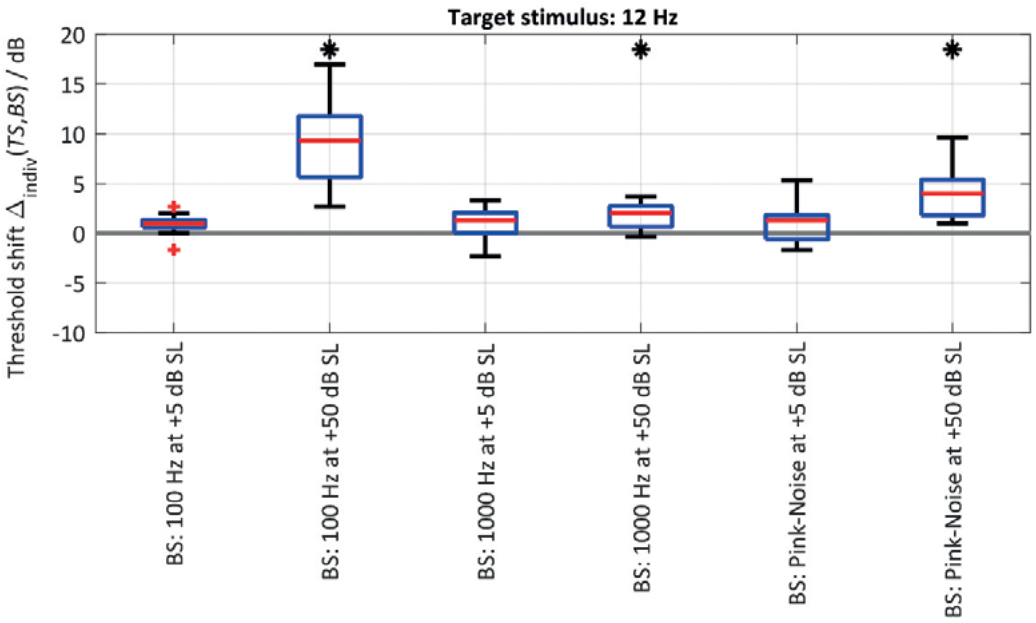

Figure 4: Threshold shifts for an infrasound pure tone at 12 Hz caused by the presence of audible sound as background stimulus (BS) presented at 5 and at 50 dB above the individual threshold level, i.e. at +5 dB and at +50 dB Sensation Level (SL). Significant threshold shifts were indicated by an asterisk.

aluminium housings, each with a sound outlet in the front plate and connected by means of sound tubes to an Etymotic ER-10B+ low-noise microphone system (Etymotic Research Inc., USA).

The volume that is enclosed by the membrane of the earphone transducers, the tubes, and the ear is small. It acts as a pressure chamber for low frequencies, enabling acoustic stimulation with the DD45 earphone transducers down to the infrasound frequency range.

It was shown that the system generates sufficiently high sound pressure levels with distortion product levels more than 45 dB below the hearing threshold levels. By means of an incorporated low-noise microphone, the system allows to monitor the sound and to detect possible distortions in the ear canal. The system is capable of presenting sound signals with frequencies ranging from 4 Hz to 5 kHz with loudness levels of up to 40 phon [22].

6. Challenges for future work

Medical acoustics and audiology highly profit from quantitative analyses and quantitative characterisation of hearing and its conservation. Today quality management is mandatory for every diagnostic, therapeutic or preventative operation and rely on a metrological fundamentals, such as traceability via the calibration of devices or the provision of reference data, methods or materials. Future developments in the field need to be incorporated into this comprehensive frame of quality assuring activities.

In the case of objective audiometry, methods based, for example, on auditory evoked potentials or the detection of otoacoustic emissions in the ear canal will become more important in the future. Objective audiometry is used for diagnostics or the support of a diagnosis of various symptoms or disorders. It has also the potential to deliver reliable quantitative data, describing the hearing ability. Objective audiology methods could, finally and at least in part, detach the subjective pure-tone threshold determination as the gold standard. Such an important step has to be accompanied by the development of new strategies of testing the devices driven by taking into account novel properties of these new technologies. Procedures and regulations need to be installed which require mandatory quality tests of daily measurement or diagnostics. This could also mean that objective audiology devices need to be classified as medical devices with measuring function.

Another result of such a development is that all standards and reference values, which hold for pure-tone audiometry will require a critical review. In many cases, a completely new definition and quantitative determination using hearing experiments will become necessary. Finally, these new approaches have to be included into international standards for broader applications. In addition, improved data management will allow more efficient meta-analyses and artificial intelligence will help in structuring, organising or interpreting data. All these novel methods will require quality assurance and currently only very rough visions exist how this could be managed in the future.

Hearing is a very important sense and it is reasonable that people are interested in their own quantitative status as an important factor of personal health and wellbeing. As in the case of sight, for example, where the individual status can be obtained at any optician shop, people could learn their individual hearing status by a visit of an audiologist. Today, the trend goes into the direction of the possibility to obtain a quick and direct information using consumer products, such as the own smartphone together with simple earphones, to determine hearing parameters. This is comparable to wearables providing other body information and will be more and more popular. Nevertheless, the quality of such data is not always clear and urgently needs to be determined and ensured in order to avoid significant risks due to wrong conclusions in the public. On the other hand, well defined and accurate wearables for hearing assessment can improve an early diagnosis of hearing disorders. New questions will arise if those devices will be developed onto the level of a medical product. They have to fulfil the full set of requirements as the established devices already on the market and they need also an appropriate quality control as described in section 4. The contribution to the maintenance of the currently well-working regime and the adaptation of future technologies into a safety ensuring system will be on the agenda for PTB also in the future.

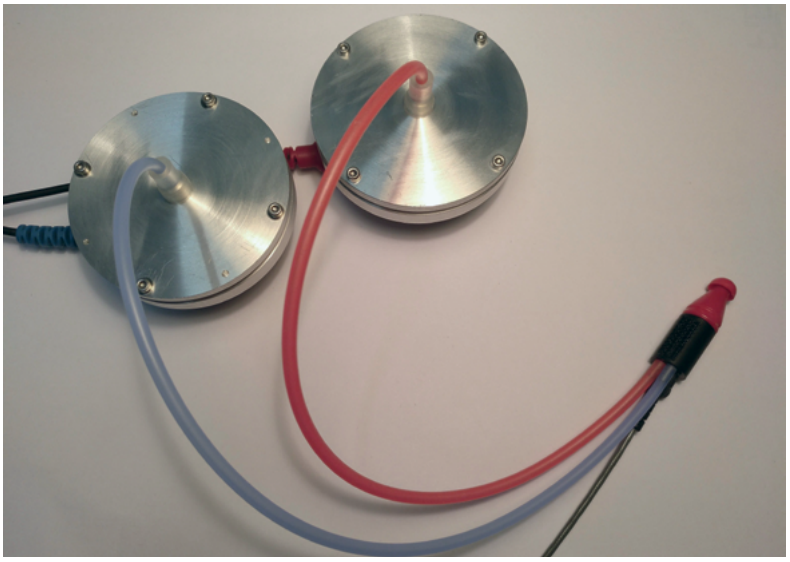

Figure 5: Photograph of the sound reproduction system consisting of two DD45 earphone transducers (top left) coupled with the Etymotic ER-10B+ system (bottom right) via two tubes.

7. Acknowledgement

This publication contains parts of a project that has received funding from the EMPIR programme co-financed by the Participating States and from the European Union's Horizon 2020 research and innovation programme.

8. References

[1] COUNCIL DIRECTIVE 93/42/EEC of 14 June 1993 concerning medical devices – Medical Device Directive.

[2] Regulation (EU) 2017/745 of the European Parliament and of the Council of 5 April 2017 on medical devices – Medical Device Regulation.

[3] Verordnung über das Errichten, Betreiben und Anwenden von Medizinprodukten (Medizinprodukte-Betreiberverordnung - MPBetreibV) 2002 (BGBl. I 3396)

[4] Leitfaden zu messtechnischen Kontrollen von Medizinprodukten mit Messfunktion (LMKM), Guidelines for metrological verifications of medical devices with a measuring function, PTB-Bericht MM11.

[5] World Health Organisation, Environmental Noise Guidelines for the European Region, WHO, 2018.

[6] European Environment Agency, Noise in Europe 2014, EEA report 10/2014.

[7] ISO 389-9:2009, Acoustics — Reference zero for the calibration of audiometric equipment — Part 9: Preferred test conditions for the determination of reference hearing threshold levels. International Organization for Standardization, Geneva.

[8] ISO 8253-1 2010. Acoustics – Audiometric test methods – Part 1: Pure-tone air and bone conduction audiometry. International Organization for Standardization, Geneva.

[9] IEC 60318-1 2009. Electroacoustics – Simulators of human head and ear – Part 1: Ear simulator for the measurement of supra-aural and circumaural earphones. International Electrotechnical Commission, Geneva.

[10] Elberling, C., Don, M., Cebulla, M., Stürzebecher, E.: Auditory steady-state responses to chirp stimuli based on cochlear traveling wave delay, J. Acoust. Soc. Am. 122, 2772-2785, 2007.

[11] Elberling, C., Don, M. A direct approach for the design of chirp stimuli used for the recording of auditory brainstem responses. J. Acoust. Soc. Am. 128, 2955-2964, 2010.

[12] Elberling, C. and Esmann, L.C.: Calibration of brief stimuli for the recording of evoked responses from the human auditory pathway. J. Acoust. Soc. Am. 141, 466–474, 2017.

[13] Fedtke, Thomas; Bug, Marion U. (2020): Equivalent hearing threshold levels for the RadioEar IP30 insert earphone and short-term stimuli: comparison of peak-equivalent and RMS-based measures. In: International Journal of Audiology 59 (5), S. 398–402. DOI: 10.1080/14992027.2019.1682690.

[14] Koch, C.: Hearing beyond the limit: Measurement, perception and impact of infrasound and ultrasonic noise. In: Brink, M. (Hrsg.): 12 th ICBEN Congress on noise as a public health problem., 2017.

[15] Moller, H. & Pedersen, C. S.: Hearing at low and infrasonic frequencies. Noise and health 6, Nr. 23, 37, 2004.

[16] Kuehler, R.; Fedtke, T. & Hensel, J.: Infrasonic and low-frequency insert earphone hearing threshold. The Journal of the Acoustical Society of America 137, 4, EL347– EL353, 2015.

[17] Drexl, M.; Otto, L.; Wiegrebe, L.; Marquardt, T.; Gürkov, R. & Krause, E.: Low-frequency sound exposure causes reversible long-term changes of cochlear transfer characteristics. Hearing Research 332 (2016), 87–94

[18] Marquardt, T. & Jurado, C.: Amplitude Modulation May Be Confused with Infrasound. Acta Acustica united with Acustica 104 (2018), Nr. 5, 825—829.

[19] Burke E., Hensel J., Fedtke T., Uppenkamp S., Koch C., Detection Thresholds for Combined Infrasound and Audio-Frequency Stimuli. Acta Acustica united with Acustica, 105, 2019.

[20] Burke, Elisa; Hensel, Johannes; Fedtke, Thomas; Uppenkamp, Stefan; Koch, Christian (2019): Detection Thresholds for Combined Infrasound and Audio-Frequency Stimuli. In: Acta Acustica united with Acustica 105 (6), S. 1173–1182. DOI: 10.3813/AAA.919394.

[21] Salt, A. N.; Lichtenhan, J. T.; Gill, R. M. & Hartsock, J. J.: Large endolymphatic potentials from low-frequency and infrasonic tones in the guinea pig. The Journal of the Acoustical Society of America 133 (2013), Nr. 3, 1561–1571.

[22] Joost, H., Friedrich, B., Verhey J. L., and Fedtke, T.: How to present pure-tone infrasound to the ear. Proceedings of the 23rd International Congress on Acoustics, Aachen (2019), 1470–1477.

New Sensors for Biosignal Detection

Rainer Körber[1], Victor Lebedev[2], Thomas Middelmann[3], Jens Voigt[4], Tilmann Sander[5]

Abstract

The non-invasive measurement of magnetic fields generated by electrophysiological activities in the human body is an important method in clinical applications and basic research. This includes the measurement of electrical activity with high temporal resolution of the brain, heart, muscles, and nerves. All such magnetic biosignals are extremely small in comparison to the Earth magnetic field and technical magnetic fields in urban environments. Traditionally, highly sensitive superconducting quantum interference devices (SQUID) are used together with advanced magnetic shields. Recently they have been complemented in usability by a new class of sensors, optically pumped magnetometers (OPM). These quantum sensors offer high sensitivities without requiring cryogenic temperatures allowing the design of small and flexible sensors for clinical applications. The PTB has a track record in developing highly sensitive magnetic field measurement devices together with advanced magnetic shielding approaches. In this paper, new developments in the sensor types together with system design strategies will be presented. Potential applications in clinical practice and basic research will be discussed.

1. Introduction

Biosignals usually refer to small electric signals produced by the sum of electrical potential differences in biological tissue or cell systems such as the nervous system. This includes electrical activity of the heart by measuring electrocardiograms (ECG), muscle activity by recording electromyograms (EMG) or neuronal activity in electroencephalograms (EEG). These signals are measured between electrodes attached to the skin and are widely used in clinical diagnosis.

Alternatively, the magnetic field generated by electrical currents can also be measured using sensitive magnetometers. Best known is magnetoencephalography (MEG), which is a functional neuroimaging technique for mapping brain activity occurring naturally in the brain. MEG has been in development since the 1980s but interest in the technique has been reignited by recent advances in hardware and machine learning algorithms to decode temporal patterns. Although EEG and MEG signals originate from the same neurophysiological processes, there are important differences. Magnetic fields are less distorted than electric fields by the skull and scalp, which results in a better spatial resolution of the MEG. Whereas scalp EEG is sensitive to both tangential and radial components of the current sources, MEG detects only its tangential components. Therefore, EEG detects activity both in the sulci and at the top of the cortical gyri, whereas MEG is more sensitive to activity originating in sulci and can thus be localized with better accuracy. Importantly, while scalp EEG relies on a reference electrode attached to a reference point on the body, MEG is reference-free, which often makes the interpretation easier. Furthermore, EEG relies on conductivity models of the tissue, which are not important for MEG. Both MEG and EEG allow for a temporal resolution in the order of one millisecond, enabling brain connectivity analysis in contrast to indirect methods such as functional magnetic resonance imaging (fMRI) or functional near infrared spectroscopy (fNIRS). MEG is applied clinically to localize abnormal brain activities, so called seizures in epilepsy or to examine abnormal patterns of activity in Parkinson's disease, schizophrenia and other brain disorders. In addition, magnetic field measurements are also used to study biosignals of the heart (MCG), muscles (MMG), and peripheral nerves (MNG).

All magnetic biosignals are extremely small

[1] Dr. Rainer Körber, ORCID: https://orcid.org/0000-0001-7052-5134; email: rainer.koerber@ptb.de

[2] Dr. Victor Lebedev, ORCID: https://orcid.org/0000-0002-0577-0763, email: victor.lebedev@ptb.de

[3] Dr. Thomas Middelmann, email: thomas.middelmann@ptb.de

[4] Dr. Jens Voigt, email: jens.voigt@ptb.de

[5] Dr. Tilmann Sander, ORCID: https://orcid.org/0000-0003-2984-5579, email: tilmann.sander-thoemmes@ptb.de

in comparison to the Earth magnetic field and technical fields in urban environments. Therefore, a biomagnetic measurement setup consists of a dedicated magnetic shield (often large enough to walk in) and sensitive magnetic field sensors operable only inside the shield. The most common magnetometer for several decades were superconducting quantum interference devices (SQUIDs) and therefore magnetically shielded rooms were optimised for SQUIDs, e.g., preventing radio frequency (RF) electro-magnetic fields in the room. Furthermore, SQUIDs require complex cooling in a cryogenic vessel which must be regularly filled with liquid helium. Since the arrangement of the SQUIDs inside the cryogenic vessel is fixed, they cannot be optimally placed for different applications and subjects. Recently, new optically pumped magnetometers (OPMs) have been investigated as future devices, which exploit the spin exchange relaxation-free (SERF) mode. These new sensors are insensitive to RF interference and can be more flexibly placed for different biomedical applications.

The PTB has a track record in developing highly sensitive magnetic field measurement devices together with advanced magnetic shielding approaches. Recently, the German Research Foundation has funded the Core Facility "Metrology of Ultra-Low Magnetic Fields" at PTB. This facility provides external scientists access to unique equipment for the measurement of extremely small magnetic fields. In particular the world-wide best walk-in magnetically shielded room (BMSR-2), which offers an overall (active + passive) shielding factor of more than 6 000 000 at 0.01 Hz and exceeds 100 000 000 above 5 Hz – unique conditions for magnetic field measurements – is thus also accessible for external scientists. This core facility benefits from PTB´s expertise as one of the world-leading institutes for highly sensitive SQUID magnetometers, which can detect very low magnetic fields down to just a few femtotesla (fT). PTB has now also established the new working group "Optical Magnetometry" to develop new optical quantum sensors with high sensitivity, which in contrast to SQUIDs do not require cryogenic temperatures. With these OPMs it is possible to design small and flexible sensor arrays that enable new clinical applications and facilitate existing ones. In the following, two different magnetic field sensor types and their application will be discussed followed by a description of shielding strategies to allow optimal operation of such sensors.

2. Ultra-sensitive SQUID systems for biomagnetism

The SQUID is the most sensitive detector of magnetic flux to-date and relies on quantum

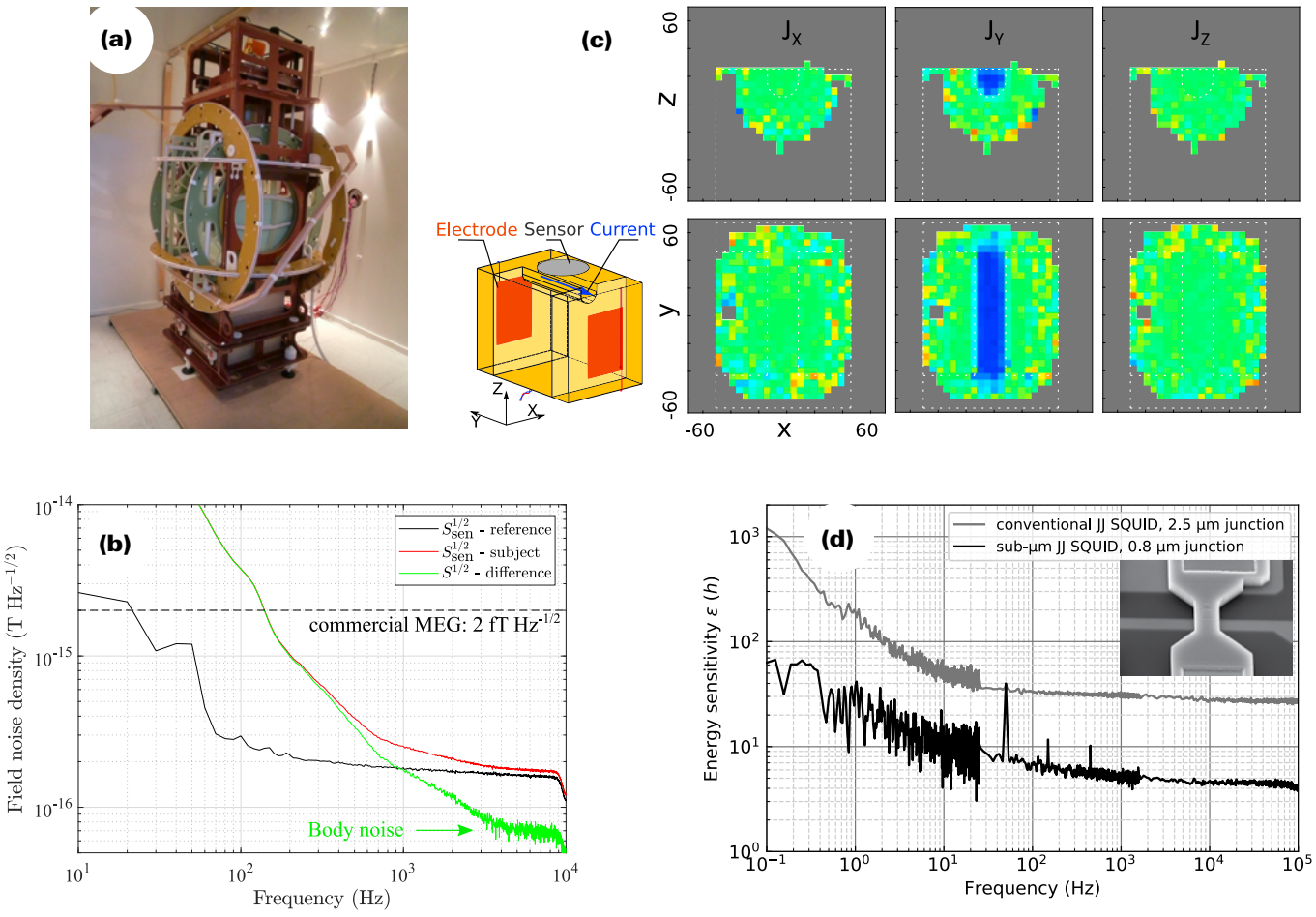

Figure 1:
a) PTB ULF MRI scanner,
b) Detection of body noise,
c) 3D imaging of impressed currents in phantoms,
d) Energy sensitivity of conventional SQUID vs. sub-µm-Junction SQUID.

interference effects in superconducting circuits. It is typically operated at liquid Helium temperature requiring the use of a cryogenic dewar vessel. Due to its high sensitivity it has been extensively used in biomagnetism to measure the tiny magnetic fields generated by ionic currents within the human body, and more recently as sensors in magnetic resonance imaging performed at ultra-low magnetic fields (1). Such a device built by PTB is shown in Figure 1a) inside a shielded room with the SQUID dewar inside a coil system.

Advances in sensor and cryogenic technology have enabled the elimination of the magnetic noise emanating from the liquid Helium dewar to reach noise levels as low as 150 aT/√Hz (2) and it is now possible to detect the thermal noise from the human body directly (3) as shown in Figure 1b). The determined level of body noise is in excellent agreement with theoretical predictions and consistent with estimations in the literature. The body noise represents the ultimate limit and, compared to commercial systems, an improvement by an order of magnitude in sensitivity was achieved. This paves the way for exploring new regimes in biomagnetic measurements as for instance the non-invasive investigation of neuronal spiking activity at the single trial level, a feature so far only possible by invasive microelectrodes.

Recently, the sensitivity of SQUIDs has been improved by miniaturising the tunnel junctions to below 1 µm (5) to get close to the quantum limit. We also follow this route and first demonstrator SQUIDs show a reduction in the energy sensitivity by a factor of 5 compared to our conventional SQUIDs as shown in Figure 1d). Combined with the improvement in low-noise dewar vessel construction one can expect a significant impact on biomagnetic measurements, but also in fundamental science experiments where SQUIDs are used in a noiseless shielded environment.

SQUID-based ultra-low field magnetic resonance imaging has the potential advantage of higher image contrast compared to high-field MRI, enabling methodologies currently unavailable. These include the combination of MEG and ultra-low field MRI in one instrument reducing co-registration errors. At PTB, the focus is directed towards imaging of impressed and intrinsic currents with exemplary results shown in Figure 1c). The 3-dimensional imaging of impressed currents has been demonstrated in phantom studies (4) and can potentially allow the extraction of conductivity maps, an indispensable ingredient in the solution of the ill-posed biomagnetic inverse problem encountered in MEG/EEG. The imaging of intrinsic neuronal currents relies on the direct detection of frequency shifts around an activated neuronal ensemble and its successful implementation would circumvent the localization ambiguity due to the inverse problem. Currently, the achieved sensitivity is close-to sufficient to realize this goal and ongoing efforts are required to succeed.

3. Compact OPM sensors for biomagnetic applications in medicine

Another class of magnetic field quantum sensors, the optically pumped magnetometers (OPMs), improved drastically in performance over the last two decades thanks to advances in laser and MEMS technologies (6). In these recently developed OPMs a hot atomic vapor in a microfabricated gas cell is optically pumped into a collective spin state by a sub-millimeter-sized spectroscopic diode laser. In an external magnetic field, the evolution of the quantum coherence in such spin-polarized atomic ensembles is equivalent to the

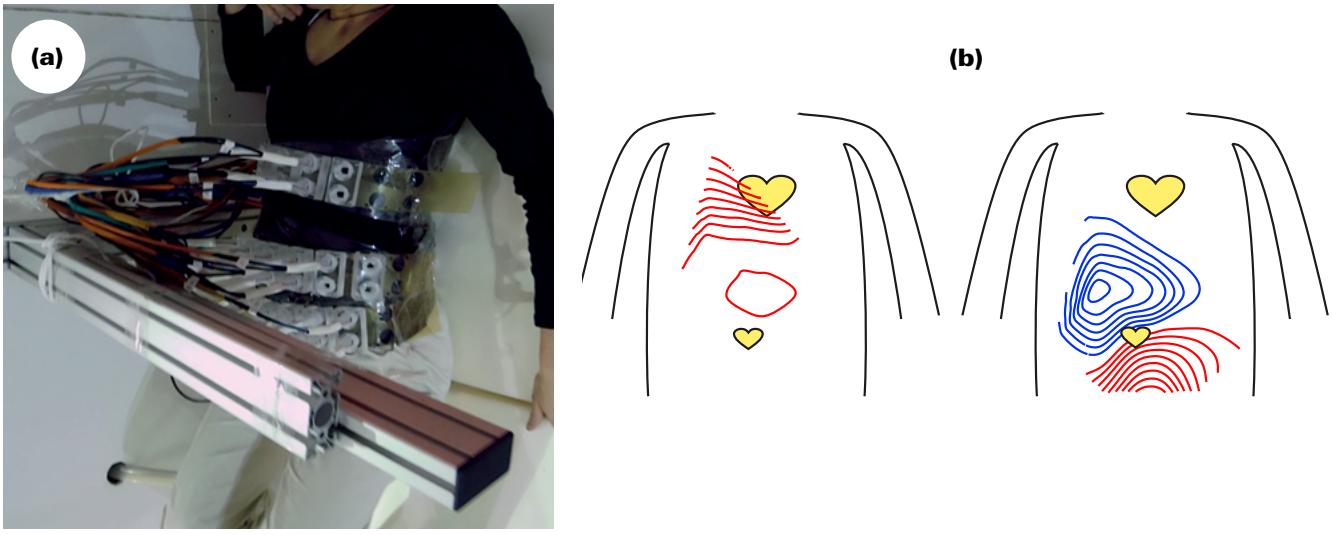

Figure 2: a) OPM sensor belts to detect fetal MCG b) Field maps of maternal and fetal MCG extracted by machine learning.

precession of a macroscopic magnetic moment. The Larmor frequency of the spin precession is proportional to the applied magnetic field and can be directly tracked by the pump laser or an additional laser. In a narrow frequency band an intrinsic sensitivity in the sub-femtotesla range has been demonstrated with a SERF OPM (7). Even in this advanced spin exchange relaxation-free (SERF) operation mode, a simple design, sub-watt power consumption, and minuscule size of the sensor components allow packaging of sensors in a housing of 5 cubic centimeters as demonstrated by QuSpin Inc. (USA) in 2018 with their QZFM-gen-2 sensors. Well-established semiconductor electronic technologies used in the design paved the way for mass production of the moderately priced OPMs. First commercial micro manufactured vector OPMs (Figure 3a), featuring a sensitivity of 10-20 fT/√Hz and 135 Hz bandwidth, already entered the market in 2016 and readily challenge their SQUID-based competitors in usability. While losing to SQUIDs in bandwidth and dynamic range, those instruments can be powered even by the USB port of a notebook and require no maintenance by qualified personal. Such OPMs can be easily deployed in an application ready multichannel array. The unique properties of OPMs attract great attention not only in the academic community (8), but also in the industrial applications and, most notably, in medicine.

As PTB has established a dedicated magneto-optical laboratory a thorough investigation of the operation principles and properties of generic and novel OPMs became feasible in close connection to the practical demands. Reference magnetic field setups for operation in magnetically well-controlled environment and with state-of-art lasers and electronic equipment are being developed. This is a necessary foundation not only for contributions to academic science, but even more for evaluation of medical and industrial applications, as well as for the development of novel magnetometer prototypes.

4. Stress-MCG recorded with OPMs during exercise

Ultra-compact OPMs assembled in a multisensory array enable a new level of biomagnetic investigations. The flexibility in placing the sensor heads facilitates adaptation to the individual shape of the body. For example, in magnetocardiography (MCG) the sensors can be attached to the body on top of the clothes as shown in Figure 2a) or Figure 3b). In this way fetal MCG was recorded in PTB's magnetically shielded room BMSR-2 (9,10). OPM usability is clearly superior to SQUIDs as, e.g., fetal magnetocardiography can be implemented without the need to design a unique application device. Figure 2a) shows that belts of OPM sensors are simply attached to the body of a pregnant woman to record heart signals. The recorded data can be separated by machine learning into maternal and fetal contributions, where Figure 2b) shows the respective field patterns.

In a recent pilot measurement adult MCG was registered before, during, and after exercise stress with two arrays of 8 OPMs each (QuSpin, QZFM-gen-1) attached to chest and back of the subject. In Figure 3b) the subject is pedaling on an ergometer and the attachment of sensors to the subject reduces relative position changes between sensors and field sources and is of great benefit for paradigms in which the subject is moving.

An SNR of up to 300 was realized which allows for distinguishing details in single heart beats already without averaging. Remaining artifacts due to the OPM's motion in the residual magnetic gradient can be strongly reduced by averaging without motional blurring, since relative positions between sensors and subject are fixed. The absence of jitter artifacts enables averaging over many heart beats also during motion as shown in Figure 2c). In SQUID-based stress-MCG stress is often induced pharmacologically (11), which is only

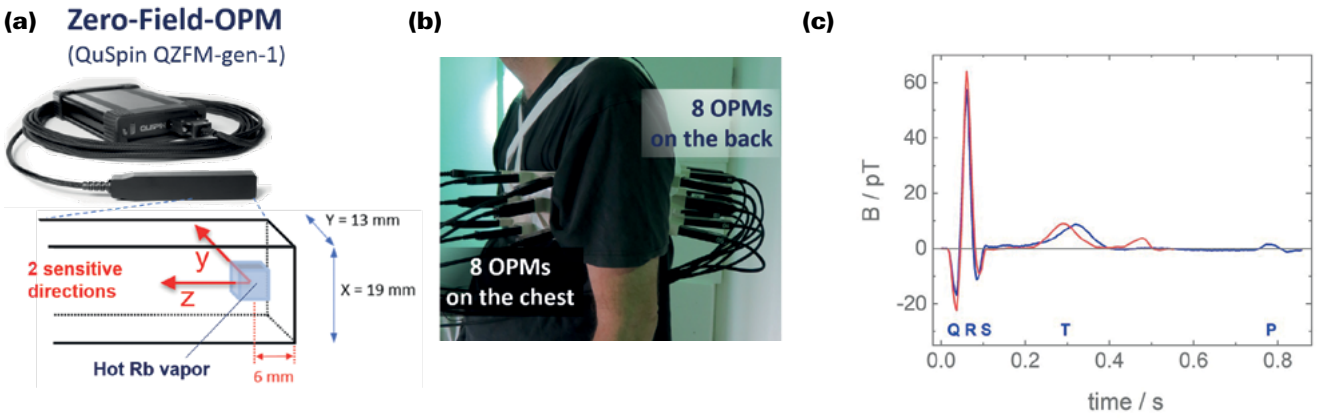

Figure 3:
a) Commercial OPM sensor, b) Experimental setup for exercise MCG, c) Averaged MCG-signal at rest in blue and during exercise in red. Clearly visible is the change in the T-wave.

partially relevant to assess heart performance.

OPM-based MCG can be applied with the same flexibility as conventional ECG based on gel filled electrodes. OPM MCG is even less invasive since no direct contact of sensor and body is needed, thus the subject can remain dressed and no electrodes need to be attached to the skin. Like in ECG a patient measured with an OPM MCG can sit upright during exercise or even walk or perform squats. The added information found in SQUID-based MCG (12,13) for ischemia and stenoses highlights the potential for OPM MCG with its much simpler operation.

5. Developing MEG for real-world settings

The study of electrical brain signals using SQUID sensors has a long history (14). Initial hope of a quick uptake in medicine did not occur, but it has become an indispensable tool for some clinical applications and especially in neuroscience. Since there are many almost intractable diseases of the brain, research up to the diagnostic applications is performed. For example, Parkinson´s disease or other movement disorders lead to a severe loss of quality of life and can start at young age and persist through the remainder of life. MEG is used in patients selected for deep brain stimulation, where the electrode leads of the implanted stimulating electrode can be used to measure local field potentials, while the patients head is in the MEG. Important results based on SQUID MEG (15) reveal a role of the cerebellum, which is generally not easy to study.

The aim to decode movement related brain signals in the healthy population leads to the necessity of wearable devices operating in normal environments, which clearly cannot be fulfilled by SQUID MEG. Portable and only by radio transmission connected EEG devices have been developed (16). An option to record magnetic brain signals of subjects in a close to normal setting is the application of the already mentioned OPMs (8,17). For MEG they cannot yet compete in noise performance or bandwidth with SQUIDs, but their usability is superior as demonstrated in a seminal work (8), which inspired the setup shown in Figure 4 a).

For MEG, usability is not the only requirement. Therefore, OPM MEG needs to be benchmarked against non-portable SQUID MEG in terms of signal-to-noise ratio, information content, precision, and repeatability. To test for signal to noise ratio and repeatability an exemplary approach is described here. Subjects listen to an acoustic stimulation for 20 minutes wearing an OPM-MEG helmet. Then subjects transfer to the SQUID MEG and the same stimulation runs and signals are recorded again. As shown in Figure 4b) the amplitudes recorded with OPMs are about 4 times higher compared to SQUID sensors. The result for the signal-to-noise ratio is still an open question as effects of sensor number and inverse solutions still need to be explored.

6. Magnetically shielded rooms

Electrophysiological signals of the human body are generally modified by conducting tissue surrounding an electrical current source. Nevertheless, magnetic biosignals have the advantage that the free propagation of magnetic fields through the body yields information complementary to electrical surface signals. Electrical propagation can be severely degraded by compartments of different conductivity in the body. The drawback of biomagnetic signals is the low amplitude in the range of fT to pT. A common method to reach an environment with low magnetic disturbances is the use of a magnetically shielded room (MSR) made of high permeability ferromagnetic material, so called Mu-metal (18). Disturbances inside the MSR

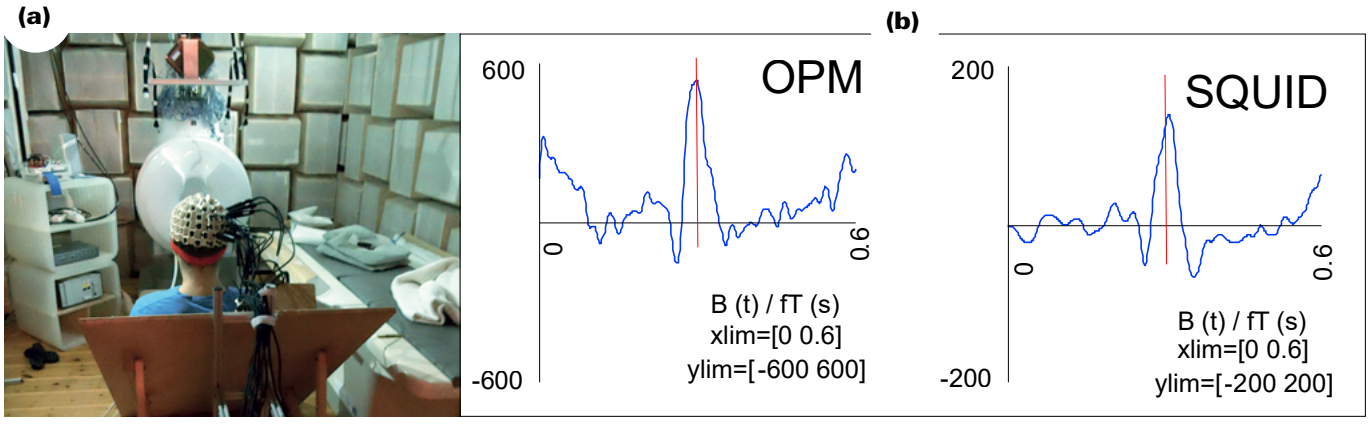

Figure 4:
a) SQUID- and OPM-MEG systems together inside a magnetically shielded room allowing rapid method evaluation, b) Amplitude comparison between SQUID and OPM data for the auditory M100 response on a single subject. OPM measured amplitudes are four times the value measured by SQUID.

can be divided into external and internal sources. External sources are the Earth magnetic field and urban technical sources, internal sources can be any installation inside the room and the residual magnetization of the MSR walls.

The two main characteristics of an MSR are the shielding factor given by the damping of an external signal and the static remnant field inside the MSR. The shielding factor depends on the frequency of the distortion, the permeability, the number of the damping layers and on their geometric shape (19). For commercial MSRs with two layers of Mu-metal a shielding factor between 100 and 300 can be achieved. It was shown in (20,21) that by a proper degaussing of the Mu-metal shield the static residual field inside a common two Mu-metal + 1 aluminium layer MSR, like the Ak3b from VAC/Germany (recent commercial naming is VACOSHIELD Advanced), is not depending on the external static Earth magnetic field, but on the residual field of the shielding walls.

For SQUIDs mainly the damping factor is relevant as even high residual fields of several µT do not prevent their operation. Usually a high residual field is accompanied by respective gradients and if the sensor is vibrating in the gradient field a time varying signal is observed. The typical frequency of such building or intrinsic setup vibrations are in the range of 4 Hz to 30 Hz where also brain activity is strong. Therefore, even for SQUIDs a low gradient is desirable and the MSR should be equipped with an optimized degaussing system to minimize this gradient. An additional requirement for SQUIDs is an MSR with an RF-shield as the bandwidth of SQUIDs reaches the MHz range, where RF fields can be quite strong.

For SERF OPMs both dynamic and residual fields should not exceed the dynamic range of these sensors, which can be about 10 nT. An MSR with a residual field of 50 nT is unsuitable for bare SERF-OPM operation. Fortunately, commercial SERF OPMs can compensate for residual fields in this range, but the compensation is static and too large gradients in combination with vibrations can still generate signal variations saturating OPMs. The 8+1-layer room of PTB, BMSR2, is uniquely suitable for high quality SERF-OPM operation with residual fields of less than 1 nT and respectively small gradients. The time varying magnetic field of external sources in a two-layer shield is reduced by the frequency dependent shielding factor. Inside the Ak3b from VAC/Germany an outside peak-to-peak distortion of 600 nT at 10mHz from the Berlin metro will be reduced to 6 nT inside the shielding. To measure in this field with current SERF OPMs the sensor-internal compensation coils need to be used already. To further reduce such time varying magnetic distortion an active field compensation (AFC) or additional Mu-metal layer can be used, and an additional shielding factor of 5 to 50 can be achieved.

Overall the shielding strategy depends on the type of sensor used and best performing biomagnetic measurement setups are rather a combination of magnetic shielding and sensor system. The different MSRs of PTB allow optimal SQUID and OPM operation.

7. Conclusion

PTB operates several arrays of either ultra-sensitive SQUIDs or single unit OPMs inside shielded rooms. With these systems we study the non-invasive detection of magnetic brain and heart signals of the human body. The systems are application ready and exemplary studies address the diagnostic potential for cognitive, psychiatric, and cardio-vascular diseases, which are a burden for patients and the health system alike.

Rapid progress is expected if the measurement advances are combined with fine grained physiological modelling and automated analyses based on, e.g., machine learning. This will help in single-event detection of brain responses using ultra-sensitive SQUIDs. Despite technical progress the hardware still consists of dedicated rooms adapted to the sensing units. Future work will need to reduce system complexity for, e.g., Parkinson´s research. In case of OPMs this could be achieved by truly wearable sensors and wall-paper like magnetic shields combined with field compensation coils.

Acknowledgements

The authors are indebted to Lutz Trahms, Martin Burghoff and Allard Schnabel for long lasting support.

References

[1] Körber R, et al. SQUIDs in biomagnetism: a roadmap towards improved healthcare. Supercond Sci Technol. 2016;29:113001.

[2] Storm JH, et al. An ultra-sensitive and wideband magnetometer based on a superconducting quantum interference device. App Phys Lett. 2017;110:072603.

[3] Storm, JH, et al. Detection of body noise with an ultra-sensitive SQUID system. Meas Sci Technol. 2019;30:215103.

[4] Hömmen P, Storm JH, Höfner N, Körber R. Demonstration of full tensor current density imaging using ultra-low field MRI. Magnetic Resonance Imaging. 2019;60:137-144.

[5] Schmelz M, et al. A new family of field-stable and highly sensitive SQUID current sensors based on sub-micrometer cross-type Josephson junctions. Supercond Sci Technol. 2017;30:074010.
[6] Shah V, Knappe S, Schwindt PDD, Kitching J. Subpicotesla atomic magnetometry with a microfabricated vapour cell. Nature Photon. 2007;1:649–652.
[7] Kominis IK et al. A subfemtotesla multichannel atomic magnetometer. Nature 2003;422:596-599.
[8] Boto E, Holmes N, Leggett J et al. Moving MEG towards real-world applications with a wearable system. Nature 2018;555:657–661.
[9] Alem O, Sander TH, Mhaskar R, LeBlanc J, Eswaran H, Steinhoff U, Okada Y, Kitching J, Trahms L, Knappe S. Fetal magnetocardiography measurements with an array of microfabricated optically pumped magnetometers. Phys Med Biol. 2015;60:4797–4811.
[10] Alem O, Mhaskar R, Jiménez-Martínez R, et al. Magnetic field imaging with microfabricated optically-pumped magnetometers. Opt Express. 2017;25:7849–7858.
[11] Brockmeier K, et al. Magnetocardiography and 32-Lead Potential Mapping. J of Cardiovascular Electrophysiology. 1997;8:615.
[12] Lant J, et al. Complementary nature of electrocardiographic and magnetocardiographic data in patients with ischemic heart disease. J of Electrocardiology. 1990;23:315.
[13] Park J-W, et al. Dobutamine stress magnetocardiography for the detection of significant coronary artery stenoses--a prospective study in comparison with simultaneous 12-lead electrocardiography. Clinical hemorheology and microcirculation. 2008;39:21.
[14] Sander TH. Biomagnetism. In: Rogalla H, Braginski A, eds. Handbook of superconductivity. 2nd ed. Taylor and Francis. 2020:In press.
[15] Neumann WJ, Jha A, Bock A, et al. Cortico-pallidal oscillatory connectivity in patients with dystonia. Brain. 2015;138:1894-906.
[16] von Luhmann A, Wabnitz H, Sander TH, Muller KR. M3BA: A Mobile, Modular, Multimodal Biosignal Acquisition Architecture for Miniaturized EEG-NIRS-Based Hybrid BCI and Monitoring. IEEE Trans Biomed Eng. 2017;64:1199–1210.
[17] Knappe S, Sander TH, Trahms L. Optically Pumped Magnetometers for MEG. In: Supek S, Aine C, eds. Magnetoencephalography. Cham:Springer; 2019:1–8.
[18] Cohen D. A Shielded Facility for Low Level Magnetic Measurements. J Appl Phys. 1967;38:1295.
[19] Summer TJ, Pendlebury JM, Smith KF. Convectional magnetic shielding. J Phys D: Appl Phys. 1987;20:1095–1101.
[20] Voigt J, Knappe-Grüneberg S, Schnabel A, Körber R, Burghoff M. Measures to reduce the residual field and field gradient inside a magnetically shielded room by a factor of more than 10. Metr Meas Syst. 2013;20:237–248.
[21] Altarev I, et al. A magnetically shielded room with ultra low residual field and gradient. Rev Sci Instr. 2014;85:075106.

Electrolytes in Human Serum – Two Decades of SI Traceability

Olaf Rienitz, Karin Röhker, Carola Pape, Silvia Ulbrich, Ursula Schulz, Jessica Towara, Volker Görlitz, Reinhard Jährling, Anita Röthke, Detlef Schiel, Rainer Stosch

Abstract

The ions lithium, sodium, potassium, magnesium, calcium, and chloride are important constituents of the electrolytes in human serum. Since electrolytes play an important role in the human body, the concentrations of the above-mentioned ions in human serum are meaningful markers for several diseases. For this reason, PTB has developed primary methods of measurement for the SI-traceable determination of these ions in the past more than two decades, as well as a routine method based on ion chromatography. The equivalence of the results of the primary method on the one hand and the routine method on the other hand as well as the international comparability of the results was demonstrated through successful participation in CCQM key comparisons. As a consequence, PTB holds eight serum-related CMC claims in the according BIPM database. The routine method was continuously improved over time resulting in relative measurement uncertainties of less than 0.5 % nearly on par with the ones obtained with the primary methods. Important improvements discussed in this work are the optimization of the serum digestion, the gravimetric preparation of reference solutions starting from primary monoelemental solutions, and the development of the exact matching one-point calibration as well as the combination of chemical and CO_2-suppression.

1. Introduction

In chemical analysis, compounds that dissociate into ions when dissolved in water and this way increasing its electrical conductivity are usually called electrolytes [1]. They are of major physiological importance for numerous processes in the human body, among them the adjustment of the pH, the osmotic pressure, and the heart rate as well as saltatory conduction and bone growth. Their concentrations in human serum are therefore meaningful markers for several diseases such as renal calculus, tumors, osteoporosis, gastric ulcer or malnutrition. In case of a lithium medication for the treatment of various mental disorders, its serum level has to be monitored regularly [2]. Because of their great medical importance and due to the high frequency of their measurements in routine laboratory medicine, the several ions forming or influencing the electrolytes in human serum, namely lithium (Li), sodium (Na), potassium (K), magnesium (Mg), calcium (Ca), and chloride (Cl) are considered priority measurands in the guideline of the German Medical Association (Richtlinie der Bundesärztekammer zur Qualitätssicherung laboratoriumsmedizinischer Untersuchungen – Rili-BÄK [3]). For the measurands listed in the Rili-BÄK, routine laboratories are obliged by law to participate in so-called External Quality Assessment Scheme (EQAS) as part of the external quality control, whereby reference method values are explicitly required for the specified electrolytes. Triggered by the Rili-BÄK [4] and an increased common awareness towards metrological concepts, a cooperation between PTB and the Medizinische Hochschule Hannover (MHH) was initiated in 1997. As a direct consequence, the working group for Inorganic Analysis (AG 3.11) started developing measurement methods for the determination of Li, Na, K, Mg, and Ca in human serum based on ion chromatography (IC). Already one year later the development of primary methods for the above-mentioned analytes as well as for Cl was tackled [5]. In addition to IC as the potential routine method, a variety of methods was assessed, further improved, and established: Gravimetry for Na [6], isotope dilution mass spectrometry (IDMS) using inductively coupled plasma (ICP) or thermal (TI) ion sources for Li, K, Mg, Ca, and Cl, inductively coupled optical emission spectrometry (ICP OES) for Na, K, Mg, and Ca, as

All authors:
Department "General and Inorganic Chemistry", PTB Braunschweig,
ORCID: https://orcid.org/ 0000-0002-5087-5812,
email: olaf.rienitz@ptb.de

well as titrimetry for Cl [5]. Through the regular participation in international comparisons, the fitness of all methods developed during the last two decades was rigorously assessed [7–11].

2. Problems at the outset

However, it became clear that the arsenal of sophisticated methods led to mediocre results, because several very basic prerequisites were not paid the necessary attention. First and foremost, state of the art analytical methods at the turn of the millennium simply required the purest water available. In 1998, the laboratory water was purified sequentially via complete demineralization followed by a one-step distillation in stainless steel and a two-step distillation in a quartz-apparatus. This purification protocol lead to unavoidable elemental trace-level impurities (problematic especially in case of mass spectrometric techniques like ICP-MS and TIMS), because the distillation does in principal not remove organic impurities like humic acids potentially present in ground water. The IC system (Dionex, USA) applied a so-called electrochemical suppressor which purpose it is to reduce the conductivity of the eluent (methanesulfonic acid) used to separate the analyte ions on a column. This conductivity suppression enables the detection of the analytes via their electrolytical conductivity in the first place, because the conductivity of the eluent exceeds the conductivity of the analytes by several orders of magnitude rendering measurements without conductivity suppression almost impossible [12]. The suppressor within the IC system used OH^- – generated by electrolysis – to replace the methanesulfonate through ion-selective membranes and form poorly dissociated water, this way dramatically reducing the background conductivity. The downside is a high sensitivity of the membranes to organic impurities in the water used affecting the stability of the baseline. Figure 1 compares the baseline acquired with demineralized and triple-distilled water to the baseline measured using water produced with a water-purifier system (Merck-Millipore) consisting of several purification steps, among them reverse-osmose, triple UV-treatment and three column-separations, resulting in water purified with regard both to inorganic but also organic impurities.

Figure 1:
Baseline of the conductivity σ acquired with the IC routine method using demineralized and subsequently triple distilled water (black line) and using ultra-pure water produced with a dedicated water purification system (blue line).

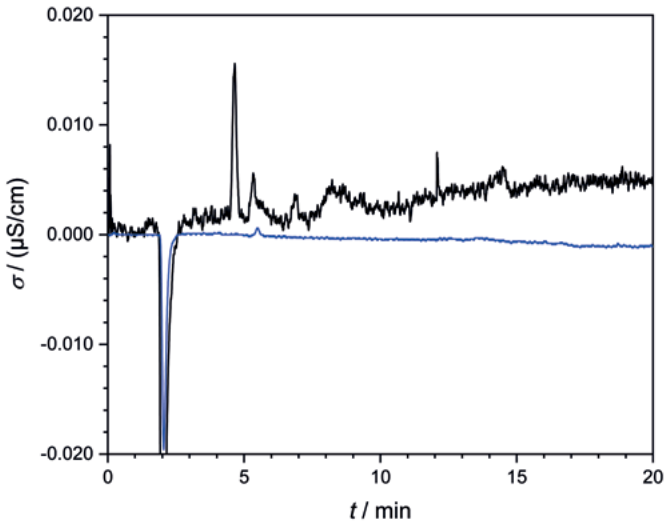

Human serum contains not only electrolytes but also a variety of organic compounds like sugars, proteins, and fats. Table 1 shows a representative composition of human serum [2].

The organic components of the serum cause strongly biased results, e.g. by shifting the response of the measurement device used. Therefore, the organic components have to be either removed or completely converted into inorganic compounds such as nitrate, water or carbon dioxide (mineralization). This so-called digestion was classically done by heating the serum with an (oxidizing) acid (mixture) on a hot-plate. After evaporating the acid serum mixture to near dryness and re-dissolving it in dilute acid or water, it was ready for the measurements. But in the ion chromatograms of the digested serum samples several unknown peaks appeared, not

Table 1:
Representative composition of human serum of a healthy patient, adapted from [2].

Constituent	per 100 g human serum
Water	92 g
Proteins and N-containing compounds	6.6 g
Sodium	330 mg
Potassium	15 mg
Magnesium	2.4 mg
Calcium	10 mg
Chloride	360 mg
Hydrogencarbonate	165 mg
Phosphate	10 mg
Sulfate	5 mg
Organic acids	21 mg
Glucose	81 mg
…enzymes, lipids, …	

present in the calibration solution prepared from pure salts.

Figure 2a shows such a chromatogram with several unknown peaks, presumably originating from amides resulting from incompletely digested proteins behaving similarly on the separation column as the cations. When these amide peaks appear close to the actual peaks, a precise and reproducible integration might be difficult, but in case they appear under the actual peaks, biases of unknown magnitude result. Therefore, several digestion methods (like ashing in an oven or oxygen bomb) were assessed and compared to each other. The best suited method proved to be a pressurized microwave assisted acid digestion in closed microwave-transparent vessels made of a highly pure fluoropolymer. In open systems the digestion temperature is always restricted to the boiling temperature of the acid used (in case of 0.25 g/g nitric acid approximately 105 °C). Working in closed vessels overcomes this restriction, because the acid vapor increases the pressure preventing the acid from boiling. This way, the temperature is limited by the vessel material, its temperature and pressure resistance [13]. The microwave ovens (Ethos 1600 and ultraCLAVE III, MLS, Germany) applied at PTB allow for routine digestion temperatures of 200 °C and 260 °C, respectively. Using a mixture of nitric acid and hydrogen peroxide enables the complete mineralization of all organic constituents of human serum.

The chromatogram in Figure 2b demonstrates a clean baseline and perfectly shaped peaks suggesting the absence of any interfering compounds and proving a complete or at least sufficiently complete digestion of all organic constituents of the serum samples. The development of a suitable digestion method was not only a requirement for the IC method but also crucial for the gravimetric and IDMS methods, because both gravimetry and IDMS require the chromatographic separation of the analyte(s) from the matrix. This preparative chromatographic separation is interfered in pretty much the same way as IC. Besides the water purification and complete digestion, the preparation, handling, and maintenance of primary calibrators, in this case monoelemental solutions with a well-known mass fraction of the element, was uncharted territory. One has to consider that the Consultative Committee for Amount of Substance (CCQM) was founded only five years ago back then and the idea of metrological concepts like traceability and measurement uncertainty applied to analytical chemistry were just that: ideas [14]. Therefore, a protocol for the gravimetric preparation and evaporation correction consequently taking into account the air buoyancy correction had to be developed from scratch [15] to be able to prepare the necessary calibration solutions. To bring this protocol to life, a weighing room was installed and equipped with a laminar flow air condition, measures to avoid electrostatic charges (e.g. a humidifier in the air condition), and sensors measuring the ambient conditions (temperature, humidity and pressure of the air), necessary to be able to correct for air buoyancy. In parallel, the established volumetric liquid handling using e.g. volumetric flasks was superseded by an exclusively gravimetric protocol.

3. Primary methods and a routine one

Especially IDMS based methods were applied to establish primary methods for the determination of the electrolytes in human serum. Table 2 summarizes all methods along with their measurement uncertainties in comparison to the routine IC method [16]. In case of IDMS, several improvements were made and resulted in a special kind of IDMS: Double IDMS with exact matching and a ratio of the ratios R_{bx}/R_{bz} adjusted to be close to unity [5], [17], [18]. The IC routine method is

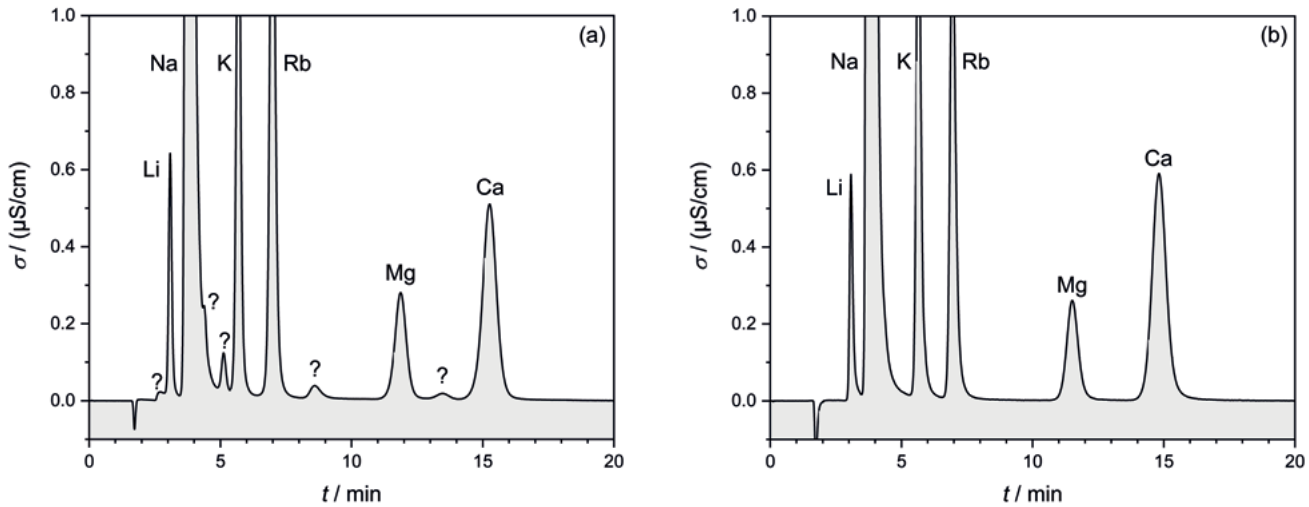

Figure 2: Chromatograms of digested human serum acquired with the IC method revealing an incomplete digestion with several unknown peaks (a) and a perfect microwave-assisted digestion with only the analyte peaks visible (b).

Analyte	Primary method		IC
		U_{rel} / %	U_{rel} / %
Li	ID-ICP-MS	0.33	0.90
Na	gravimetry	0.14	0.40
K	ID-TIMS	0.30	0.70
Mg	ID-ICP-MS	0.62	0.80
Ca	ID-TIMS	0.32	0.70
Cl	titrimetry	0.40	

Table 2:
Primary methods and associated relative expanded uncertainties U_{rel} (coverage factor k = 2) compared to those achieved with the IC routine method in 2001.

based on a one-point-calibration and requires an iterative adjustment of all analyte concentrations in the calibration solution so that the peaks measured in the sample and in the calibration solution match within 1 %.

Figure 3 illustrates impressively how similar the chromatograms of reference and serum sample are, provided the serum was digested completely and both solutions were matched properly in terms of the analyte contents.

While time-consuming in the beginning, an experienced technician produces such a perfect agreement usually with just one iteration based on the evaluation of a first rough measurement. The measurement makes use of an internal standard. In case of serum, rubidium (Rb) is added prior to the digestion. Due to a similar behavior of Rb and the analytes as well as an evaluation based on peak area ratios related to Rb rather than absolute peak areas, especially losses during the digestion or any other liquid handling step do not affect the final result. A big problem was the precipitation of Mg and to minor extends of Ca and Li on the suppressor membrane due to the extremely high OH^- concentrations on the membrane surface causing too low Mg and Ca results. The iterative matching scheme solved the problem, because the calibration solution was affected in exactly the same way, resulting in virtually unbiased results. Another problem the IC method suffered from was the not entirely perfect separation of K from Na resulting in accordingly larger uncertainties due to the limited reproducibility of the peak integration. Again, the exact matching scheme mitigated this problem. Therefore, until some five years ago the method was at its limits. In 2015 the change from the electrochemical suppression to chemical suppression helped to improve the IC method substantially. In the new IC system (Metrohm, Switzerland) the eluent is dilute nitric acid with an extremely high conductivity. The chemical suppression is based on the exchange of the nitrate anions originating from the eluent acid with hydrogencarbonate. The hydrogencarbonate together with the remaining protons from the eluent acid forms intermediate carbonic acid which in turn decomposes into water and carbondioxide (CO_2). The CO_2 has a very low solubility in the acidic environment. This way the background conductivity is perfectly reduced without the precipitation of especially Mg, but the CO_2 bubbles would render a conductivity measurement impossible. A so-called CO_2-suppressor (Metrohm, Switzerland) after the chemical suppression degasses the eluent through PFA-membrane capillary packs. The resulting background conductivity is on par with the conductivity achieved with electrochemical suppression but without losing analyte ions resulting in substantially larger analyte peaks in case of Li, K, Rb, Mg, and Ca. Furthermore, due to an improved separation column, Na and K are now perfectly baseline-separated. This way the uncertainties associated with the analyte contents were reduced approximately by a factor of two. Figures 4a and 4b show the different

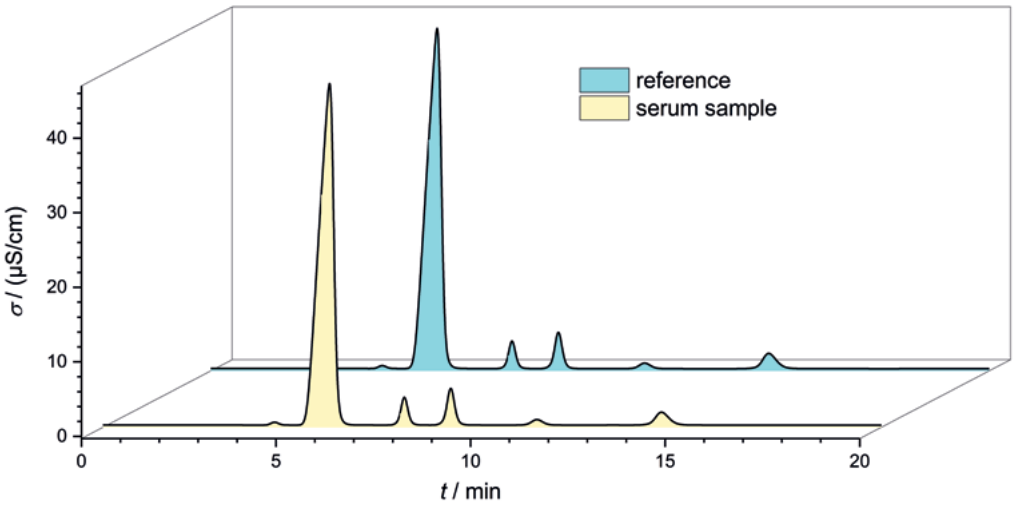

Figure 3:
Exact matching: Both the reference and the serum sample were digested and prepared in exactly the same way. They were matched with regard to their analyte contents perfectly, so that in a 2D-plot the chromatograms agree within their line widths. Virtually all potential biases become negligible.

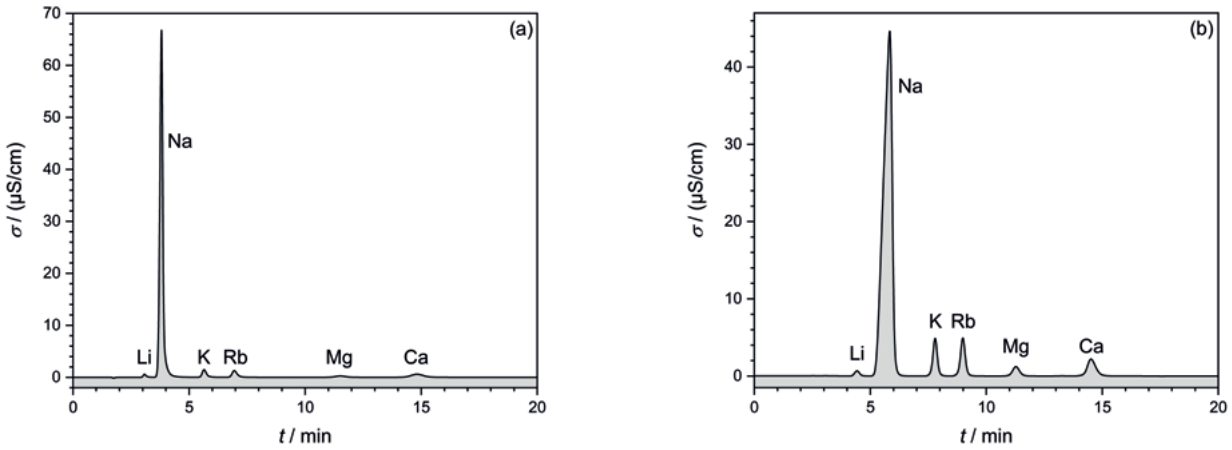

Figure 4: IC chromatograms of completely digested serum samples with exactly the same analyte contents. (a) Acquired with the first IC system using electrochemical and (b) with the improved IC system using chemical and subsequent CO_2 suppression. Especially the Mg peak, but to a minor degree also the peaks of Ca, Rb, K, and Li as well as the peak separation benefit from the improvements achieved over the last two decades reducing the uncertainties to nearly 50 % of the original value.

peak separation and areas of the first IC system compared to the improved one based on combined chemical and CO_2 suppression using measurement solutions with exactly the same analyte mass fractions.

Table 3 compares the uncertainties achieved routinely with the different IC systems during the participation in comparison measurements [19] in 2001 and 2017, respectively. Even more remarkable than the improvement itself is that the uncertainties associated with the results determined with the IC routine method now come really close to those achieved with the primary methods (Table 2) or in case of Mg are even smaller.

	IC routine method	
Analyte	**2001**	**2017**
	U_{rel} / %	
Li	0.90	0.39
Na	0.40	0.40
K	0.70	0.39
Mg	0.80	0.45
Ca	0.70	0.40
Cl	0.40	0.41

Table 3: Relative expanded measurement uncertainty U_{rel} (coverage factor k = 2) achieved with the IC routine method in the framework of comparison measurements [19] in 2001 and after several improvements in 2017. The uncertainty associated with the chloride content determined using titrimetry remained constant, but on an already exceptional level.

4. How accurate and reliable is the routine method?

Even though the uncertainties associated with the results achieved with the IC routine method were already exceptionally low in the beginning more than two decades ago and were further improved about five years ago, the accuracy of the routine method had to be assessed. In a first attempt this was done with certified reference sera like NIST SRM 909b. Both the primary methods and the routine one were able to reproduce the certified values well within the limits of their uncertainties [5], [16]. Already in 2001, within the framework of the international pilot study CCQM-P14 (Ca) [7] and the European comparison IMEP-17 (Li, Na, K, Mg, Cl) [8], the performance of the IC routine method was compared to the primary methods and to the comparison reference values. Figure 5 as an example clearly demonstrates the perfect agreement of the Ca mass fractions determined using the IC routine method and the values measured by the primary ID-TIMS method as well as the perfect agreement of all values with the reference value from the comparison.

Whenever serum related CCQM comparisons [9–11] were organized, PTB put their primary methods to the test to ensure international long-term comparability and claim and maintain their so-called "Calibration and Measurement Capabilities" (CMC). As of the end of 2019 PTB holds eight serum related CMCs in the BIPM database [20]. Figure 6 shows PTB's performance in serum-related CCQM comparisons over the last two decades in terms of the so-called normalized errors E_n [21]. Since the normalized errors compare the difference between the participant's value and the comparison reference value to their combined uncertainty, $-1 \leq E_n \leq +1$ indicates perfect agreement with the reference value. Even though the complete variety of methods like ID-TIMS, ID-ICP-MS, and titrimetry was tested, all results were flawless.

5. RELA-IFCC – the IC method routinely applied

In Germany, the dissemination and traceability scheme in clinical chemistry is maintained via reference laboratories and regular comparison measurements. The "*Referenzinstitut für Bioanalytik*" RfB (Bonn, Germany) organizes annually an international comparison measurement with a large variety of analytes under the umbrella of the *International Federation of Clinical Chemistry and Laboratory Medicine* (IFCC), the so-called "RELA – IFCC External Quality Assessment Scheme for Reference Laboratories in Laboratory Medicine"

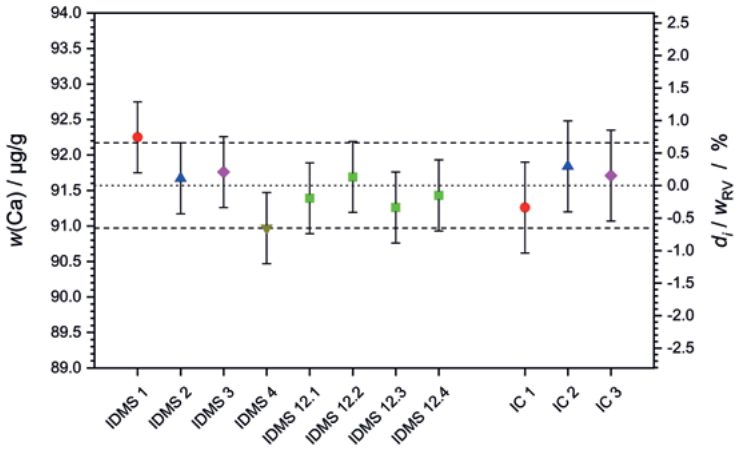

Figure 5: In the framework of PTB's participation in the international comparison measurement CCQM-P14 "Calcium in Serum" the IC routine method was compared to the primary ID-TIMS method. The results achieved with both methods agree perfectly with each other and with the reference value w_{RV} (dotted black line). The range of the expanded uncertainty associated with the reference value is shown as dashed black lines. The right axis indicates the relative deviation from the reference value. ID-TIMS results are labelled "IDMS 1" through "IDMS 12.4". IC results are labelled "IC 1" through "IC 3". Each data point represents a separately prepared aliquot of the original pool of sample vials. Points of the same color and shape represent aliquots from the same vial.

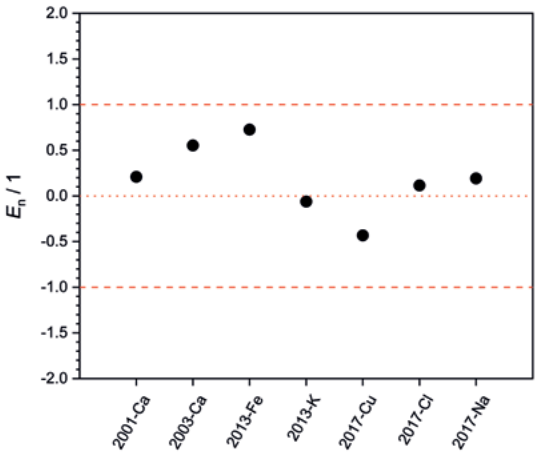

Figure 6: PTB's record of participation in serum related CCQM comparison measurements. The data points show the so-called normalized errors $E_n = d_i/U(d_i)$. An E_n between –1 and +1 demonstrates perfect agreement with the reference value and this way a successful participation (for more details refer to the text above and [21]). The year represents the according comparison: 2001: CCQM-P14, 2003: CCQM-K14, 2013: CCQM-K107, 2017: CCQM-K139. A variety of methods were put to the test: Ca and K: exact matching double IDMS on an MC-TIMS with prior matrix removal; Fe and Cu: exact matching double IDMS on an HR-ICP-MS; Cl: exact matching argentometric titration with potentiometric end-point detection; Na: ion chromatography with exact matching one-point calibration.

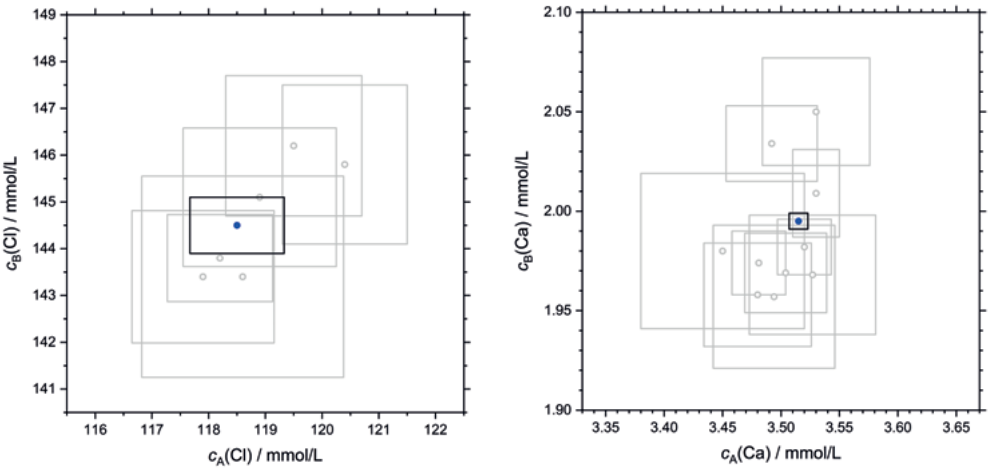

Figure 7: RELA 2018 comparison measurement. All participants were provided with serum samples on two different concentration levels (A and B). Results are visualized as so-called Youden-plots. PTB participated in the Cl and Ca measurements with the argentometric titration method and an ICP OES bracketing method, respectively.

[19]. PTB AG 3.11 has been participating in this comparison scheme since 2003, usually covering all electrolytes by applying the IC method, but sometimes also by applying primary methods. In the latest comparison "RELA 2018" the electrolytes Ca and Cl were measured by PTB using an ICP OES bracketing method with yttrium as an internal standard [5], [15] and an argentometric titration with exact matching and a potentiometric end-point determination [11], respectively. Figure 7 depicts the Cl and Ca results as so-called Youden-plots, demonstrating the successful outcome.

6. Outlook

In recent years, the ability to measure ions in human serum has been expanded to include the elements iron and copper and proven by successful participation in the CCQM key comparisons K107 [10] and K139 [11], respectively. Future work will cover especially toxic elements in human serum, but this requires the accurate measurement of much lower contents. The necessary efforts can be kept to a minimum since the Inorganic Analysis working group can draw on many findings gathered in the field of trace metal analysis in matrices other than human serum in the past two decades. This work will complement the analysis of toxic elements in fresh water [17] or pharmaceuticals [14], [22], two fields PTB is already involved in.

References

[1] Daniel C. Harris, *Quantitative Chemical Analysis*, W. H. Freeman and Company, New York, 1998

[2] Klaus Dörner (ed.), *Klinische Chemie und Hämatologie*, Ferdinand Enke Verlag, Stuttgart, 1999

[3] Deutsches Ärzteblatt, 2019; 116(51-52): A-2422 / B-1990 / C-1930

[4] Deutsches Ärzteblatt, 2014; 111(38): A-1583 / B-1363 / C-1295

[5] Olaf Rienitz, *Entwicklung chemisch-analytischer Primärmethoden zur Bestimmung physiologisch relevanter anorganischer Bestandteile in Humanserum*, PTB-Bericht, PTB-ThEx-19, Wirtschaftsverlag NW, Bremerhaven, 2001

[6] Rance A. Velapoldi, Robert C. Paule, Robert Schaffer, John Mandel, John R. Moody (eds.), *Standard Reference Materials: A Reference Method for the Determination of Sodium in Serum*, NBS Special Publications 260-60, 1978

[7] Ulf Örnemark, Yetunde Aregbe, Lutgart Van Nevel, Ioannis Papadakis, Philip D. P. Taylor, Adam Uldall, *CCQM-P14, Calcium in Serum, Final Report*, 2001

[8] Lutgart Van Nevel, Ulf Örnemark, Peggy Smeyers, Philip D. P. Taylor, *IMEP-17: Trace and Minor Constituents in Human Serum. Report to Participants*, EUR 20657 EN, 2003, https://ec.europa.eu/jrc/en/publication/eur-scientific-and-technical-research-reports/imep-17-trace-and-minor-constituents-human-serum-report-participants

[9] Lutgart Van Nevel, Yetunde Aregbe, Philip D. P. Taylor, *CCQM-K14: Calcium amount content in serum*, Metrologia 2004, 41 08003, https://doi.org/10.1088/0026-1394/41/1A/08003

[10] Heidi Goenaga Infante, *Final report for CCQM-K107: total elements and selenomethionine in human serum*, Metrologia, 2016, 53 08008, https://doi.org/10.1088/0026-1394/53/1A/08008

[11] Richard Shin, Fransiska Dewi, Benny Tong, Leung Ho Wah, David Saxby, Paul Armishaw, Veronika Ivanova, Liuxing Feng, Jun Wang, M Estela del Castillo Busto, Paola Fisicaro, Olaf Rienitz, Wai-Hong Fung, Michael Ho-pan Yau, Yong-Hyeon Yim, Mirella Buzoianu, Suleyman Z. Can, Betul Ari, Oktay Cankur, Heidi Goenaga Infante, Ramiro Pérez-Zambra, Elizabeth Ferreira, Stephen Long, W. Clay Davis, Regina A. Easley, *Elements in human serum—CCQM-K139*, Metrologia, 2018, 55 08006, https://doi.org/10.1088/0026-1394/55/1A/08006

[12] Joachim Weiß, *Ionenchromatographie*, Wiley-VCH, Weinheim, 2001

[13] Howard M. Kingston, Stephen J. Haswell (eds.), *Microwave-Enhanced Chemistry*, American Chemical Society, Washington, DC, 1997

[14] Anita Röthke, Volker Görlitz, Reinhard Jährling, Heinrich Kipphardt, Ralf Matschat, Silke Richter, Olaf Rienitz, Detlef Schiel, *SI-traceable monoelemental solutions on the highest level of accuracy: 25 years from the foundation of CCQM to recent advances in the development of measurement methods*, Metrologia, 2019, http://iopscience.iop.org/10.1088/1681-7575/ab5636

[15] Angela Kaltenbach, Janine Noordmann, Volker Görlitz, Carola Pape, Silke Richter, Heinrich Kipphardt, Gernot Kopp, Reinhard Jährling, Olaf Rienitz, Bernd Güttler, *Gravimetric preparation and characterization of primary reference solutions of molybdenum and rhodium*, Analytical and Bioanalytical Chemistry, 2015, 407, 3093-3102

[16] Karin Röhker, Olaf Rienitz, Detlef Schiel, *Ion chromatographic precision measurement procedure for electrolytes in human serum: validation with the aid of primary measurement procedures*, Accreditation and Quality Assurance, 2004, 9, 671–677

[17] Olaf Rienitz, Detlef Schiel, Bernd Güttler, Michael Koch, Ulrich Borchers, *A convenient and economic approach to achieve SI-traceable reference values to be used in drinking-water interlaboratory comparisons*, Accreditation and Quality Assurance, 2007, 12, 615–622

[18] Mike Sargent, Chris Harrington, Rita Harte, *Guidelines for Achieving High Accuracy in Isotope Dilution Mass Spectrometry (IDMS)*, Royal Society of Chemistry, Cambridge, MA, 2002, eISBN 978-1-84755-930-2

[19] http://www.dgkl-rfb.de:81

[20] https://www.bipm.org/kcdb/cmc/advanced-search?area=8

[21] Dieter Richter, Wolfgang Wöger, Werner Hässelbarth (eds.), *Data analysis of key comparisons*, PTB-Bericht, PTB-IT-10, Wirtschaftsverlag NW, Bremerhaven, 2003

[22] Anita Röthke, Janine Noordmann, Silke Richter, Heinrich Kipphardt, Matthias Weber, Olaf Rienitz, *Toxischen Elementen auf der Spur – Gravimetrische Herstellung und Charakterisierung SI-rückgeführter Monoelementlösungen*, GIT-Labor – Portal für Anwender in Wissenschaft und Industrie, 28.06.2019, https://www.git-labor.de/forschung/pharma-drug-discovery/toxischen-elementen-auf-der-spur

Assuring SI Traceable Measurement Results in Germany for Organic, Peptide and Protein Biomarkers

Gavin O'Connor[1], André Henrion[2], Claudia Swart[3], Cristian Arsene[4], Rüdiger Ohlendorf[5], Christine Brauckmann[6], Claudia Frank, Rainer Stosch[7], Bernd Güttler[8]

Abstract

The international comparability of measurement results can be achieved by anchoring these measurements to the international System of Units (SI). Both the mechanisms and infrastructure for achieving this in the area of clinical chemistry are relatively new when compared to those for physical measurements. For the past two decades, PTB has been comparing the equivalence of its clinical measurement services with those of other NMIs. The development of high accuracy isotope dilution methods has enabled the provision of accurate results, whereby, all contributions to the measurement uncertainty can be appropriately estimated. These methods have been applied to priority clinical biomarkers, assuring the results provided by the German clinical reference laboratories are fully SI traceable. This, in turn, ensures the reference methods and routine clinical laboratories produce "fit for purpose" measurements as defined by RiLi-BÄK.

Previously simple protein biomarkers were considered too complex for the application of the high accuracy methods developed by NMIs. Improvements in analytical technology combined with simpler protein expression systems that enabled the production of isotopically labelled peptides and proteins enabled these methods to be applied to this group of analytes for the first time. The developed methods enabled full traceability to the SI through a stepwise approach, whereby, protein-specific peptides can be used to determine the amount of protein present in a biological sample. These methods can be easily applied to simple proteins but alternative approaches using protein metal complexes, that could infer a protein's structural integrity are currently been investigated.

The metrology community has developed and compared their measurement services at the highest level for several important clinical markers. Greater effort is required to further disseminate these services, with the final goal of improving the comparability of patient measurement results on a continuous and global basis, for a broader range of biomarkers. If this is to become a reality much greater collaboration is required between the NMIs, reference laboratories, IVDD manufactures, and routine laboratories. This collaboration is essential if the benefits of metrological traceability are to be realised in full.

1. Introduction

Approximately 70 % of clinical decisions are based on results provided by *in-vitro* diagnostic tests [1]. Reliable test results are a prerequisite for medical diagnostics and, by law, must be based on internationally comparable standards [2]. Such traceability of clinical laboratory measurement results requires a concerted effort from many sectors if the benefits of comparable measurement results are to be realised [3].The patient and economic benefits of measurement traceability have been studied for a small number of important measurands, with the concluded cost benefits running into the hundreds of thousands of Euros per annuum for each [4]. Through initiatives like the Joint Committee on Traceability in Laboratory medicine (JCTLM) [5] and the International Consortium on Harmonisation in Clinical Laboratory Results (ICHCLR), National Measurement Institutes (NMIs), accreditation bodies, reference laboratories, laboratory proficiency testing (PT) providers, clinical laboratories and *in-vitro* diagnostic manufacturers

All authors: Division "Chemical Physics and Explosion Protection", Physikalisch-Technische Bundesanstalt Braunschweig

[1] Prof. Dr Gavin O'Connor, ORCID: https://orcid.org/0000-0002-7812-6717, email: gavin.oconnor@ptb.de

[2] Dr. Andre Henrion, ORCID: https://orcid.org/0000-0002-8444-640X, email: andre.henrion@ptb.de

[3] Dr. Claudia Swart, email: claudia.swart@ptb.de

[4] Dr. Cristian Arsene, ORCID: https://orcid.org/0000-0002-9963-5027, email: cristian-gabriel.arsene@ptb.de

[5] Dipl.-Ing.(FH) Rüdiger Ohlendorf, email: rudiger.ohlendorf@ptb.de

[6] Dr. Christine Brauckmann, email: christine.brauchman@ptb.de

[7] Dr. Rainer Stosch, ORCID: https://orcid.org/0000-0001-7694-5519, email: rainer.stosch@ptb.de

[8] Dr. Bernd Güttler, ORCID: https://orcid.org/0000-0001-8293-2773, email: bernd.guettler@ptb.de

are coordinating activities. A major aim of these services is to improve both the standardisation and harmonisation of patient results. Such combined efforts are essential if standardised reference ranges are to be agreed internationally, thereby enabling clinicians to form decisions from a consistent pool of data [6]. The availability of data with an assured quality is essential if the aspirations of personalised medicine and the use of artificial intelligence (AI) for clinical diagnosis are to be fully realised. The role of NMIs in these activities is essential. Where SI units are used, an NMI is responsible, not only for the primary realisation of the units but also for assuring the successful transfer of these to end users. For clinical chemistry this needs to be achieved in a "fit for purpose" style that does not over burden routine measurement laboratories, whilst at the same time ensuring a patient's measurement results are comparable, independent of where or when the measurements were obtained.

The International Committee for Weights and Measures (CIPM) is responsible for promoting the global uniformity of units. The CIPM Mutual Recognition Agreement (CIPM-MRA), which has been signed by representatives from over 100 countries, is the framework through which NMIs demonstrate the equivalence of their calibration and measurement service capabilities. Consultative Committees (CCs) organise comparisons whereby NMIs or Designated Institutes (DIs) benchmark the equivalence of their services. This results in internationally recognised, peer reviewed Calibration and Measurement Capabilities (CMCs) which are catalogued in the CIPM MRA databases. For chemical and biological measurements this work is performed in the working groups of the CC for Amount of Substance: Metrology for Chemistry and Biology (CCQM).

The German Medical Association has published guidelines (RiLi-BÄK)[7] containing the measurement ranges and maximum permissible measurement error for 93 priority measurands in blood, serum or plasma, which should not be exceeded by routine clinical laboratories. To assure the labs are operating within these legal limits they must participate in a recognised proficiency testing (PT) scheme within the framework of the external quality control of the German Medical Association [7]. Where a reference method is available, this is used to assign the target value to the PT materials which is used in assessing if a laboratory is performing as obliged. The *in-vitro* diagnostic testing devices (IVDD) used within a clinical laboratory are often supplied by an external provider complete with the reagents and calibrators required for the measurement. Regulation (EU) 2017/746 requires that calibrators provided with these IVDD must have a statement on the metrological traceability of the calibrators[2]. This metrological traceability can be obtained from certified reference materials (CRM) or reference measurement procedures. To help IVDD manufactures meet these requirements the JCLTM reviews and curates a database of materials, reference procedures and reference laboratories which have the relevant accreditation and experience to provide these services. These reference laboratories also participate in the International Federation for Clinical Laboratory Medicine (IFCC) external quality control for reference laboratories (RELA) PT schemes, organised by the German Referenzinstitut für Bioanalytik (RfB). PTB plays an important role in providing SI traceable reference points assuring "fit for purpose" results are produced by German clinical reference and testing laboratories (Figure 1).

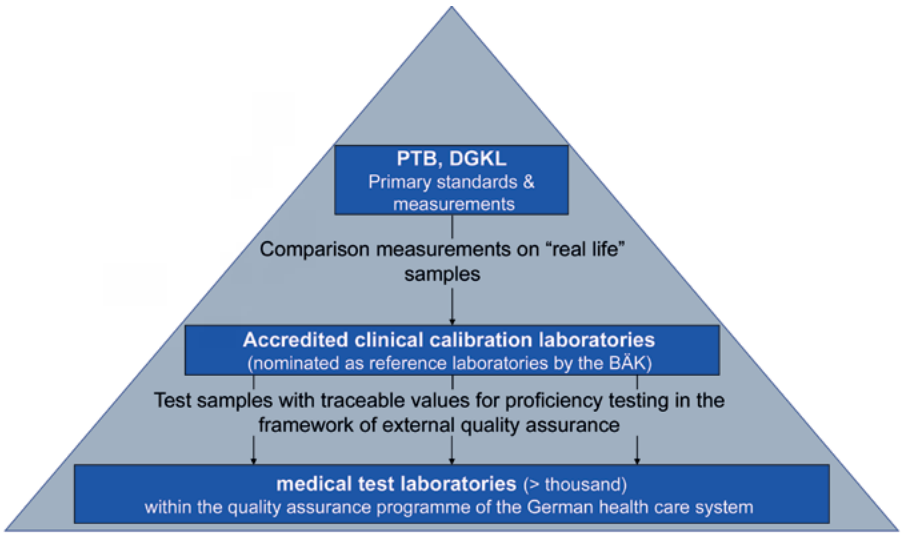

Figure 1
Measurement hierarchy for well-defined molecules in clinical laboratory medicine in Germany.

2. Small organic molecules of clinical relevance

The molecules covered by the Organic Analysis Working Group (OAWG) of the CCQM from the RiLi-BÄK list and their reference ranges are shown in Figure 2. To cover the wide range of different priority measurands for clinical chemistry, in terms of molecular complexity and their concentrations ranges in biological fluids is challenging. Enabling comparability, both within a single country and between different countries would take a huge amount of an NMI's resources, if key comparison were to be required for every measurand. A more pragmatic approach, whereby NMIs could prove general competence that could be extended to a wider range of measurands was required.

The (OAWG) of the CCQM is responsible for designing and organising studies to assess the CMCs claimed by NMIs for well-defined molecular entities in different matrices [8]. Although the group was established in 1995 it did not complete its first Key comparison (KC) study in the clinical area until 2000. From the outset, CCQM made a requirement that, where possible, NMIs participate in studies using a primary method of analysis. The definition of a primary method was agreed at the first meeting of the CCQM in 1995. "*A primary method of measurement is a method having the highest metrological qualities, whose operation can be completely described and understood, for which a complete uncertainty statement can be written down in terms of SI units, and whose results are therefore, accepted without reference to a standard of the quantity being measured*". It was also concluded that for the application of this general description to chemical measurements the following requirements would also have to be met. "*Measurements of amount of substance, to be considered primary, must be made using a method which is specific for a defined substance and for which the values of all parameters, or corrections which depend on other species or the matrix, are known or can be calculated with appropriate uncertainty*". From this it was concluded that: isotope dilution with mass spectrometry (IDMS); coulometry; gravimetry; titrimetry; and the determination of freezing point depression; all had the potential to be primary methods. Therefore, NMIs with an interest in clinical measurements had to develop IDMS methods for determining the mass fraction of the specific measurand in biological fluids.

At PTB, an active research programme already existed for developing IDMS methods. The exact matching approach, first described by Henrion [9] formed the basis for most IDMS methods applied by NMIs for clinical measurements. The approach requires: a pure substance reference material of the target analyte to be studied; an isotopically labelled analogue of the same substance; gravimetric preparation of, fully equilibrated, sample and calibration mixtures; and finally, precise, interference free isotope ratio measurements. A pictorial depiction of the exact matching IDMS method is shown in Figure 3, along with the reduced form of the organic IDMS equation. The procedure involves the preparation of sample and calibration blends or mixtures, containing both the natural and labelled molecules of interest. The interference free measurement of the isotope amount ratios in both blends enables the amount

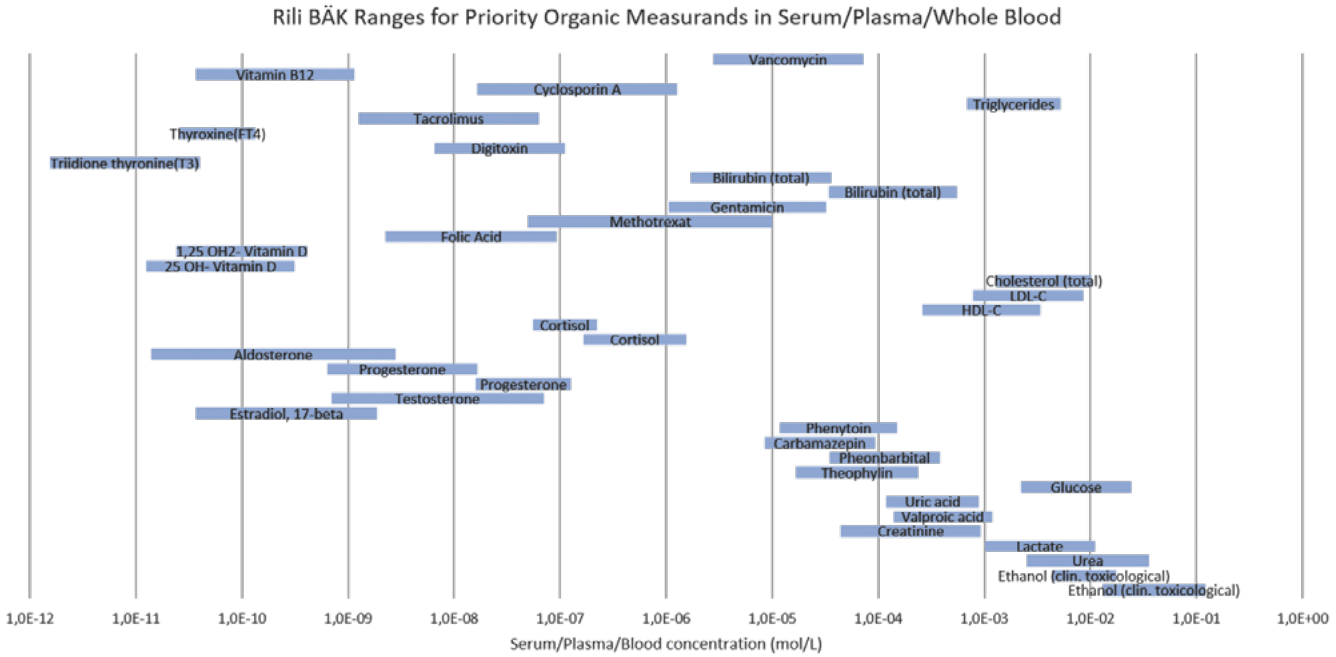

Figure 2: Reference ranges for priority small organic molecules as stated by RiLi-BÄK.

of substance concentration in the sample to be determined. The measurement results are fully traceable to the SI by using a pure substance CRM of known purity and the gravimetric preparations of the blends and calibration standards. The exact matching criteria are reached when the measured ratio of the natural and labelled analyte signals in the calibration and sample blends is equal and the ratio of ratios between sample and calibration blends reaches unity. Under these conditions the gravimetrically prepared amount-of-substance concentration in the primary calibrator can be transferred to the sample via a fixed equation, where all components can be described in terms of SI units and a full uncertainty estimate assigned. Therefore, in terms of the final measurement, this approach meets the requirements of a primary method as requested by the CCQM.

An initial set of studies were chosen for the clinical sector that would help build confidence that the different participant institutes had the required skills to perform all aspects of the IDMS procedures and appropriately assess, estimate and combine all required components of the measurement uncertainty. A suite of three studies, each containing two different samples covering the clinical range of interest for each measurand, was selected. The measurands were chosen based on several criteria including the requirement that pure substance reference materials and isotopically labelled analogues needed to be readily available worldwide. Also, while the IDMS methods had the potential to reduce many of the errors, the first set of studies were particularly chosen as they had extra challenges where interferences, non-equilibration or incomplete conversion from the measurand to the analytical target would cause a bias if not appropriately addressed. For these reasons, creatinine, glucose and total cholesterol were chosen as the initial set of clinical comparisons by the OAWG. CCQM KC studies are governed by strict rules and result in a permanent record of degrees of equivalence for each participating institute. Therefore, in the late 1990s pilot studies were performed for each measurand. During this period each institute developed their IDMS methods and made many presentations on their procedures and their approach to estimating the measurement uncertainty.

The first KC was reported for cholesterol in serum in 2000 and for creatinine and glucose in serum in 2001. All three molecules are on the list used for general blood screening. Cholesterol is an important biomarker in estimating a patient's risk of developing heart attacks, creatinine is used as an indicator of kidney function and elevated glucose levels can indicated a wide range of medical issues. These three measurands have become the basic

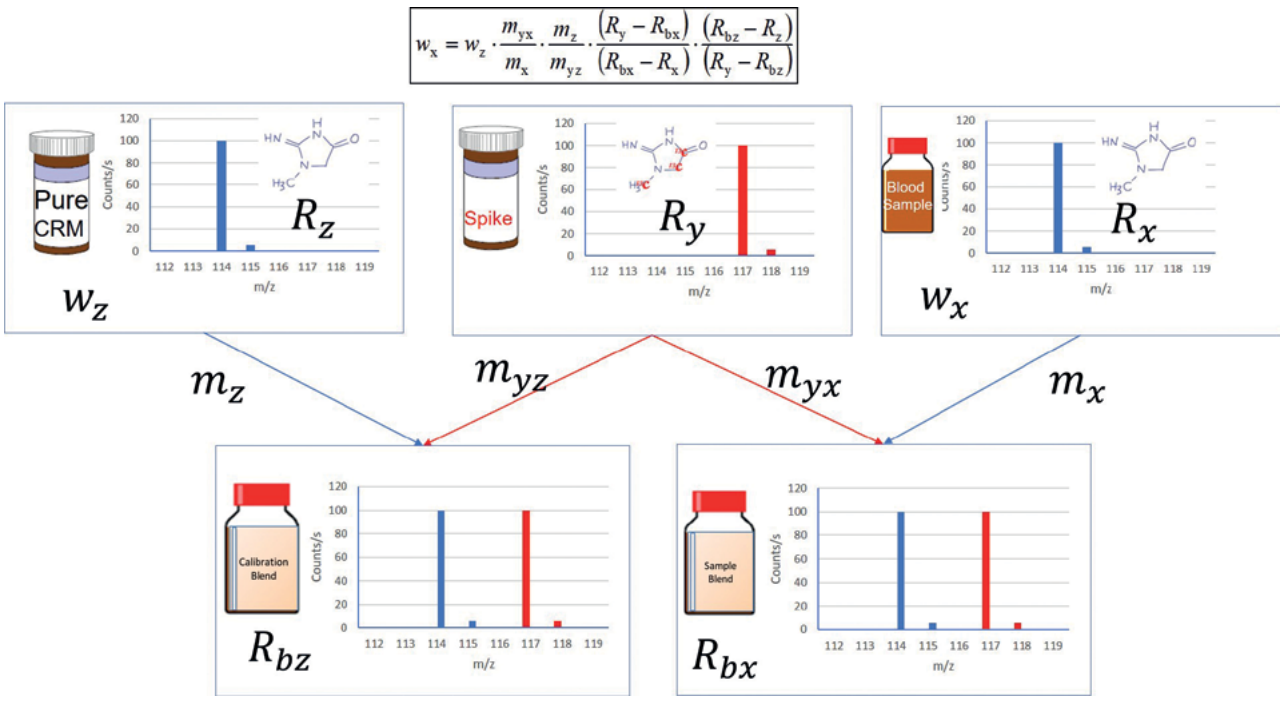

Figure 3:
Schematic diagram of the principle of exact matching IDMS. Where, w_x is the unknown amount-of-substance concentration of the measurand in the sample; w_z, is the gravimetrically prepared amount-of-substance concentration of the measurand in the calibration standard; m_z is the mass of the calibration standard used to prepare the calibration mixture; m_{yz} is the mass of the isotopically labelled spike solution used to prepare the calibration blend; m_{yx} is the mass of the isotopically labelled spike solution added to the sample blend; m_x is the mass of the sample used to make the sample blend; R_y is the isotope ratio of the isotopically labelled material; R_x is the isotope ratio of the natural molecule in the sample; R_z is the isotope ratio of the natural molecule in the calibration material; R_{bz} is the isotope ratio of the calibration blend; R_{bx} is the isotope ratio of the sample blend.

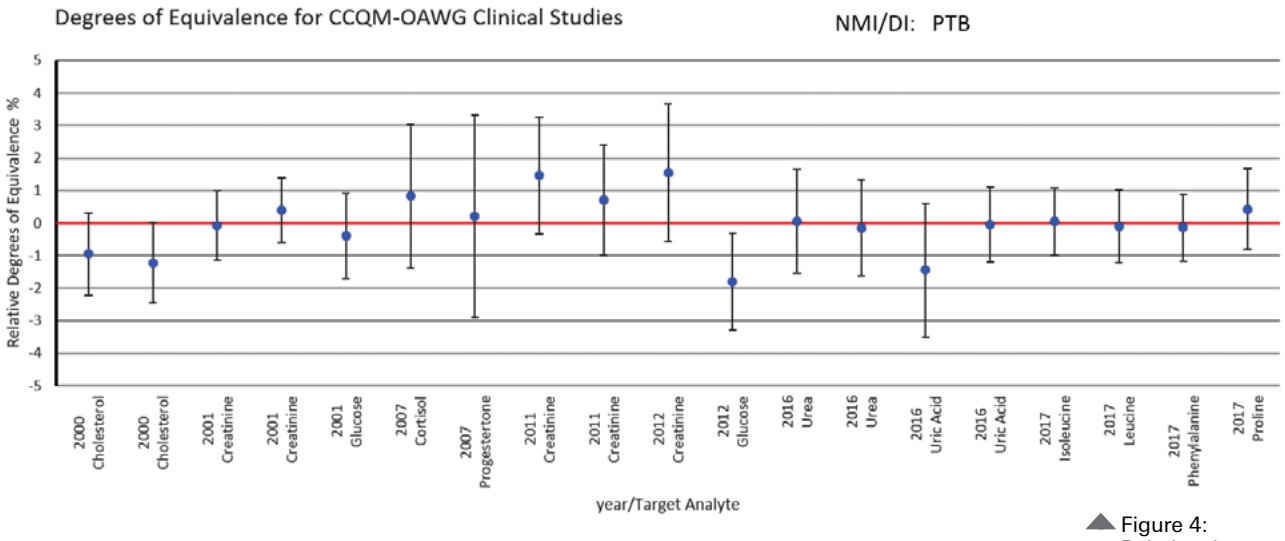

Figure 4:
Relative degrees of equivalence ($[X_{ptb}-X_{ref}]/X_{ref}$) % with their associated expanded uncertainties (95 %) recorded by PTB in CCQM OAWG clinical key comparison studies between the year 2000–2017.

benchmarks for NMIs and DIs offering services in clinical chemistry. They have been repeated many times over the last two decade (Creatinine: 2010, 2012; Glucose: 2005, 2012; Cholesterol: 2012) enabling more established institutes to prove equivalence over time and acting as ideal studies for new institutes starting a clinical programme for the first time. As well as repeating these initial studies, the OAWG identified other areas where NMIs had CMCs or services. For many of these other molecules, participation in these initial studies did not provide enough practical evidence to support these claims, as the measurement challenges were considered different. An example of this was in the area of steroid and vitamin analysis where the clinical levels were much lower than those previously studied. Therefore, in 2007-2008 three KC studies targeting steroids were completed.

On completion of a KC a reference value (KCRV) is calculated, along with its associated uncertainty. The degree of equivalence (DoE) for each institute is simply the difference between the labs reported result and the KCRV. The expanded uncertainty for the DoE is also calculated by combining the standard uncertainties from the KCRV with the individual labs reported standard uncertainty, in quadrature and expanding this with a coverage factor (normally k=2) to give a 95 % confidence level. These can be reported in relative terms (%DoE) and can be used to indicate an institutes performance for different measurands over a wide range of concentrations. The relative DoE (%DoE) obtained by PTB from the relevant OAWG key clinical studies for serum and aqueous standards is shown in Figure 4. For this period the

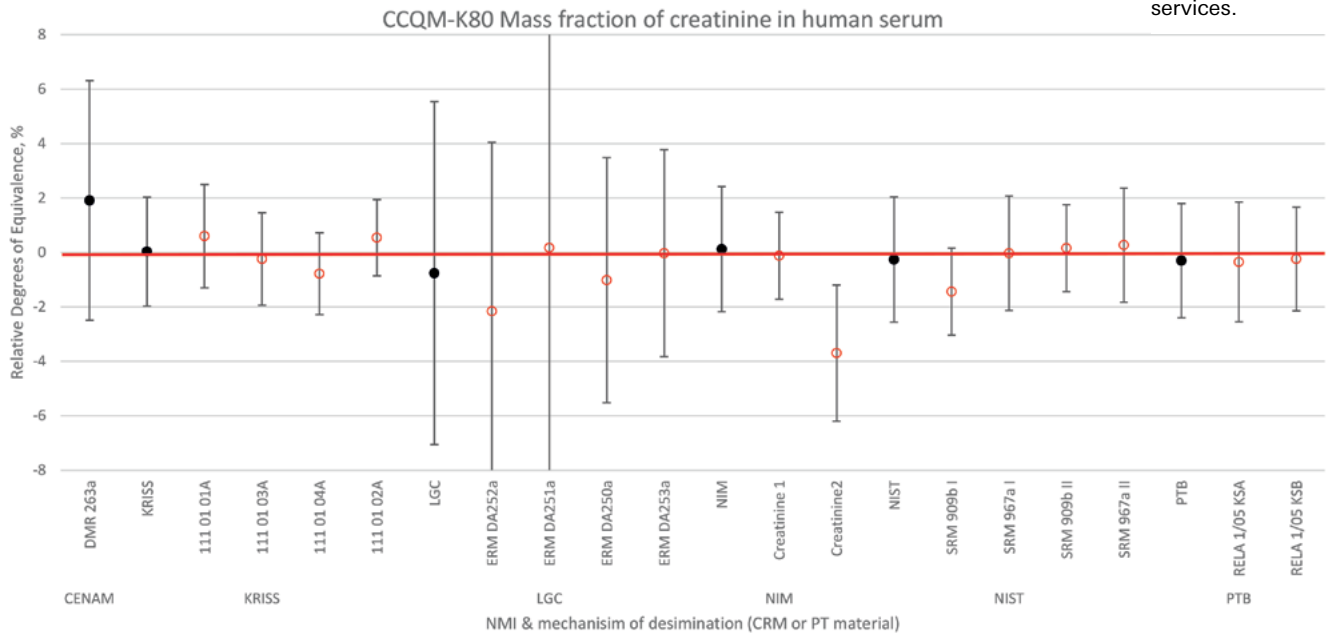

Figure 5:
Relative degrees of equivalence for individual CRMs and PT samples assigned by NMIs (red dots) and an overall calculated DoE% for each NMI (Black dots) used by NMIs in the dissemination of services.

average absolute %DoE for PTB was 0.6 % with an average expanded uncertainty of 1.5 %. The studies ranges were from 10 nmol/L (progesterone in serum) to 2 mmol/L (cholesterol in serum) which is consistent with the current services offered and CMCs held by PTB.

NMIs and DIs may choose to disseminate their services in many ways. Some chose to produce CRMs which are characterised using approaches which have been validated by participation in KC of the OAWG. Others provide reference measurement services performed on request. In order to validate the equivalence of these routes of dissemination, an alternative approach to assess NMIs' services has also been used by the OAWG. Where NMIs are providing services for the same measurand using CRMs or providing reference values for PT materials, a simple comparison study can be run via a single experiment on the same instrument at the same time in one NMI. This is achieved by all NMIs sending their CRMs or PT samples to a central coordinating lab for measurement. The coordinating NMI uses a precise method which has a proven linear range for the study materials. Simple linear regression models are then used to establish the best fit between the values assigned by the CRM producing NMI and the linear fit. The results for such a study, for creatinine in serum CRMs and a PT material characterised by PTB, are shown in Figure 5.

PTB determines reference values for the IFCC RELA inter-comparisons in order to provide SI traceability to German reference laboratories and also a large number of clinical reference laboratories on a global scale simultaneously. Since these reference laboratories are used to set the target values for German clinical PT schemes this is also the most effective way to provide SI traceability to the very large number of testing laboratories in Germany. Agreement between the PTB value and those from the German reference laboratories assures that full traceability to the SI has been demonstrated. These reference laboratories assign the target values by which routine clinical laboratories are assessed. The agreement demonstrated for a series of creatinine in serum ring trials, performed in 2005, 2010 and 2018 shows the agreement achieved between PTB and the German reference laboratories, in Figure 6.

Several factors have changed over the two decades that PTB has been providing these services. At the outset, the availability of isotopically labelled molecules was limited to a small number of materials. Also, the high-resolution mass spectrometers, required to provide precise and specific isotope ratio measurements, were normally coupled with gas chromatographic separation and were expensive and considered difficult to use. The pace of developments in MS instrumentation has resulted, not only in improved precision, higher resolution and direct interfacing of liquid chromatography, but also their increased use in reference laboratories. This in turn has fuelled the market for isotopically labelled materials resulting in the ready availability of a much wider range of molecules. Early studies also highlighted the need for pure substance reference materials characterised via methods providing measurement results fully traceable to the SI. Although not covered in this report, this requirement still proves challenging for the wide range of small complex biological molecules required.

Figure 6: Relative degree of equivalence for creatinine in serum observed between the result obtained by PTB and the two German clinical reference laboratories from 2005 to 2018 when participating in IFCC-RELA PT studies.

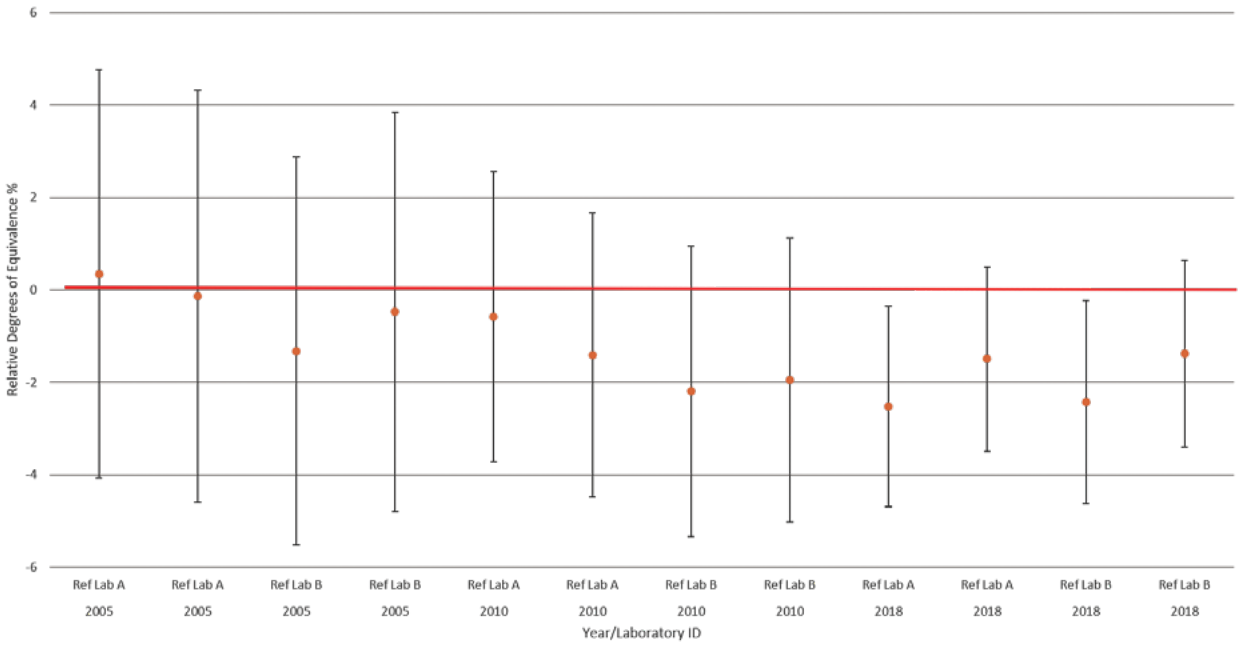

3. Extending the approach to peptides and proteins

There are a large group of clinical measurands where SI traceable measurement results are simply not achievable. This can result from the measurand being poorly defined or the molecule being so complex that measurement approaches do not meet the criteria of a "primary method". When the OAWG was established this set of measurands included all protein biomarkers of clinical interest. In 2003, PTB, LGC and NIST were asked to devise a strategy for providing SI traceable results for simple proteins. It was requested that, if possible, the methods selected should be capable of providing SI traceable measurement results for proteins in biological fluids in the future.

The direct application of IDMS to intact proteins is complicated by several practical realities. The MS analysis of intact proteins is only possible via electrospray ionisation (ESI) or matrix assisted laser desorption ionisation (MALDI). ESI of intact proteins normally results in the addition of multiple protons to the protein molecule thereby separating the signal across many channels (m/z) in the mass spectrometer. MALDI requires the isolation, purification and matrix preparation of the protein prior to analysis. The variability of signal intensity, due to matrix inhomogeneity, results in poor quantitative measurements. These sensitivity issues aside, the number of carbons in the average protein yields a mixture of isotopologues where the monoisotopic form of the molecule is rarely observed or is present at very low abundance. Isotopically labelled recombinant proteins were and are very costly, as are the natural isotopic composition pure proteins in the quantity needed to produce a fully characterised calibrator. Therefore, a stepwise approach was suggested, whereby proteins were digested to their constituent peptides. If specific peptides were found to be unique to the target protein and the protein could be digested completely to yield equimolar quantities of the peptides, these could be used to derive the amount of initial protein present [10]. The emerging field of proteomics had fuelled the development of LC-MS/MS instruments that could readily separate and selectively detect peptides. The relevant peptides could be synthesised and purified so that the amount of substance of each amino acid could be used to determine the amount of peptide initially present. Also, isotopically labelled peptides, where the choice and number of atoms to be labelled can be chosen, could be specified and synthesised. This stepwise approach established the required unbroken chain from amino acids of known purity, through specific peptides to the amount of protein present. A schematic diagram of the approach is shown in Figure 7.

Although simple in concept, the devised approach required proof that: peptides could be purified and fully characterised with the required uncertainty to be used a calibrators; that digestion methods could be developed to fully release equimolar amounts of peptides; that proteins and peptides were stable during the complete extraction and digestion procedures. For this initial work human growth hormone (hGH) was selected as an example protein. Originally the higher order standard for hGH was a pituitary extract and was assigned in non-SI traceable international units (IU). All following preparations of the standard were compared to the previous isolated material until a recombinant protein was provided. PTB and LGC assessed the selection of specific stable peptides and developed digestion methods for their equimolar release. At the time, the most quantitative proteomic methods used a generic 8 to 16-hour tryptic digestion protocol. The systematic study of enzyme to substrate ratio and multiple additions of enzyme over a prolonged time course revealed that, when using conventional protocols, peptides were still being released after 36 hours of digestion and that these curves differed greatly depending on peptide position in the protein and the protein being studied. The initial study concluded in a bilateral comparison determining the concentration of hGH in a calibration solution via four separate peptides [11]. The results of this initial study are shown in Figure 8. These approaches have been further refined and the digestion methods have been proven to work in biological matrices enabling the direct analysis of hGH in serum [12–15]. These initial studies enabled the fully SI traceable quantification of proteins in serum for the first time and form the basis for inter-comparisons between NMIs.

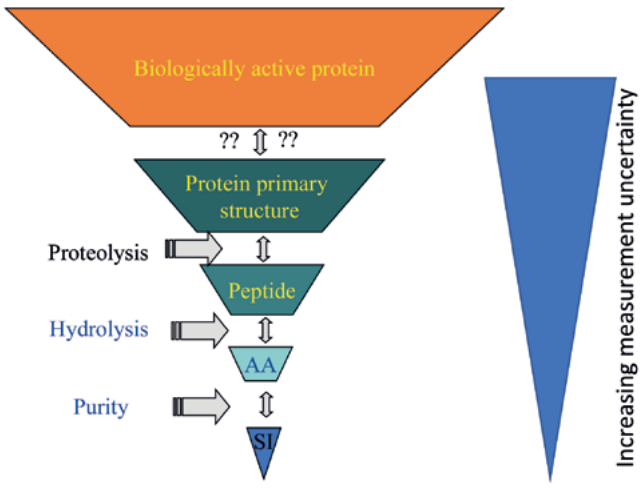

Figure 7: Schematic diagram for the provision of traceable measurement results for the quantification of proteins.

The initial cost constraints concerning the manufacture of isotopically enriched proteins has somewhat subsided over the years. Therefore, more recent approaches using IDMS for the quantification of proteins have used isotopically labelled protein internal standards [16]. However, careful consideration into how the recombinant protein is equilibrated within the natural samples is required, if accurate measurement results are to be obtained. PTB has successfully used these approaches for collaborations with the IFCC working group on haemoglobin variants (HbA2) [17], cystatin C [18], C-reactive protein and in assessing the suitability of reference materials for the calibration of hGH antibody-based testing methods [15].

The peptide-based IDMS methods have proven capable for the direct quantification of a total specific primary sequence of a protein in serum. While this is of considerable benefit, it provides little information on the heterogeneity of the molecule caused by post translational modifications, or on the secondary, tertiary or quaternary structure of the protein that may be essential for biological activity. Metals play an important role in protein structure and function. They can be covalently bound to other organic molecules (e.g. heme group), non-covalently bound or simple trapped within the protein structure. An alternative approach for the quantification of intact protein molecular assemblies is via the quantification of protein bound/associated metals that have a known stoichiometric ratio to the total protein amount present. For this approach to be successful the intact protein molecular assembly must be isolated and separated from other proteins that contain the same element, before the accurate amount concentration of the selected element is determined. To achieve this, PTB has investigated the coupling of advanced separation science with the element specific detection of inductively coupled plasma mass spectrometry (ICP-MS) [19]. For a purified protein, the direct quantification of the metal content via elemental IDMS may yield accurate results. However, for complex biological samples the incorporation of the isotopically enriched element into the protein target is more beneficial. This enables species specific IDMS and if the isotopically enriched protein assembly can be equilibrated with the natural protein, the full advantages of molecular specific IDMS can be achieved. As a proof of principle exercise, this approach was applied to the quantification of total haemoglobin in blood [20]. This is an important health status marker where the current reference method does not yield measurement results that are fully SI traceable. The developed method used a heme group enriched with ^{57}Fe or ^{54}Fe, which had been fully incorporated into the tetrameric structure of haemoglobin. The isotopically enriched protein was added to the blood sample and the natural and enriched protein were chromatographically separated from the matrix before being completely atomised and ionised in the ICP. A comparison of the results obtained from different IDMS procedures using elemental and peptide-based approaches with that of molecular signals from isotope dilution Raman spectroscopy (IDRS) are shown in Figure 9. The advantage of this is that the resulting elemental signals are much less complex then those provided by organic mass spectrometry instruments and if these can be obtained, interference free, the basic principles of IDMS can be used to yield measurement results whereby full traceability to the SI can be achieved. These approaches are being extended to investigate a wider group of elements including amino acid specific sulfur, non-covalently bound metal tags and naturally occurring metals.

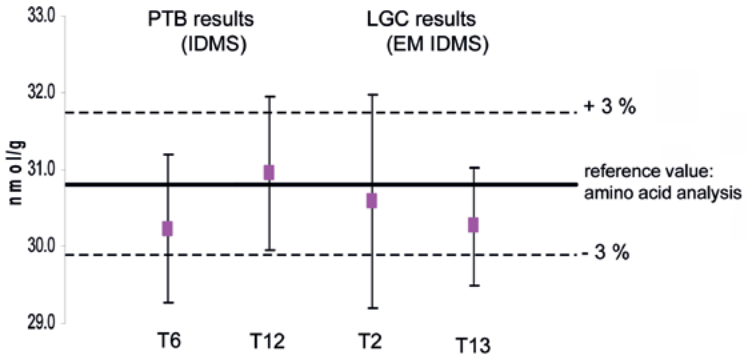

Figure 8:
Comparison of peptide based IDMS results obtained for four hGH peptides in different NMIs.

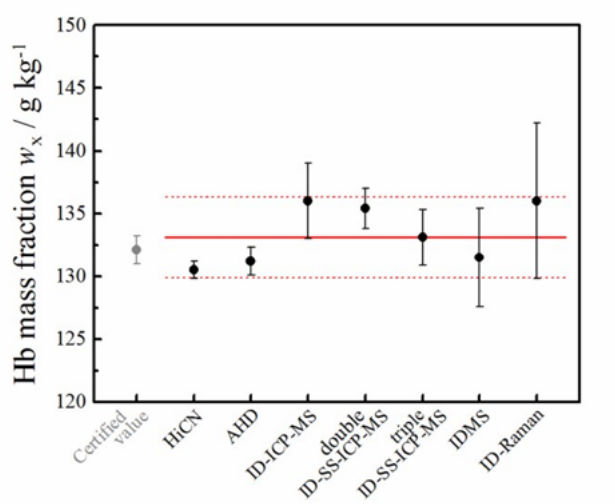

Figure 9:
Determined mass fraction of haemoglobin as determined by IDMS based reference methods

These IDMS approaches are now becoming more established within the metrology community, with many NMIs developing these capabilities. In 2014, the CCQM established a specific protein analysis working group to design a set of studies to benchmark the current services of the NMIs in this area. As would be expected, clinical biomarkers are a high priority for this working group. To date, the group's activities have concentrated on the purity assessment of peptide standards and the value assignment of primary calibrators [4]. KCs have already been completed in this area and the BIPM has developed a strategic plan to address the required studies to demonstrate the equivalence of services in this area. An initial set of matrix studies are currently at the pilot stage. PTB is coordinating two pilot studies on haemoglobin in blood and hGH in serum, with the results due to be reported in 2020. The successful outcome of these pilot studies will result in commencing the first protein related KCs enabling the global equivalence of these measurands to be realised for the first time.

4. Beyond current capabilities

The issues of providing traceability for protein biomarkers has been hampered from the outset by several factors. One of the very first requirements in achieving measurement traceability is having a full and detailed knowledge of the measurand (the quantity intended to be measured). On discovering a clinical biomarker, the output from a measurement response is often correlated with the traits of disease or a biological activity. This response may be attributed to a specific protein (as identified by its primary protein sequence) but may equally be attributed to a group of similar molecules or modified forms of the same primary sequence. However, the gap between what is the subject of measurement (analytical target) and the measurand is often forgotten (i.e. has no uncertainty contribution associated with it) or is not well understood. This sometimes leads to a "chicken and egg" type quandary whereby in order to get a greater understanding of a biomarker you need more comparable measurements across a greater population. However, more accurate measurements may require a better understanding of the biomarker for metrological principles to be applied to the measurements. The IU for protein measurements were established to deal with complex biomolecules that could not be fully characterised by physical methods. However, the pace of development of modern instrumentation has resulted in a greater understanding of the specific biomarkers of interest and, thus, in reference methods that meet the criteria of providing SI traceable results being applied to reference materials assigned in IU. This will continue to be a subject of much debate over the coming years and the benefits of metrological traceability will need to be proven to the broader biologicals' community. However, the role of NMIs in finding new approaches for the quantification of protein structural/function measurement will continue to shed light on this debate and at the very least aid in the better description of the measurand. PTB has active research programmes in developing new methods for the quantification of biological complexes and protein-protein interactions [22].

5. Plans for immediate future

After two decades of CCQM activities, having completed 14 key comparisons covering 13 different measurands of relevance to the clinical sector, PTB has proven the equivalence of the services that it provides to the German reference laboratory network, at the highest level. Initially CMCs were limited to "like-for-like" claims, whereby participation in a specific KC resulted in a specific claim for the measurand and range covered. Future studies are now designed to cover a much broader range of claims. This will enable an NMI to base their evidence for a specific claim on participation in several KCs that addressed the quantification of different measurands. The initial set of studies were designed to gain confidence that an NMI had the required skills, not to run a routine method of analysis, but to define the research project required to ensure fully traceable measurement results could be obtained from the IDMS procedures as applied in their institute. The collected evidence will enable PTB to work with the German reference laboratories to select priority measurands and broaden the range of services to address the increasing list of molecules requested by RiLi-BÄK.

The issue of the availability of pure primary calibrators from NMIs, which are essential to support CMCs continues to cause concern. Quantitative nuclear magnetic resonance (NMR) spectroscopy offers an approach to provide the traceability and low uncertainties required for the primary calibration standards. PTB will investigate approaches for the provision of pure substance reference materials to support the expanding range of measurands required.

Clinical laboratory medicine is not only a medical necessity but a global industry. The anchoring of results to the SI ensures a level playing field for all IVDD manufacturers. It also stimulates innovation as new testing methods are compared to the "true" amount of substance present and not to any observable difference to older competing technologies. Finally, if a patient's clinical laboratory results are to be used

to inform models for AI or personalised medicine, it is essential that all data used to inform these models are comparable. The current SARS-CoV-2 crisis is a good example, at the highest level, that highlights the importance of accurate and worldwide comparable results for this purpose. SI traceable results is a mechanism whereby this can be achieved.

References

[1] https://www.bivda.org.uk/The-IVD-Industry/The-Value-of-IVDs. BIVDA (The IVD technologies industry body) UK. The Value of IVDs

[2] REGULATION (EU) 2017/746 OF THE EUROPEAN PARLIAMENT AND OF THE COUNCIL of 5 April 2017 on in vitro diagnostic medical devices and repealing Directive 98/79/EC and Commission Decision 2010/227/EU. http://data.europa.eu/eli/reg/2017/746/2017-05-05

[3] Vesper HW, Thienpont LM (2009) Traceability in laboratory medicine. Clinical chemistry 55(6):1067–1075

[4] David P Leech (2000) The Economic Impacts of NIST'S Cholesterol Standards Program. 00-4 Planning report

[5] Armbruster D, Miller RR (2007) The Joint Committee for Traceability in Laboratory Medicine (JCTLM): A Global Approach to Promote the Standardisation of Clinical Laboratory Test Results. The Clinical Biochemist Reviews 28(3):105–114

[6] Panteghini M, Braga F (2020) Implementation of metrological traceability in laboratory medicine: where we are and what is missing. Clinical chemistry and laboratory medicine

[7] www.bundesaerztekammer.de/rilibaek2019

[8] Teo TL, Lippa KA, Mackay L, Yong S, Liu Q, Camara JE, Delatour V, Lee TK, Lalere B, O' Connor G, Henrion A, Kato M, Numata M, Kwon H-J, Jeong J-S, Xu B, Song D, Nammoonnoy J, Wollinger W (2019) Enhancing the accuracy of measurement of small molecule organic biomarkers. Analytical and bioanalytical chemistry 411(28):7341–7355

[9] Henrion A (1994) Reduction of systematic errors in quantitative analysis by isotope dilution mass spectrometry (IDMS): an iterative method. Fresenius J Anal Chem 350(12):657–658

[10] Burkitt WI, Pritchard C, Arsene C, Henrion A, Bunk D, O'Connor G (2008) Toward Système International d'Unité-traceable protein quantification: from amino acids to proteins. Analytical biochemistry 376(2):242–251

[11] Arsene CG, Ohlendorf R, Burkitt W, Pritchard C, Henrion A, O'Connor G, Bunk DM, Güttler B (2008) Protein quantification by isotope dilution mass spectrometry of proteolytic fragments: cleavage rate and accuracy. Analytical chemistry 80(11):4154–4160

[12] Wagner IV, Paetzold C, Gausche R, Vogel M, Koerner A, Thiery J, Arsene CG, Henrion A, Guettler B, Keller E, Kiess W, Pfaeffle R, Kratzsch J (2014) Clinical evidence-based cutoff limits for GH stimulation tests in children with a backup of results with reference to mass spectrometry. European journal of endocrinology 171(3):389–397

[13] Arsene C, Schulze D, Röthke A, Thevis M, Henrion A (2018) Growth hormone isoform-differential mass spectrometry for doping control purposes. Drug testing and analysis 10(6):938–946

[14] Arsene CG, Schulze D, Kratzsch J, Henrion A (2012) High sensitivity mass spectrometric quantification of serum growth hormone by amphiphilic peptide conjugation. Journal of mass spectrometry: JMS 47(12):1554–1560

[15] Boulo S, Hanisch K, Bidlingmaier M, Arsene C-G, Panteghini M, Auclair G, Sturgeon C, Schimmel H, Zegers I (2013) Gaps in the traceability chain of human growth hormone measurements. Clinical chemistry 59(7):1074–1082

[16] Pritchard C, Groves KJ, Biesenbruch S, O'Connor G, Ashcroft AE, Arsene C, Schulze D, Quaglia M (2014) Quantification of human growth hormone in serum with a labeled protein as an internal standard: essential considerations. Analytical chemistry 86(13):6525–6532

[17] Arsene CG, Kaiser P, Paleari R, Henrion A, Spannagl M, Mosca A (2018) Determination of HbA2 by quantitative bottom-up proteomics and isotope dilution mass spectrometry. Clinica chimica acta; international journal of clinical chemistry 487:318–324

[18] González-Antuña A, Rodríguez-González P, Ohlendorf R, Henrion A, Delatour V, García Alonso JI (2015) Determination of Cystatin C in human serum by isotope dilution mass spectrometry using mass overlapping peptides. Journal of proteomics 112:141–155

[19] Gleitzmann J, Raab A, Schulze D, Wätzig H, Feldmann J, Swart C (2016) Accurate and precise quantification of Cu,Zn-SOD in human red blood cells using species-specific double and triple IDMS. J. Anal. At. Spectrom. 31(9):1922–1928

[20] Frank C, Brauckmann C, Palos M, Arsene CG, Neukammer J, Del Castillo Busto ME, Zakel S, Swart C, Güttler B, Stosch R (2017) Comparison of potential higher order reference methods for total haemoglobin quantification-an interlaboratory study. Analytical and bioanalytical chemistry 409(9):2341–2351

[21] Josephs RD, Martos G, Li M, Wu L, Melanson JE, Quaglia M, Beltrão PJ, Prevoo-Franzsen D, Boeuf A, Delatour V, Öztug M, Henrion A, Jeong J-S, Park S-R (2019) Establishment of measurement traceability for peptide and protein quantification through rigorous purity assessment—a review. Metrologia 56(4):44006

[22] Henrion A (2013) Integrating chemical cross-linking with mass spectrometric analysis of peptides and proteins. In: Farkas E, Ryadnov M (eds) Amino Acids, Peptides and Proteins, vol. 38. Royal Society of Chemistry, Cambridge, pp 151–171

Quantitative Magnetic Resonance Imaging

Christoph Kolbitsch[1], Sebastian Schmitter[2], Tobias Schaeffter[3]

Abstract

Magnetic Resonance Imaging (MRI) is a widely used medical imaging modality. Due to its excellent soft tissue contrast, it is often used in brain imaging but also for many other applications such as cardiovascular imaging or tumour diagnosis. The majority of MRI scans provide qualitative images, where the contrast (i.e. the difference in signal intensity) between healthy and diseased tissue is used for diagnosis. Quantitative MRI on the other hand provides physical (e.g. relaxation times) and biophysical parameters (e.g. blood flow velocities, blood perfusion), which can be used for an objective assessment of pathologies. Quantitative MRI does not depend on hardware or acquisition related parameters, making it much easier to combine data from multiple hospitals in multi-centre studies and allowing for monitoring of disease progression or treatment outcome.

PTB is working on novel techniques in order to ensure that the full potential of quantitative MRI can be utilised for patient care. We have developed novel signal models to provide more accurate measurements and ensure negative effects during data acquisition (e.g. breathing motion of the organs) are taken into consideration to minimize measurement errors. In addition, we have combined quantitative parameter estimation with statistical approaches in order to be able to assess not just the biophysical quantities but also their uncertainty. Finally, we are also working on novel hardware designs to ensure best possible measurement quality.

1. Introduction

Medical imaging is the backbone of modern clinical diagnosis. More than 5 billion imaging investigations are performed worldwide each year. Medical imaging modalities today can acquire morphological information with high spatial resolution in a relatively short time. This technical progress has led to the current radiological practice to make decisions based on visual inspection of images and to rate diseases in qualitative terms. Over the last decade significant effort has been made to transform medical imaging from qualitative to quantitative measurement of biophysical properties. Quantitative medical imaging offers the possibility for objective diagnosis based on well-defined reference values rather than interpretation-based assessment of image intensity changes. Especially for the current development of automated medical image assessment, quantitative imaging will play an important role to enable more reproducible diagnosis. This is supported by the two largest societies in this field. The Radiology Society of North America (RSNA) have organized the Quantitative Imaging Biomarkers Alliance (QIBA) and the European Society for Radiology (ESR) have started the European Imaging Biomarkers Alliance (EIBALL), which are both committed to making medical imaging a more quantitative science.

The trend of quantitative imaging holds especially for Magnetic Resonance Imaging (MRI), which is a widely used medical imaging modality providing excellent soft tissue contrast. The image contrast of MRI depends on wide range of intrinsic tissue properties such as the density of hydrogen nuclei (spin density ρ) and the interaction of nuclear spins with the magnetic field (relaxation times T_1 and T_2)[1]. The image contrast is also determined by acquisition specific parameters, such as the timing of data acquisition (e.g. echo and repetition times), the order of magnetic field gradients and radiofrequency-pulses (so-called MR sequences) and hardware related influences. Because of this dependency on both tissue and acquisition related parameters, MRI is commonly

[1] Dr. Christoph Kolbitsch, Department "Biomedical Magnetic Resonance", PTB Berlin, ORCID: https://orcid.org/0000-0002-4355-8368, email: christoph.kolbitsch@ptb.de

[2] Dr. Sebastian Schmitter, Department "Biomedical Magnetic Resonance", PTB Berlin, ORCID: https://orcid.org/0000-0003-4410-6790, email: sebastian.schmitter@ptb.de

[3] Prof. Dr. Tobias Schaeffter, Steering Committee "Metrology in Medicine", Division "Medical Physics and Metrological IT", PTB Berlin, ORCID: https://orcid.org/0000-0003-1310-2631, email: tobias.schaeffter@ptb.de

[1] The relaxation times also depend on the magnetic field strength. Nevertheless, for a given clinical field strength of 1.5 tesla or 3 tesla, T_1 and T_2 can be considered only dependent on the tissue type.

used as a qualitative imaging modality, i.e. the intensity difference between different tissue types or diseased and healthy tissue (image contrast) is used for diagnosis, rather than the actual pixel intensity values. Therefore, many diagnostic MR techniques rely on localised pathologies in order to have a contrast between healthy and diseased tissue. In addition, the dependency on the acquisition parameters makes it difficult to compare qualitative MR images across patients and MR scanners. This has strong implications for research to ensure reproducibility of results, for clinical multi-centre trials to pool data and in clinical practice to diagnose and to monitor treatments.

Quantitative MRI promises to overcome these challenges by providing quantitative maps of biophysical parameters, which are independent of any acquisition or hardware related parameters.

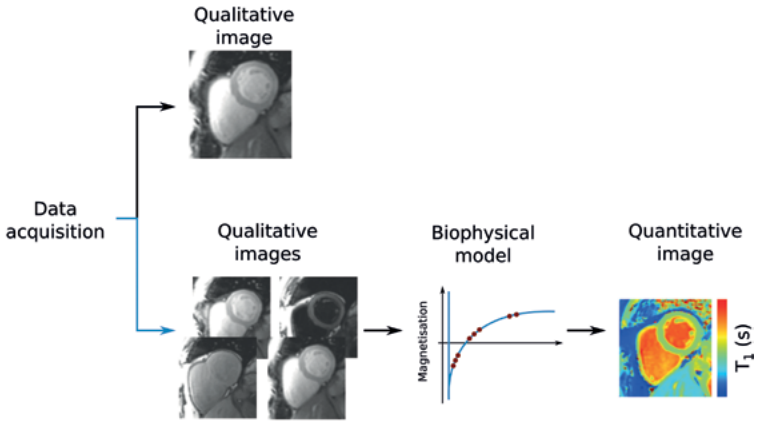

Figure 1:
For qualitative MR images the pixel intensities depend on tissue specific parameters but are also influenced by sequence and hardware related parameters. Quantitative MRI directly describes biophysical parameters. Commonly multiple qualitative images are required in order to calculate quantitative parameters using a biophysical model.

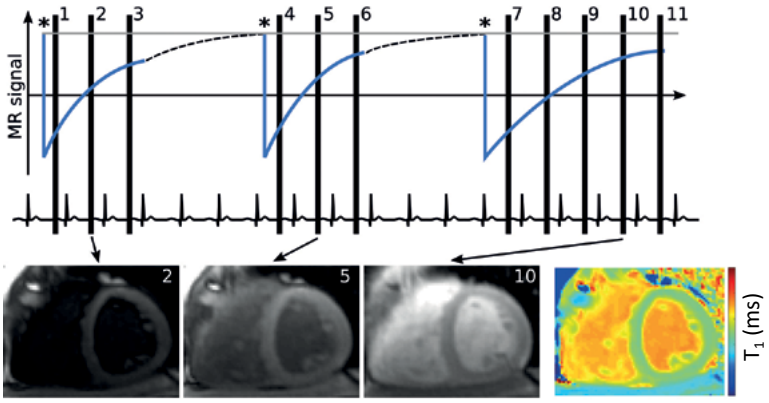

Figure 2:
MOLLI obtains multiple qualitative images (1 to 11 for MOLLI 3(3)3(3)5 (4), grayscale images) in mid-diastole after three inversion pulses (*). Rest-periods without data acquisitions are inserted (dashed lines) to allow magnetization to recover to equilibrium state (grey line). A model is then fitted on a pixel-by-pixel basis to obtain quantitative T_1 maps (colour).

This makes quantitative MR images easier to compare between different scans and patients allowing for monitoring of treatment response and multi-centre studies. Figure 1 compares the acquisition of a 2D qualitative and quantitative MR images of the heart. Commonly multiple qualitative images with different image contrast are required and a biophysical model is fitted to the data to obtain a quantitative parameter map.

At PTB we are developing a range of different quantitative MR approaches in order to improve the accuracy and reliability of quantitative MRI. In the following we show four examples of our current research work: i) For cardiac T_1 mapping we used sophisticated physical signal models in order to make data acquisition more efficient and ensure more accurate measurements; ii) 4D Flow MRI provides quantitative blood flow velocities during the cardiac cycle. Novel approaches developed at PTB aim at reducing scan times in order to make this method applicable in clinical practice. iii) For cardiac perfusion imaging we employed statistical approaches not just to improve blood perfusion quantification but also to obtain an uncertainty measure for each estimate. iv) Respiratory motion is one of the biggest challenges of dynamic contrast enhanced (DCE) MRI hampering quantification. By accurately determining the motion of the organs due to breathing, we were able to correct for motion artefacts and ensure accurate quantitative assessment of liver tumours even during free-breathing of patients.

All of this work was carried out in close collaboration with clinical partners (Charité Berlin and King's College London) in order to ensure that our developed techniques get evaluated in a clinical setting as early as possible.

2. Cardiac T_1 Mapping

One of the most important quantitative MR approach for cardiac tissue differentiation is T_1 mapping, which provides a map of T_1 relaxation times measured in seconds. Pathological changes of tissue (e.g. fibrosis) in the heart has different T_1 values compared to healthy myocardium. Therefore, T_1 mapping can be used to diagnose a wide range of different cardiac pathologies, especially for entities, which otherwise would look healthy with preserved ejection fraction (1–3).

Currently the most commonly used cardiac T_1 mapping approach is the so-called modified Look-Locker inversion recovery (MOLLI) (4). For MOLLI multiple 2D qualitative images are acquired at different time points after an inversion pulse (so called inversion times, TI), which provide snapshots of the recovery of the longitudinal magnetization during T_1 relaxation

(Figure 2). In order to minimize motion artefacts due to heart motion, data acquisition is restricted to a short acquisition window of 200 to 300 ms. Most commonly a two or three parameter mono-exponential model is used to estimate T_1 values. Although this is very robust, it is a simplification of the MR signal evolution and requires additional rest periods where no data is acquired to ensure full recovery of magnetization for accurate results. Acquiring data only in a small window of each cardiac cycle and using a simple model means that MOLLI is an inefficient technique, because only a small percentage of the total scan time is used to acquire diagnostic information.

In order to overcome this challenge, we developed a novel approach, which utilises a flexible 2D Golden radial data acquisition approach to obtain data continuously over multiple cardiac cycles (Figure 3) (5). We used a model that accurately describes the MR signal during the entire acquisition process and hence no rest periods are required. This approach yields T_1 maps of different cardiac phases and additional diagnostic information about cardiac function, i.e. how much blood is pumped into the body with every heartbeat. Our signal model describes the evolution of the MR signal with a millisecond resolution. Therefore, physiological variations during data acquisition (e.g. changes in the heartrate) do not affect the accuracy of our approach. Figure 4 compares the T_1 times measured in a phantom for different tissue types. Our approach provides highly reproducible measurements, whereas the standard approach shows a clear heartrate dependency.

With this new technique we were able to improve the accuracy and efficiency of cardiac T_1 mapping. Future work will focus on extending this approach from 2D slices to full 3D coverage of the entire heart.

3. 4D Blood Flow

The velocity of the human blood and the velocity of moving tissue such as the cardiac muscle is one of these quantitative parameters, which gained substantial clinical and scientific interest since initial human applications in the early 1980ies (6). Today, MRI allows quantifying the time-resolved 3D velocity vector field, meaning that the magnitude and the direction of the velocity can be measured at typical spatial resolutions of 0.5–3 mm for each point within a three-dimensional object (e.g. the vessel) and as a function of the cardiac cycle (7). This technique is often termed "4D flow MRI", referring to the 3D spatial plus the temporal coverage. MR-based velocity quantification is not only used in clinical cardiovascular exams on a regular basis, it also gains increasing interest for engineering purposes to study the dynamics of fluid in various applications.

The acquisition of the time-resolved blood velocity vector field allows the calculation of velocity-derived parameters such as the total blood flow within a cardiac cycle, the reversed flow through the cardiac valves, and also the wall shear stress (WSS). The latter denotes the tangential force of the blood at the vessel wall, which is assumed to be an important parameter in the development of atherosclerotic plaques.

Beside the potential of this technique there are also limitations that still hinder a broader clinical application of this method. A correct quantification of the hemodynamic parameters, in particular the calculation of WSS, requires high spatial and high temporal resolution. However, acquisition times increase approximately linear with temporal resolution and super-linear with spatial resolution, and furthermore, high resolution requires a high signal-to-noise ratio (SNR). Thus, overall scan times of 10–20 minutes are often needed for a 4D flow scan, which are too

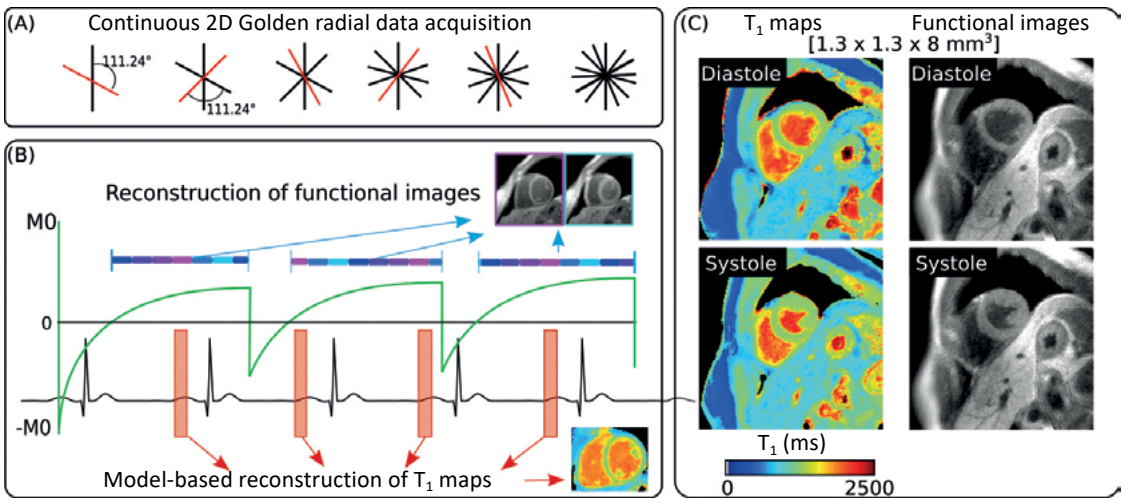

Figure 3: Iterative model-based reconstruction providing 2D high-resolution T_1 maps and functional images of the heart. A continuous 2D Golden radial acquisition is carried out during a single breathhold. Multiple-inversion pulse are applied at fixed time points. Data is retrospectively selected to provide functional (cine) images and T_1 maps.

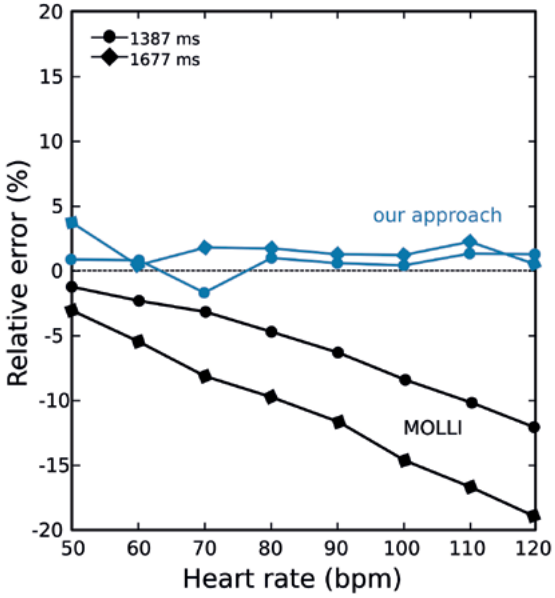

Figure 4:
Dependency of T_1 estimation on different heart rates. The standard approach (MOLLI) leads to an underestimation of T_1 values especially for high heart rates. This effect is corrected for using our proposed signal model (blue).

long for clinical routine and acceleration of 4D flow is highly required.

At PTB we aim to improve the quantification of 4D flow scans and to accelerate acquisition times. Recent works have addressed the acceleration in several orthogonal ways. First, acceleration is achieved by using dedicated radiofrequency pulses to image the spins only within a restricted 3D volume. Developments at PTB now allow to restrict the volume in two dimensions, which reduces time by more than two-fold (8) as shown in Figure 5. To maintain the temporal resolution of conventional scans, additional techniques are employed that make use of the temporal dynamics of the acquisitions (9). In an orthogonal strategy, we investigate acceleration techniques by applying compressed sensing, which makes use of the high redundancy of the different velocity components of the 4D flow vector field. This approach allows high undersampling of data during acquisition. In a second work, velocity scans covering a 2D slice as performed typically in clinical routine are accelerated by acquiring multiple slices simultaneously. This approach can also be used to quantify motion of tissue in two slices (10). In addition to such efforts, a main goal of PTB's efforts are to improve the quantification by increasing the resolution, which however requires high SNR. To address this issue, PTB investigates flow quantification using MRI scanners operating at a field strength of 7 tesla instead of 1.5 tesla and 3 tesla that are most often used in clinical routine (Figure 6). Using this field strength, resolutions of 0.5 mm are feasible, which opens the door to investigating a large range of medical conditions such as intracranial aneurysms or arteriovenous malformations.

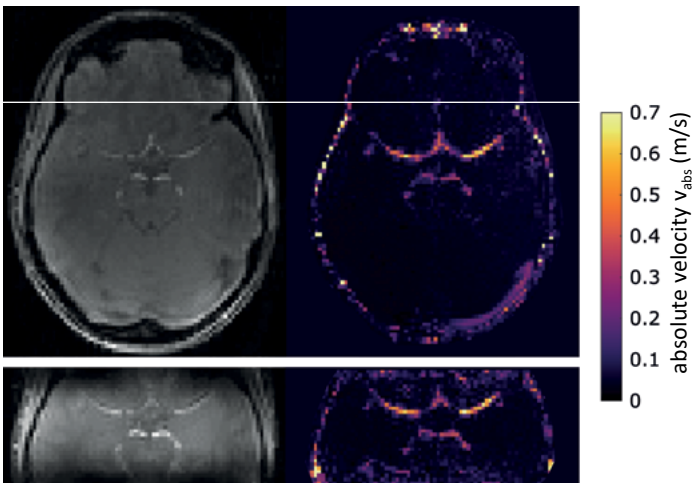

Figure 5:
Magnitude (left) and velocity image (right) obtained in the human brain of an entire transversal view (top row) and a view restricted to the Circle of Willis (bottom), the main cerebral arteries. Detailed analysis revealed identical velocity values within the arteries while the volume of interest was reduced more than 2-fold. Data was acquired at 7 tesla field strength.

Another important factor for accurate quantitative flow is motion. An example is shown in Figure 6 for 4D flow MRI acquired during free breathing (11). Respiratory motion led to blurring of anatomical structures such as the heart and the liver (white arrows) in the qualitative images. In the quantitative 4D flow maps, physiological motion leads to errors in quantification. Without correcting for respiratory motion, blood flow velocities appear lower, potentially leading to wrong diagnostic interpretation. This demonstrates that for quantitative MRI, accurate motion compensation is even more important than for qualitative MRI.

In clinical practice the standard approach to minimize the negative effect of motion is gating. For this, data in a certain motion gate is only used for the final image reconstruction, whereas it is discarded outside the gate. However, motion gating requires periodic and reproducible motion patterns to ensure enough data can be acquired in a pre-defined motion state such as end-expiration (12). The ratio between gated data and total data (acquired and discarded data) is called scan efficiency. Breathing patterns can vary strongly between different subjects leading to scan efficiencies between 20 % and 60 %. Changes in the breathing motion, e.g. change from deep breathing to shallow breathing or drifts can lead to long scan times or even scan abortions (13). To overcome these problems motion correction methods have been proposed in order to utilise all the acquired data with a 100 % scan efficiency.

4. Cardiac Perfusion

The myocardium (i.e. the heart muscle) is supplied with oxygen and nutrients via the coronary arteries. If these arteries get blocked (so-called stenosis), not enough blood reaches the heart

muscle (perfusion defect) and cardiac arrest can occur. Early diagnosis of patients at risk is vital for successful treatment and to reduce mortality and morbidity. One promising non-invasive technique is first-pass myocardial perfusion imaging (14, 15). For this measurement an MR contrast agent is injected into the patient's blood stream. The MR contrast agent leads to an increase of the MR signal and therefore the blood flow can be assessed by monitoring the changes in the MR signal strength. If the entire myocardium is supplied well with blood and there is no stenosis, contrast agent reaches the myocardium simultaneously and leads to a homogenous MR signal enhancement. If certain parts of the coronary arteries are narrowed and hence at risk of a blockage, signal enhancement is reduced in these areas which can be easily identified.

Cardiac perfusion MRI yields a series of 2D images showing contrast enhancement in the myocardium over time. Commonly, these images are diagnosed visually by a clinical expert. Quantitative approaches to measure the myocardial blood flow have been proposed, but are not widespread used and often suffer from low signal-to-noise-ratios (16). Often, quantitative perfusion MRI relies on image segmentation and only provides perfusion values in a few myocardial segments rather than utilising the high spatial resolution of the MR images. In addition, only single estimates of blood perfusion are usually provided without any measure of uncertainty.

We developed a novel approach to quantitatively asses myocardial perfusion parameters and their uncertainty using Bayesian inference (17). In particular, the approach determines the perfusion rate (F) and the time delay between arrival of contrast agent in the left ventricle and myocardium. So called, Gaussian Markov Random Field priors were used in order to utilise the spatial smoothness of myocardial perfusion quantification. Figure 7 shows the results for patients with and without coronary stenosis. Only F is shown as it is currently believed to be the most reliable biophysical parameter to indicate perfusion defects. We achieved reliable perfusion quantification in the entire myocardium and our approach also yields an uncertainty measure for each perfusion value. This could be used to assess the reliability of the quantitative results, as a high uncertainty could indicate problems during data acquisition (e.g. residual artefacts due to respiratory motion). It could also be important to better distinguish small perfusion defects from natural signal variation in the myocardium.

Here we also determined the ischemic burden, i.e. how many voxels in the myocardium suffer from low perfusion. The ischemic burden was defined as all pixels with values of F smaller than 60 % of the median of all F values. This threshold is heuristically determined but shows how the quantitative information obtained with this approach could be used in order to automatically detect perfusion defects in patient data. This could provide an important step from subjective interpretation-based diagnosis to automated diagnosis based on biophysical reference values.

5. Tumour Perfusion

Tissue perfusion is another important parameter in the diagnosis of cancer. For this dynamic contrast-enhanced (DCE) MRI (18) is applied to measure the uptake of an injected contrast agent over time. It has been shown that DCE-MRI provides information about tumour angiogenesis, i.e. the new formation of vessels in order to meet the high demand of nutrition in lesions (19),

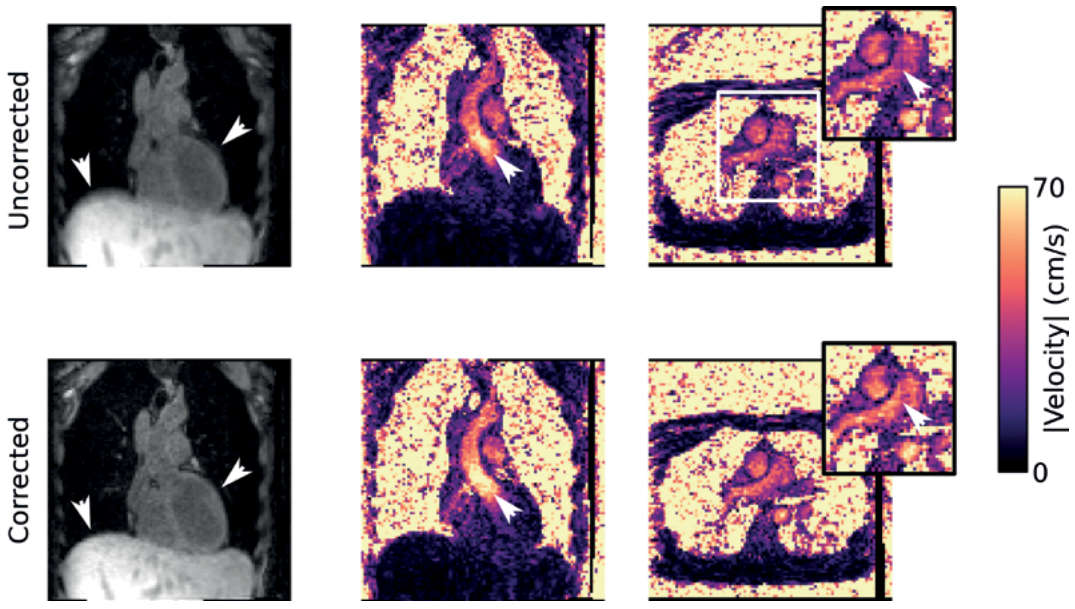

Figure 6: Uncorrected and corrected 4D flow-encoded MRI (grayscale) and corresponding quantitative 4D flow images showing the blood flow through the aorta during systole.

which often correlates with the malignancy of the tumor. In addition, it could be used to detect an early response to cancer drugs inhibiting angiogenesis.

Commonly, DCE-MRI of the liver is only acquired for a few predefined time points during contrast agent arrival, peak enhancement and early and late washout of contrast agent. One of the main challenges of quantitative MRI in the thorax or abdomen is physiological motion such as breathing or beating of the heart. In DCE-MRI of the abdomen, usually images are obtained during a single breathhold and are then qualitatively assessed (18). Often patients hold their breath at different breathhold positions, which makes it challenging to compare the images.

We developed a highly-efficient 3D acquisition approach, which yields 3D DCE-MRI with 1.5 mm^3 isotropic resolution covering the entire abdomen with a temporal resolution of 6 seconds. In order to minimize artefacts due to the breathing motion of the patient, respiratory motion information was obtained directly from the diagnostic DCE-MR data without the need of any additional scans (20). 3D high-resolution images for different breathing positions were reconstructed. Afterwards a non-rigid image registration, together with a motion-compensated reconstruction algorithm to reconstruct motion-free 3D-images, was applied. A pharmacokinetic model was then fit to the dynamic image volumes to obtain quantitative parameters such as volume transfer constant (k_{trans}), which is a measure for the angiogenesis of tumours. The hepatic artery could be used as arterial input function to the pharmacokinetic model.

We applied this approach in 11 patients and demonstrated that our respiratory motion-correction approach improved contrast-to-noise ratio of hepatic lesions by 47 % ($p < 0.01$) and k_{trans} by 62 % ($p < 0.01$). Figure 8 shows an example of a patient with malign hepatic lesions. Respiratory motion leads to blurring of the qualitative DCE-MR images and to errors in the quantification of k_{trans}. Small lesions (white arrow) are missed due to respiratory motion. In addition, the substructure of larger lesions (e.g. necrotic core) is only accurately depicted using respiratory motion correction.

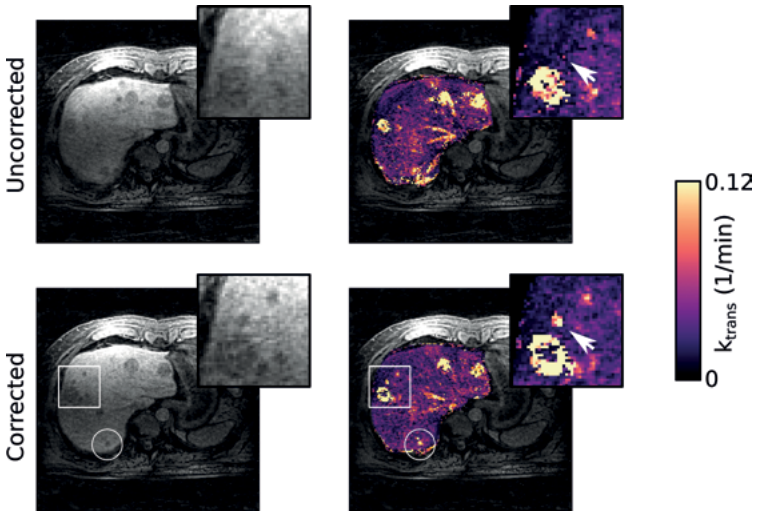

Figure 8:
Uncorrected and corrected late-phase DCE-MRI (grayscale) and corresponding maps of the volume transfer constant (k_{trans}) from a patient suffering from hepatic malign lesions.

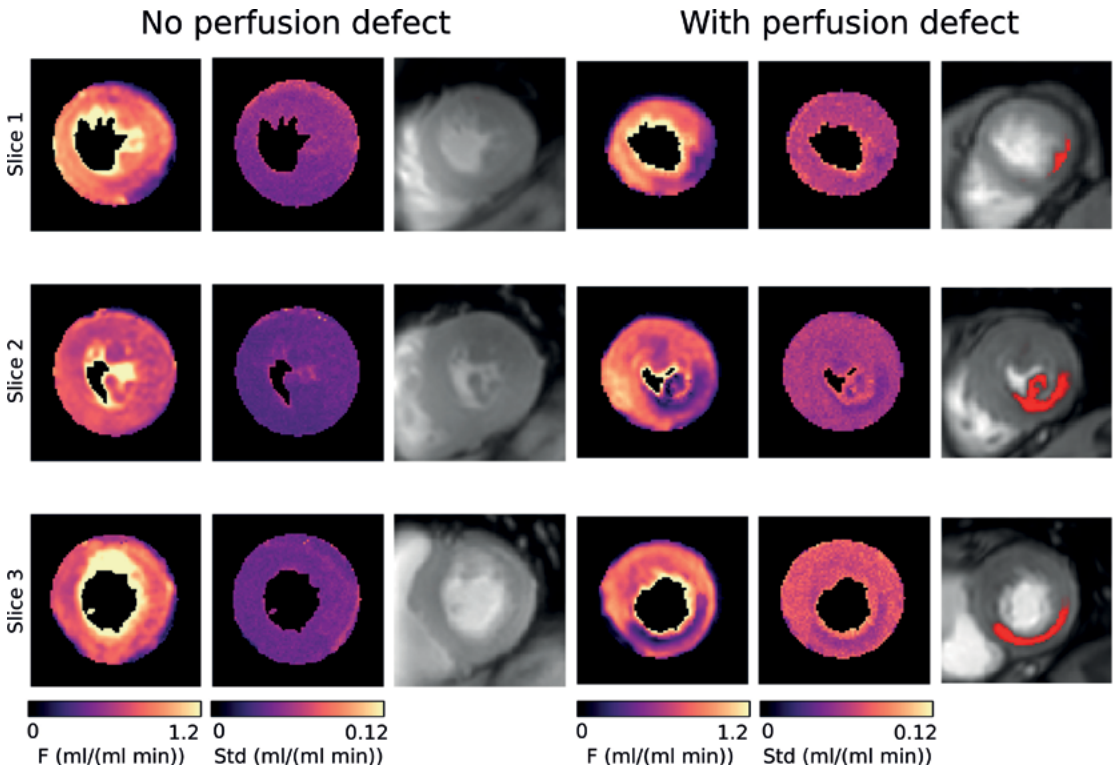

Figure 7:
Assessment of myocardial perfusion using MRI. With this statistical approach not just the quantitative perfusion frate (F) is available but also a measure for its uncertainty (Std). Here the standard deviation over all realisations was used as a measure for the uncertainty. This further allows for an automatic detection of perfusion defects marked in red.

With this method 3D DCE-MRI with high spatial resolution can be acquired without the need of any breathholds making it very easy to apply in patients. In addition to the DCE-MRI we also simultaneously acquired Positron-Emission-Tomography (PET) data using ^{18}F-FDG. This provides additional metabolic information about the tumour. In a next step, the respiratory motion information obtained from the MR, will be applied to the PET reconstruction in order to improve the PET image quality and PET tracer quantification. This will then ensure that both modalities are showing the exact same respiratory motion state and allow for a comparison of quantitative MR and PET information on a pixel-by-pixel basis. This will further improve tumour characterisation.

6. Conclusion

Quantitative MRI offers the possibility to assess a wide range of different physical and biophysical parameters. Here at PTB we have developed a range of new methods in order to improve the accuracy and precision of quantitative MRI methods and to assess their uncertainty. Improved image reconstruction ensured shorter scan times, advanced signal models reduced the dependency on physiological effects such as heart rate changes and motion correction were employed in order to allow for full 3D quantitative assessment of organs with high spatial resolution. All these developments were carried out in close collaboration with medical experts to ensure, that our methods are applied in a clinical setting as quickly as possible. We believe that our work is also an important stepping stone towards reproducible automated diagnosis.

Acknowledgements

Parts of the work shown here was supported by the German Research Foundation (DFG) grant “BioQic” (No. GRK 2260).

References

[1] Puntmann VO, Voigt T, Chen Z, et al. Native T1 mapping in differentiation of normal myocardium from diffuse disease in hypertrophic and dilated cardiomyopathy. JACC Cardiovasc. Imaging 2013;6:475–484. doi: 10.1016/j.jcmg.2012.08.019.

[2] Karamitsos TD, Piechnik SK, Banypersad SM, et al. Noncontrast T1 Mapping for the Diagnosis of Cardiac Amyloidosis. JACC Cardiovasc. Imaging 2013;6:488–497. doi: 10.1016/j.jcmg.2012.11.013.

[3] Germain, El-Ghannudi S, Jeung M, Ohlmann P, Epailly E, Roy C, Gangi A. Native T1 Mapping of the Heart - A Pictorial Review. Clin. Med. Insights Cardiol. 2014;8:1. doi: 10.4137/CMC.S19005.

[4] Messroghli DR, Radjenovic A, Kozerke S, Higgins DM, Sivananthan MU, Ridgway JP. Modified look-locker inversion recovery (MOLLI) for high-resolution T 1 mapping of the heart. Magn. Reson. Med. 2004;52:141–146. doi: 10.1002/mrm.20110.

[5] Becker KM, Schulz-Menger J, Schaeffter T, Kolbitsch C. Simultaneous high-resolution cardiac T 1 mapping and cine imaging using model-based iterative image reconstruction. Magn. Reson. Med. 2019;81:1080–1091. doi: 10.1002/mrm.27474.

[6] Moran PR. A flow velocity zeugmatographic interlace for NMR imaging in humans. Magn. Reson. Imaging 1982;1:197–203. doi: 10.1016/0730-725X(82)90170-9.

[7] Markl M, Frydrychowicz A, Kozerke S, Hope M, Wieben O. 4D flow MRI. J Magn Reson Imaging 2012;36:1015–1036. doi: 10.1002/jmri.23632.

[8] Wink C, Ferrazzi G, Bassenge JP, Flassbeck S, Schmidt S, Schaeffter T, Schmitter S. 4D flow imaging with 2D-selective excitation. Magn. Reson. Med. 2019;82:886–900. doi: 10.1002/mrm.27769.

[9] Wink C, Bassenge JP, Ferrazzi G, Schaeffter T, Schmitter S. 4D flow imaging with UNFOLD in a reduced FOV. Magn. Reson. Med. 2020;84:327–338. doi: 10.1002/mrm.28120.

[10] Ferrazzi G, Bassenge JP, Wink C, Ruh A, Markl M, Moeller S, Metzger GJ, Ittermann B, Schmitter S. Autocalibrated multiband CAIPIRINHA with through-time encoding: Proof of principle and application to cardiac tissue phase mapping. Magn. Reson. Med. 2019;81:1016–1030. doi: 10.1002/mrm.27460.

[11] Kolbitsch C, Bastkowski R, Schäffter T, Prieto Vasquez C, Weiss K, Maintz D, Giese D. Respiratory motion corrected 4D flow using golden radial phase encoding. Magn. Reson. Med. 2020;83:635–644. doi: 10.1002/mrm.27918.

[12] Nguyen TD, Spincemaille P, Cham MD, Weinsaft JW, Prince MR, Wang Y. Free-breathing 3-dimensional steady-state free precession coronary magnetic resonance angiography: comparison of four navigator gating techniques. Magn. Reson. Imaging 2009;27:807–814. doi: 10.1016/j.mri.2008.11.010.

[13] Sakuma H, Ichikawa Y, Chino S, Hirano T, Makino K, Takeda K. Detection of coronary artery stenosis with whole-heart coronary magnetic resonance angiography. J Am Coll Cardiol 2006;48:1946–1950. doi: 10.1016/j.jacc.2006.07.055.

[14] Nagel E, Greenwood JP, McCann GP, et al. Magnetic Resonance Perfusion or Fractional Flow Reserve in Coronary Disease. N. Engl. J. Med. 2019;380:2418–2428. doi: 10.1056/NEJMoa1716734.

[15] Coelho-Filho OR, Rickers C, Kwong RY, Jerosch-Herold M. MR Myocardial Perfusion Imaging. Radiology 2013;266:701–715. doi: 10.1148/radiol.12110918.

[16] Jerosch-Herold M. Quantification of myocardial perfusion by cardiovascular magnetic resonance. J. Cardiovasc. Magn. Reson. 2010;12:1–16. doi: 10.1186/1532-429X-12-57.

[17] Lehnert J, Kolbitsch C, Wübbeler G, Chiribiri A, Schaeffter T, Elster C. Large-Scale Bayesian Spatial-Temporal Regression with Application to Cardiac MR-Perfusion Imaging. SIAM J. Imaging Sci. 2019;12:2035–2062. doi: 10.1137/19M1246274.

[18] Quillin SP, Atilla S, Brown JJ, Borrello JA, Yu C-Y, Pilgram TK. Characterization of focal hepatic masses by dynamic contrast-enhanced MR imaging: Findings in 311 lesions. Magn. Reson. Imaging 1997;15:275–285. doi: 10.1016/S0730-725X(96)00226-3.

[19] Jackson A, O'Connor JPB, Parker GJM, Jayson GC. Imaging Tumor Vascular Heterogeneity and Angiogenesis using Dynamic Contrast-Enhanced Magnetic Resonance Imaging. Clin. Cancer Res. 2007;13:3449–3459. doi: 10.1158/1078-0432.CCR-07-0238.

[20] Ippoliti M, Lukas M, Winfried B, Schaeffter T, Makowski MR, Kolbitsch C. 3D nonrigid motion correction for quantitative assessment of hepatic lesions in DCE-MRI. Magn. Reson. Med. 2019:1–14. doi: 10.1002/mrm.27867.

Metrology for RF Safety in Magnetic Resonance Imaging

Frank Seifert[1]

Abstract

Magnetic Resonance Imaging (MRI) is a non-invasive medical imaging technique to obtain three-dimensional images with up to sub-millimeter resolution. Because of the remarkably high soft-tissue contrast and the avoidance of ionizing radiation, MRI is widely applied in clinic and research. Nevertheless, there are hazards that are particularly related to tissue heating due to the absorption of radiofrequency (RF) energy expressed by the Specific Absorption Rate (SAR). The distribution of local SAR in the human body is very inhomogeneous and can only be derived from numerical simulations using a variety of human voxel models. Validation of these simulations by measurements of RF field quantities is necessary to create confidence in this computational approach. Thus, the metrological concept to assess the SAR hazards of MRI is based on instrumentation for traceable in situ measurements of RF electromagnetic fields and other RF related quantities which can be operated within the MR environment. PTB developed unique measurement methods which are suitable for MRI equipment at 1.5 tesla to 7 tesla together with parallel transmission (pTx) capability. This measurement infrastructure was developed for RF safety in MRI and is independent from MR vendor specific solutions. In addition to this, it can be operated independently from the MR equipment allowing measurements in specific exposure scenarios. The measurement infrastructure allows research on future technologies in the field of sensor equipped implants which are capable to to monitor and mitigate the RF related hazards during MRI examinations.

1. Introduction

Magnetic Resonance Imaging (MR imaging) is the one of the most important medical imaging modality today. It is non-invasive, involves no ionizing radiation, and provides three-dimensional images with up to sub-millimeter resolution. Because of the superior soft-tissue contrast and the avoidance of ionizing radiation, MR imaging is widely applied in clinic and research. Nevertheless, there are hazards that are particularly related to tissue heating due to the absorption of radiofrequency (RF) energy. RF related tissue heating is a direct consequence of the radiofrequency magnetic field pulses applied to the human body to excite the nuclear spins during the imaging process. A widely accepted approach to protect the patient against excessive radio frequency energy is to limit the Specific Absorption Rate (SAR) as given by the international standard EN/IEC 60601-2-33 [1].

RF power absorption in the human body is very inhomogeneous and depends strongly on the frequency of the RF fields. For instance, for MR scanners operating at 7 tesla the RF wavelengths in tissue come down to about 12 cm, smaller than body dimensions. This brings the danger of temperature hot spots and emphasizes the need for metrological sound techniques to control local SAR distribution in the human body. At present, however, local SAR can only be derived from numerical simulations using a variety of human voxel models, e.g. the Virtual Population (VIP) [2]. Validation of these simulations by measurements of RF field quantities is necessary to create confidence in this computational approach. Thus, one of the major goals in the field of RF safety in MRI is the development of metrologically sound techniques to relate electromagnetic field simulations with in-situ measurements of diverse RF quantities. The metrological concept to assess

1 Dr. Frank Seifert, Research group, "MR Technology", PTB Institut Berlin, email: frank.seifert@ptb.de

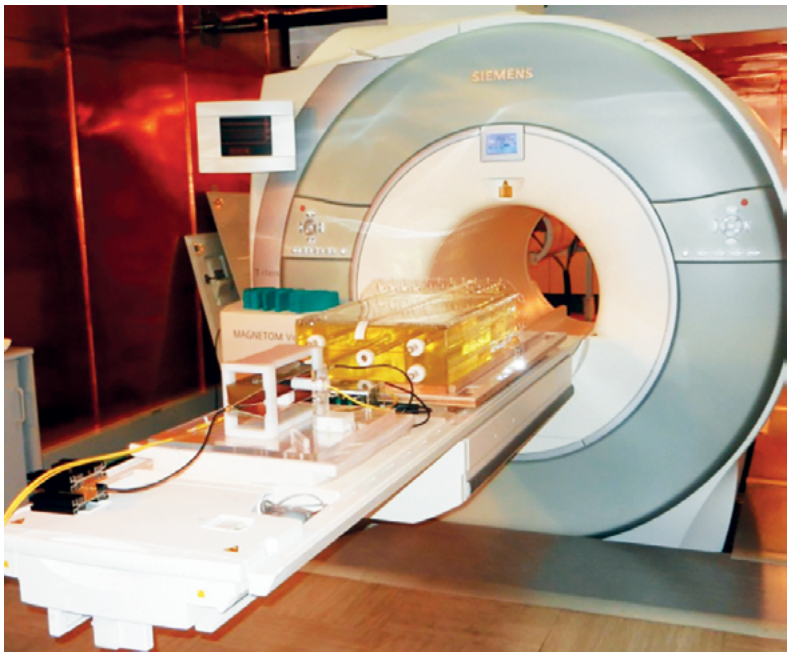

Figure 1:
Measurement setup for in-situ RF field measurements on top of the patient bed of PTB's 3 tesla MR scanner consisting of a torso phantom filled with a liquid mimicking both dielectric and MR properties of human tissue and an MR-TEM cell for in-situ calibration of RF field probes. The MR-TEM cell is a calculable field source relating RF electromagnetic field components to the gyromagnetic ratio of water protons.

the SAR hazards of MR imaging equipment is based on instrumentation providing traceable in situ measurements of RF electromagnetic fields and other RF related quantities in the MR environment. These unique measurement methods developed by PTB are suitable for either state-of-the-art MR equipment at 1.5 tesla or 3 tesla or for emerging MRI technologies such as parallel transmission (pTx) or ultrahigh magnetic fields (≥ 7 tesla) with their specific associated RF related hazards.

Furthermore, the importance of MR safety assessment of implanted metallic structures has been increased tremendously since nowadays an estimated 8 % – 10 % of the European population are carrying medical implants. Especially for patients with an active implantable medical device (AIMD) like cardiac pacemakers there is an unquestioned need for safe MR scans. For example, the European Society of Cardiology (ESC) has stated "that, after implantation, up to 75 % of patients with pacemakers develop an indication for magnetic resonance imaging examination" [3]. There are now a number of labelled AIMDs on the market that allow MRI examinations if certain conditions are met. These so called "MR conditional" devices include spinal cord stimulators (SCS), deep brain stimulators (DBS), cardiac resynchronization therapy (CRT) pacemakers, implantable cardioverter defibrillators (ICD), insertable cardiac monitor (ICM) systems, and interventional systems for cardiac catheter ablation procedures.

Besides the ASTM standard F2182-11a [4] the technical specification ISO/TS 10974 [5] is the first comprehensive standardization document applicable to active implantable medical devices intended to be used in patients who undergo an MR examination. This future ISO standard also emphasizes the need of RF field measurements to access the uncertainties of electromagnetic modelling in MRI.

PTB developed a measurement infrastructure for RF safety in MRI in terms of independence from MR vendor specific solutions. Furthermore, it can be operated independently from the MR equipment allowing measurements in specific exposition scenarios. The developed MR safe measurement infrastructure is inert with respect to strong static magnetic fields and to switched magnetic field gradients. To avoid RF field distortions and RF interferences by metallic wires for all RF probes a fiber optical link was used for signal readout. Other measurement equipment is located outside the shielded MR scanner room. To account for the complex time structure of the pulsed transmitted RF signals all measurement devices operate in the time domain regime with full phase resolution capability.

2. MR-TEM cell

To calibrate RF electromagnetic field probes a source of well-defined fields is required. A transverse electromagnetic (TEM) cell is such a source and is frequently used in RF dosimetry. A TEM cell made of non-magnetic printed circuit

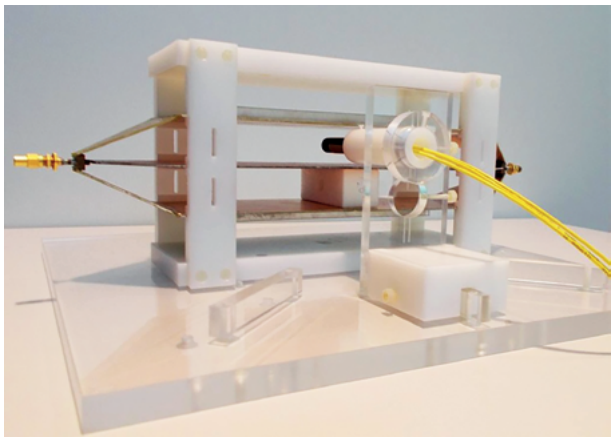

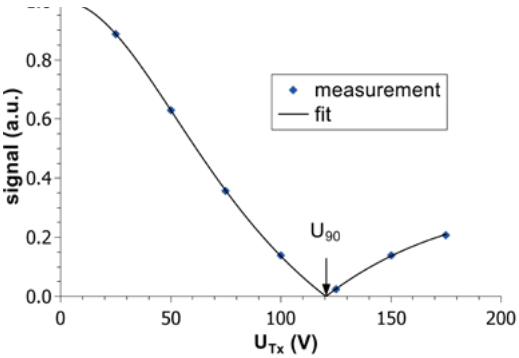

Figure 2:
MR-TEM cell made of printed circuit board material to ensure MR compatibility. In the upper compartment a fiberoptic *E*-field sensor is positioned while the lower compartment contains a water-filled polyethylene sphere inside a foam block (left). Principle of flip angle measurement using saturation pulses with different nominal transmitter voltages.

board material operated as a transmit/receive (Tx/Rx) coil directly in an MR scanner [6] allows to trace the RF magnetic field

$$B_1^+ (90°, 1\ \text{ms}) = \frac{\alpha}{\gamma\tau} \approx 5.87165\ \mu\text{T}$$

inside the compartments back to the gyromagnetic ratio γ of the proton by determining the nominal transmitter voltage U_{90} required for a α = 90° (flip angle) rectangular RF pulse with a pulse duration of e.g. τ = 1 ms which is applied it to the cell. Then, the electric field at the Larmor frequency is known from the strict relation between electric and magnetic field in a TEM cell:

$$|E_1| = 2|B_1^+|\, c_0 \approx 3520.52\ \text{V/m}$$

The actual RF voltage amplitude *U* at the port of the TEM cell is then related to the plate distance *d* via *E* = *U*/*d*. This relation can be used to determine the voltage in the transmit chain of the MRI scanner or to generate defined RF currents for the calibration of current sensors.

Since the *E*-field vector is oriented into the vertical axis, the calibration of a 3-axis fiber optic *E*-field sensor in the position shown in Figure 2 is feasible. A loop appropriate to measure the RF magnetic field needs to be inserted under an angle of 45 degrees. *E*- and *B*-field measurements with calibrated fiber optic time domain sensors inside the body coil of a 3 tesla MRI scanner [7] were successfully applied for validation of a realistic model of that coil [8]. The MR compatible TEM cell is a central part of our measurement infrastructure and allows the calibration of *E*- and *B*-field sensors as well as RF current sensors directly at the frequency of the MR scanner studied. The uncertainty of this calibration procedure is resulting mainly from imperfections of the current hardware implementation and was estimated to be less than 5 % which is sufficient for safety assessments. It was shown that an improved flip angle measurement technique allows determinations of B_1^+ with an uncertainty at the 0.1 percent level [9].

3. MR-compatible current sensor

Currents induced in wire type medical implants like electrodes for deep brain stimulators, guide wires, catheters etc. are a major safety concern in MRI. The RF fields used to excite the nuclear spin induce currents in these implants which cause heating of the implant tip within the patient. For the assessment of these currents a sensor for measuring the induced current in the implant directly at its protruding end is an invaluable tool to assess and minimize these currents [10 – 12]. The magnetic field generated by the current in the implant can be selected by a toroidal shield with a slit while the detection of unwanted signals directly from the transmitter coil of the MRI scanner is suppressed [13]. A Rogowski coil inside the shield is used to measure this field. Readout via a fiber optic transducer avoids effects of the strong electromagnetic fields inside and in the vicinity of an MR scanner. For use in an MRI scanner the sensor must not affect the image quality, i.e. needs to be non-magnetic and should avoid the generation of low frequency eddy currents by the switched magnetic field gradients of the MR scanner. Hence, a copper plated plastic was used for the toroidal shield of the sensor (Figure 3). All plastic parts of the sensor were generated using additive manufacturing methods. The shield was galvanically coated with a thin copper layer with a thickness of typically 10 µm. To further suppress undesired RF magnetic field components passing the central slit of 2 mm width in the shield a Rogowski coil was chosen as a pickup coil for the fields generated by the RF current in a wire running through the bore of the sensor. The number of loops was limited by the choice of thick wire to reduce the resistive impedance. The two parts of the shield are joined with a snap fit.

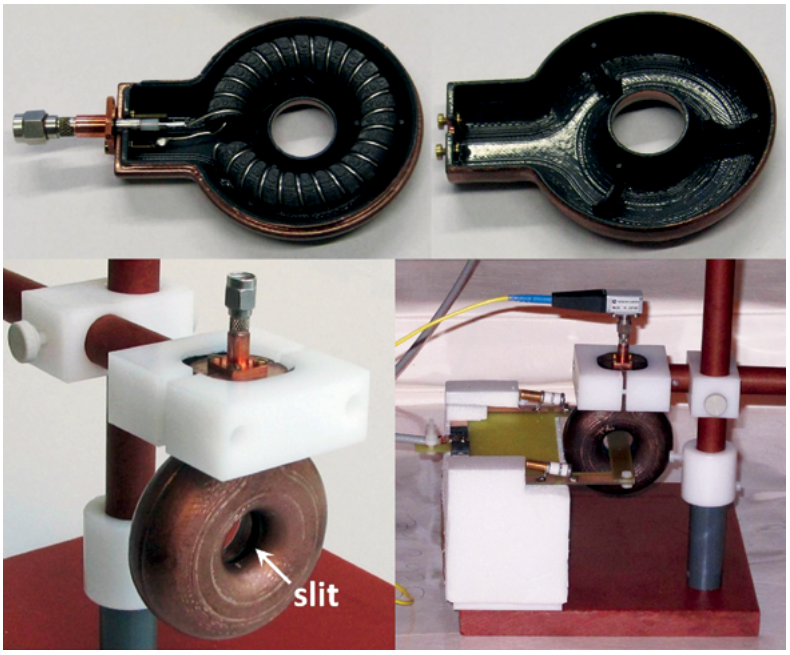

Figure 3:
The MR-compatible current sensor consists of a Rogowski coil inside a shield of copper plated plastics. The shield consists of two parts with a snap fit joint. For in-situ calibration one detachable part of the calibration coil is fed through the sensor. The calibration coil is connected to the MR-TEM cell after its calibration via a flip angle experiment. Applying $U_{\text{Tx, 90°,1 ms}}$ at the input port of the TEM cell, an RF current amplitude of approximately 2 A is generated in the calibration coil.

4. Body phantom:

One part of the measurement infrastructure for RF safety assessment are phantoms resembling the human body or parts of it. A body phantom with the outline described in the ASTM standard F2182–11 [4], was filled with a proper phantom liquid. Further, the body phantom was equipped with 5 removable tubes for EM field measurements in the interior and with feedthroughs for wire type implants (s. Figure 1). The dielectric properties

Figure 4: Measurement setup consisting of 8-channel transmitter, 4-channel receiver, 8-channel power amplifier modules and optical receiver and converter for the time-domain *E*- and *H*-field probes. The system can be used for measurements in the MR environment and for bench measurements outside the magnet. The positioning system on the left side is used for bench measurements on MR coils and implants.

of the phantom liquids were characterized using a coaxial probe. It was shown that the high conductivity of the phantom liquids developed for the use with cell phones to reproduce worst case exposure scenarios cause untypical field distributions inside the phantom when used in MRI. This is no problem as far as the phantoms are used to validate simulations and to prove the methods developed. It would however pose a problem when the phantoms are used to assess implant safety. Hence, conductivity was adapted to obtain appropriate B1-distributions and coil loading conditions. Together with the phantoms several tools for save body phantom handling (approx. 60 kg weight) and accurate phantom and sensor positioning were developed by PTB.

5. MR safe RF signal and field sensors:

A set of 8 nonmagnetic directional couplers, specially customized for PTB, is available to measure the forward and reflected RF voltages at the feeding ports of parallel transmission (pTx) coils in either 3 tesla or 7 tesla MRI magnets. A time domain electrooptic *E*-field probe (OEFS-S1B, Seikoh-Giken) is used for *E*-field measurements inside and outside of the phantoms. The system consists of a three axis sensor head (d = 12 mm), an 11 m long optical fiber link and a controller unit with RF output. The controller unit is always placed outside the RF shield of the scanner room. A time domain *H*-field probe with optical read out (H-TDS, SPEAG) is used for measurements of B_1^+ and B_1^- to characterize the body coil of the MR system. For all MR safe field probes mounting assemblies were developed and built by PTB allowing proper positioning of the field probes inside and outside the phantoms, in the surrounding of a human subject and inside the calibration devices.

6. Signal generation and data acquisition:

PTB developed a scalable system to generate and receive RF signals applicable for safety assessment of MR coils and metallic implants consisting of 8 phase-coherent transmit and 4 receive channels. The system implemented is using 16-bit arbitrary waveform generators allowing seamless transmission for RF safety testing at frequencies of up to 297 MHz (7 T). 8 broadband 20 W amplifiers are used for heating experiments. For signal reception a 14-bit 4-channel digitizer with a maximum sampling rate of 500 MS/s is used. The receiver is able to sample RF coil signals for experiments at 1.5 tesla to 7 tesla (s. Figure 4). PTB developed flexible software for digital down conversion, filtering and subsequent data processing. Furthermore, the software is performing measurement control, i.e. synchronization with the MR sequence, trigger generation and reference signal acquisition. The system is capable to acquire concurrently data from RF immune fiber-optic temperature probes. PTB is using fluoroptic probes which do not show any static magnetic field shift. For a reliable validation of simulation calculations, induced temperature changes of at least 2 K within 120 s should be aimed for.

For sampling long MR-sequences the sampled

data at a data rate of 1GB/s can be streamed through a GPU based down-converter to reduce the data rate to <1 MB/s. Thus, MR-sessions with a duration of >1 h can be recorded and used as realistic input data for e.g. thermal simulations (s. Figure 5).

7. Procedures and tools for comprehensive RF safety calculations in multichannel transmit MR systems

The development of a simulation infrastructure for multichannel transmit MR systems (pTx) is a key for comprehensive RF safety calculations in MRI [14]. To this end PTB developed a number of procedures and tools to account for the specific RF related hazards associated with pTx MRI systems in particular at ultrahigh fields. The datasets were generated by commercial FDTD solvers but procedures and tools are completely written in house. In addition, a GPU accelerated code for the Pennes' Bioheat Equation was written to correlate peak spatial SAR with local tissue temperature.

A tailored FDTD mesh generation tool was implemented using voxel models and tissue properties from commonly available databases [2]. The tool generates FDTD meshes for both the EMF and thermal simulations. The mesh generation assigns tissue types with higher conductivity a higher priority avoiding discretization artifacts due to disruption of internally connected tissue structures.

Furthermore, a procedure for the proper design of pTx coil models was established. Since tuning, matching and decoupling networks are incorporated later by the co-simulation the coil model includes additional ports for decoupling of coil elements. For each port a separate FDTD run is necessary resulting in typically 1 to 10 GB of 3D steady state field data per port. From steady state port voltages and port currents the impedance matrix and S-parameter matrix are calculated and used as input for co-simulation.

PTB developed an own co-simulation framework for tuning/matching/decoupling of pTx coils including intrinsic coil losses. As a result, for arbitrary driving voltage vectors the complete power balance and 3D field superposition can be calculated for different tuning/matching/decoupling parameters. From 3D field superposition distributions of all relevant field quantities can be deduced, e.g. B_1^+, B_1^-, E_1, local SAR and local SAR averaged over 10g.

To simplify access to local SAR (psSAR10g) the 3D power correlation matrix or Q-matrix is calculated using all previous data. Since the 3D Q-matrix is a very large data set the application of data compression schemes like the method of "Virtual Observation Points" (VOPs) is desirable. PTB developed and implemented an own algorithm to calculate VOPs with known overestimation error. An important finding was that the eigenvectors of VOPs represent all relevant scenarios in terms of local SAR including, of course, the "worst case" scenario. Thus, VOPs can be used as versatile testbed for safety assessment of pTx MR systems.

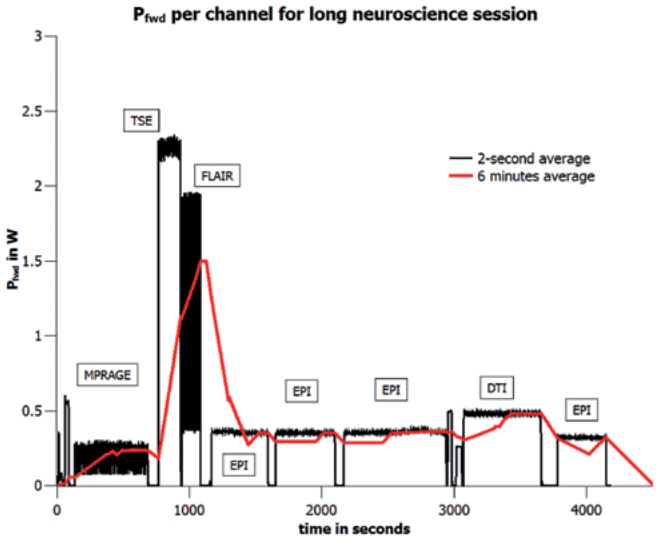

Figure 5: Recorded RF signal transmitted by the body coil during a neuroscience MR session consisting of different MR sequences (MPRAGE, TSE, FLAIR, EPI etc.). The signal is transformed into 2-second or 6-minute averages of RF forward power scaled to a maximum 6-minute average of 1.5 W. These data can be used in thermal simulations as realistic RF input.

A key result of this approach was the finding that the determination of psSAR10g at 7 tesla is prone to model variations when relying on measured multi-channel driving voltages. Hence, PTB developed a procedure for the calculation of an upper limit of psSAR10g for a fixed individual channel forward power. It was shown that this approach is simpler and more robust to demonstrate compliance with IEC 60601-2-33 [15].

PTB's GPU accelerated code to solve Pennes' Bioheat Equation is based on the OpenACC framework. To reduce discretization artifacts the same FDTD mesh was used for

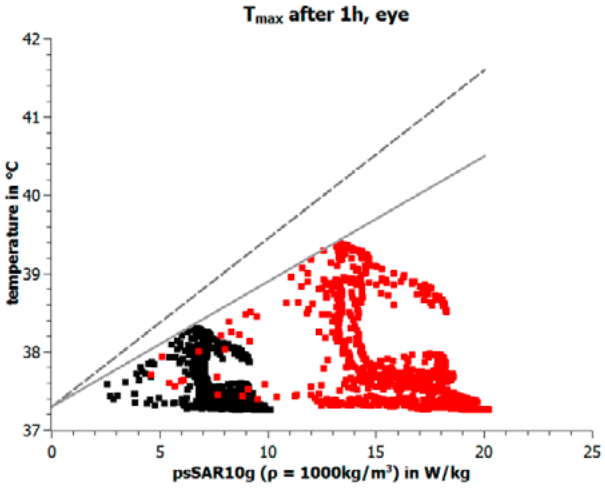

Figure 6: Peak steady state temperatures in dependence of psSAR10g for eye tissue: 2x873 different voltage vectors were used, total forward power was 8 W (red squares) or 4 W (black squares). The solid line indicates an upper limit extrapolation, the dashed line is the extrapolating line for muscle, skin and fat tissue.

thermal as well as for EMF calculations. This ensures that the heat generation terms match exactly with the right tissue type. This fast implementation of Pennes' Bioheat Equation allows to perform >1000 simulations in a reasonable time (s. Figure 6). Maximum steady state temperatures were determined for different groups of tissue types with different susceptibility to temperature rise. This is important when accessing the risk of tissue damage for large set of local SAR scenarios as given by the eigenvectors of the VOPs [16].

8. Comprehensive characterization of 3 tesla body coils

Knowledge of the EM fields in the body coils of MRI scanners is a precondition for the assessment of RF safety and of implant safety in particular. We addressed the question if it is possible to generate a reliable coil model which predicts the fields not only qualitatively but quantitatively with the limited knowledge of a commercial coil. For home build coils where all details are available the feasibility of such models is undisputed. However, the question remained what kind of external measurements would be required to parameterize the coil model.

It was possible to obtain the geometry of the body coil of PTBs 3 tesla MR scanner from the vendor together with the approximate values of the end ring capacitors. Furthermore, the coil load and the positions of the trimmers used for matching, tuning and decoupling were known as well as details of the elliptic polarized driving mode used for body imaging.

The two feeding ports of the body coil were not directly assessable to measurements, only the feeding cables. The feeding voltage amplitudes and phases were measured both for circular and elliptic polarization using a digital scope. Furthermore S-parameter and impedance spectra where measured at the feeding cables as a function of loading conditions to determine the Q factor of the body coil.

For the EM simulations CST Microwave Studio was used. The values of the end ring capacitors as well as the trimmers used for matching, tuning and decoupling were refined using co-simulations. The feeding conditions measured were used to drive the coil and coil losses were introduced to reproduce the Q factors found experimentally.

The results of the EM simulations were first compared to B_1^+ maps of the body phantom in various positions in the body coil. The model was optimized by minimizing the deviations to the measured field maps allowing for an additional phase shift caused by matching, tuning and decoupling.

The *E*-fields and *B*-fields measured with fiber optic time domain sensors inside and on top of the phantoms are then in good agreement with the simulations. The axial E field profiles are much more structured and even the multitude of minima and maxima of the minor field components are reproduced well (s. Figure 7). The residual asymmetries in *E*-field profiles arise from imperfections of the real coil which cannot be determined by the accessible measurement data.

The motivation for the effort to optimize the coils model was to predict the fields inside a human subject properly. Measurements inside the human are not feasible, however, profiles on top of the volunteer in a fix vertical position can be recorded. A comparison with the B_1 profiles above the phantom shows clearly the sensitivity of the axial profiles to the object in the coil. The B_1 fields again show good agreement, however the measured values are about 17 % higher which can be attributed to different coil loading for the human voxel model "Duke" [2] and the volunteer due to different body weight.

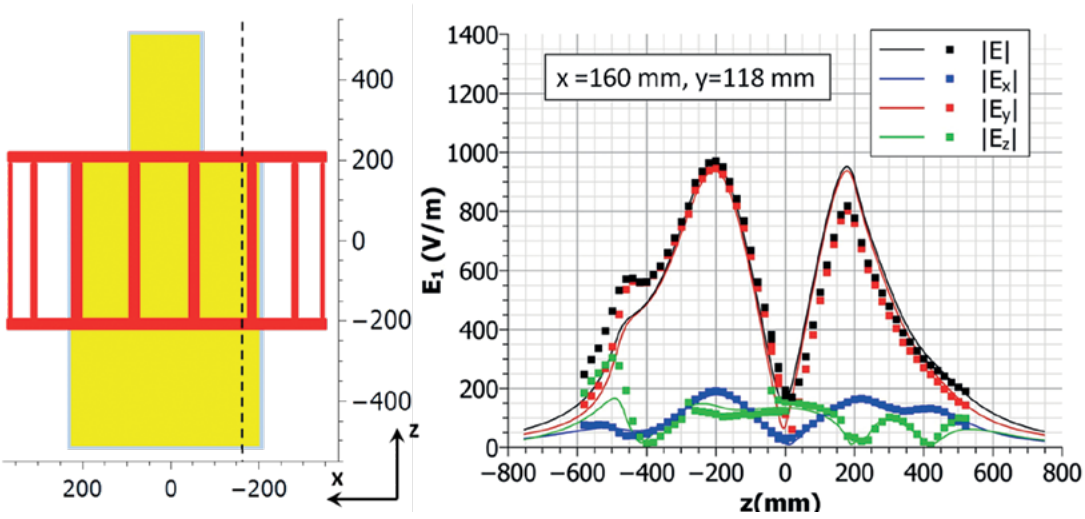

Figure 7: Measured (squares) and simulated (lines) RF *E*-field profiles along the dashed line above the phantom within the body coil (red) for 1 kW of forward power.

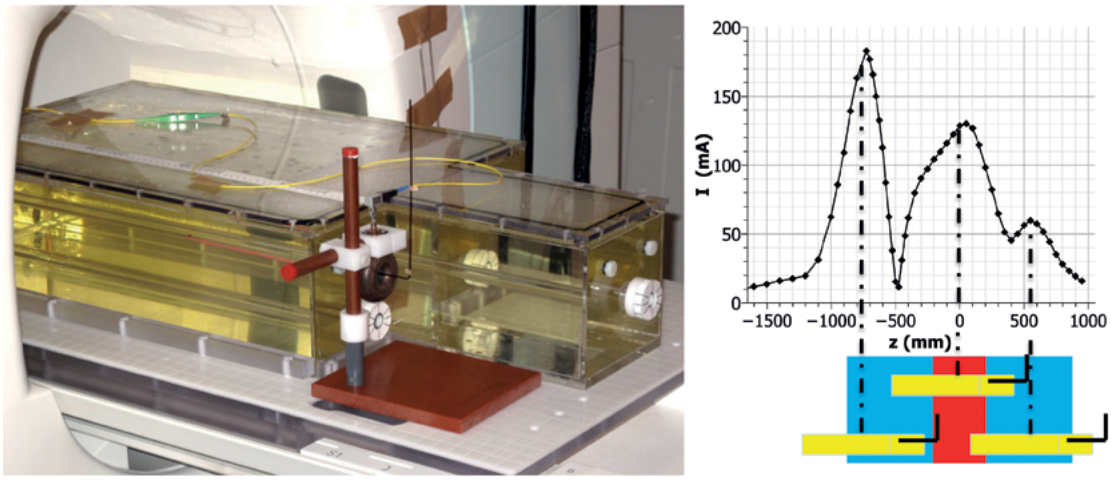

Figure 8:
left: Phantom with wire in the "shoulder" together with current sensor on patient bed of MR scanner; right: Measured RF current in the protruding part of a wire in the "shoulder" of the phantom as a function of the axial position of the phantom inside the MR scanner bore. At the bottom prominent phantom positions are illustrated with sketches of the phantom (yellow) with respect to the range of the body coil (red) and bore (blue) of the MR scanner.

9. Characterization of pTx coils for 3 tesla and 7 tesla MRI

Using the versatile measurement infrastructure we characterized a 3 tesla and two 7 tesla 8-channel pTx head coil arrays. A key result [17] is the determination of the power balance of a commercial 7 tesla 8-channell pTx head coil with internal shielding, including the power radiated into the far field. The maximum radiated power was determined for this coil to be 1 % of overall forward power. The maximum occurs when driving the elements with a phase increment of 45 degrees, i.e. in the circularly polarized mode. This experimental finding is consistent with simulation data [18]. The low portion of radiated power is due to the shielding of the individual elements and simplifies RF safety assessment of this coil.

10. In-situ measurements of RF currents in implanted wires

The RF current at the protruding end of wires implanted in the shoulder and the head of the body phantom was measured [19] as function of the axial position inside PTB's 3 tesla MR scanner (s. Figure 8). The coil was driven with 1 kW of nominal transmitter power. Phantom and sensor were placed on the patient bed and moved through the 45 cm long body coil steps of 5 cm. For each position, the sensor signal was recorded with and without wire to remove residual displacement current signals via complex subtraction. The highest currents were measured for the wire in the "shoulder" of the phantom (about 350 mA). For the wires in the head section of the phantom the maximum currents (about 180 mA) were lower. Distinct currents were measured till the rear edge of the phantom exits the body coil i.e. about 100 mA are measured for the wire in the "shoulder"

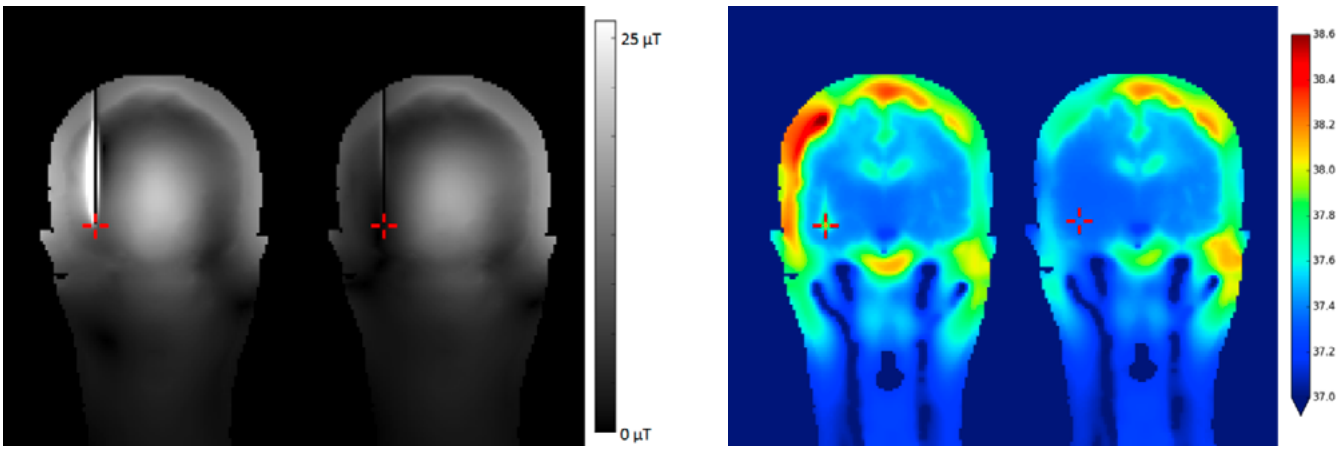

Figure 9:
Left: Coronal maps of $|B_1^+|$ for CP-mode excitation (left) and using the projection method (right) at 1kW of total forward power. $|B_1^+|$ artifacts near the implant are due to induced RF currents. For the projection method these artifacts are effectively suppressed. The red cross indicates the position of the wire's tip. **Right:** Coronal maps of steady state temperature for CP-mode excitation (left) and using the projection method (right) at 20 W of total forward power. No significant implant heating occurs when using the projection method.

when all parts of the wire are already 30 cm outside the coil and about 60 mA are measured for the wire in the head when all parts of the wire are even 60 cm outside the coil.

11. pTx for SAR managing in the presence of metallic implants

PTB developed a new method to control implant heating by transmit array coils. Utilizing the additional degrees of freedom of pTx coil arrays the hazard of excessive local tissue heating due to metallic implants can be mitigated. In this Q-matrix approach [20] the single Q matrix associated with the proximate tissue volume of a metallic implant can be used to determine the "worst case" steering conditions for implant heating. A projection technique is applied to calculate new steering conditions which result in much lower implant heating. The efficacy of this method was demonstrated by EMF and thermal simulations using a 7 tesla 8-channel head coil model (s. Figure 9).

12. Conclusion:

As a major result the established measurement infrastructure allows experimental validation of actual EMF field simulations of real MRI systems within reasonable uncertainty margins. Thus, the locally deposited RF power (peak spatial SAR averaged over 10 g, psSAR10g) can be determined at a much higher level of confidence compared to contemporary safety standards. The measurement methods are suitable for MRI equipment operating from 1.5 tesla to 7 tesla and are independent from MR vendor specific solutions. Furthermore, it can be operated standalone allowing measurements in specific exposure scenarios, e.g. for measurements with implant models. Together with the multi-channel transmit capability (pTx) the measurement infrastructure allows research on future technologies in the field of sensor equipped implants which are capable to communicate with the MR scanner to monitor and mitigate the RF related hazards during MRI examinations.

Acknowledgement:

This work was supported by the European Metrology Research Programme (EMRP; Grant no. HLT06). The EMRP is jointly funded by the EMRP participating countries within the European Association of National Metrology Institutes (EURAMET) and the European Union.

Many current and former members of the MR technology group have contributed to the results presented here. I would especially like to thank Gerd Weidemann, Antonino Cassara, Werner Hoffmann, Harald Pfeiffer, Rainer Seemann, and Bernd Ittermann

References:

[1] International Electrotechnical Commission (IEC): 60601-2-33:2010+AMD1:2013+AMD2:2015, Medical electrical equipment – Part 2–33: Particular requirements for the basic safety and essential performance of magnetic resonance equipment for medical diagnosis.

[2] Christ A, Kainz W, Hahn E G, Honegger K, Zefferer M, Neufeld E, Rascher W, Janka R, Bautz W, Chen J, Kiefer B, Schmitt P, Hollenbach H P, Shen J, Oberle M, Szczerba D, Kam A, Guag J W, and Kuster N, The Virtual Family – development of surface-based anatomical models of two adults and two children for dosimetric simulations, Physics in Medicine and Biology, 55(2) (2010) N23–N38.

[3] 2013 ESC Guidelines on cardiac pacing and cardiac resynchronization therapy, European Heart Journal 34 (2013) 2281 – 2329, doi:10.1093/eurheartj/eht150.

[4] International Organization for Standardization (ISO): Tech. Specif. ISO TS10974, Assessment of the safety of magnetic resonance imaging for patients with an active implantable medical device, second edition, 2018.

[5] ASTM International: F2182-11a, Standard Test Method for Measurement of Radio Frequency Induced Heating On or Near Passive Implants During Magnetic Resonance Imaging.

[6] T. Klepsch, T. D. Lindel, W. Hoffmann, H. Botterweck, B. Ittermann, F. Seifert, Calibration of fibre-optic RF E/H-field probes using a magnetic resonance (MR) compatible TEM cell and dedicated MR measurement techniques, *Biomed. Tech.* vol. 57, Suppl. 1 (2012) 119–122, doi:10.1515/bmt-2012–4428.

[7] G. Weidemann, I. Frese, F. Seifert, A. M. Cassara, W. Hoffmann, B. Ittermann, A system for calibrated measurements of RF electro-magnetic fields inside a clinical MR scanner, *Proc. ISMRM* 22 (2014) 1370

[8] A. M. Cassara, G. Weidemann, F. Seifert, B. Ittermann, Accurate EM modelling of a not-fully accessible RF body coil at 3T for quantitative SAR investigations, *Proc. ISMRM* 22 (2014) 1378

[9] F. Seifert and B. Ittermann, High precision MR-TEM cell for in-situ calibration of RF field probes in clinical MR systems, *Proc. ISMRM* 26 (2018) 1715

[10] Nordbeck, P., Weiss, I., Ehses, P., Ritter, O., Warmuth, M., Fidler, F., Herold, V., Jakob, P. M., Ladd, M. E., Quick, H. H. and Bauer, W. R. (2009), Measuring RF-induced currents inside implants: Impact of device configuration on MRI safety of cardiac pacemaker leads. Magn Reson Med, 61: 570–578. doi: 10.1002/mrm.21881

[11] Etezadi-Amoli M, Stang P, Kerr A, Pauly J, Scott G. Interventional device visualization with toroidal transceiver and optically coupled current sensor for radiofrequency safety monitoring. Magnetic Resonance in Medicine 2014. doi: 10.1002/mrm.25187.

[12] Etezadi-Amoli M, Stang P, Kerr A, Pauly J, Scott G. Controlling radiofrequency-induced currents in guidewires using parallel transmit. Magnetic Resonance in Medicine 2014. doi:10.1002/mrm.25543.

[13] Hagmann MJ, Babij TM . Noninvasive measurement of current in the human body for electromagnetic dosimetry. IEEE Transactions on Biomedical Engineering, 1993;40:418–23, DOI:10.1109/10.243420.

[14] Seifert F, Wübbeler G, Junge S, Ittermann B, Rinneberg H. Patient safety concept for multichannel transmit coils. Journal of Magnetic Resonance Imaging 26 (2007) 1315–1321.

[15] F. Seifert, A. Cassara, G. Weidemann, and B. Ittermann, Reliable and robust RF safety assessment of transmit array coils at ultrahigh fields, Proc. ISMRM 22 (2014) 4891.

[16] F. Seifert, G. Weidemann, and B. Ittermann, Correlation of psSAR and tissue specific temperature for 7T pTx head coils - a large scale simulation study, Proc. ISMRM 23 (2015) 380.

[17] G. Weidemann, F. Seifert, W. Hoffmann, H. Pfeiffer, R. Seemann, B. Ittermann, Measurements of RF power reflected and radiated by multichannel transmit MR coils at 7T, Magn Reson Mater Phy, DOI 10.1007/s10334-016-0551-6.

[18] A. Kuehne, S. Goluch, P. Waxmann, F. Seifert, B. Ittermann, E. Moser, and E. Laistler, Power Balance and Loss Mechanism Analysis in RF Transmit Coil Arrays, Magnetic Resonance in Medicine DOI 10.1002/mrm.25493.

[19] G. Weidemann, F. Seifert, W. Hoffmann, B. Ittermann, RF current measurements in implanted wires in phantoms by fiber optic current clamps, Proc. ISMRM 23 (2015) 1852.

[20] Seifert F, Weidemann G, Ittermann B. Q matrix approach to control implant heating by transmit array coils. Proc. ISMRM 23 (2015) 3212.

Dosimetry in Medical X-ray Imaging

Ludwig Büermann[1]

Abstract

X-ray computed tomography is by far the largest contributor to the radiation burden of patients. Therefore, good clinical practice in medical X-ray imaging requires the quantification of radiation exposure to optimize the image quality in relation to the absorbed dose ratio. This article covers the dosimetry part but not the quantification of image quality. Dose measurements in X-ray imaging are fundamental for two purposes: First, to set and check standards of good practice and second, to assist in assessing detriment or harm. Different application specific dose quantities are defined for general radiography and fluoroscopy, mammography and computed tomography. These provide the basis for quality assurance in X-ray imaging – for example, for acceptance testing, or for application-specific diagnostic reference levels. Non-invasive X-ray multimeters are used for quality control measurements in the beams of diagnostic X-ray devices. The patient dose is usually evaluated as the absorbed dose in organs and tissues from which the risk-related quantity "effective dose" is estimated. The latter quantity allows an estimate of the patient's risk to suffer from stochastic radiation effects. The effective dose is estimated from the measured application-specific dose quantities by use of dose conversion coefficients. These cannot be measured directly. Instead, they are calculated by means of Monte-Carlo simulations using computational reference models of the human body. Alternatively, they can be determined by dose measurements in adequate physical (anthropomorphic) phantoms. Simulations and dose measurements are important requirements for the development of personalized dosimetry in computed tomography.

1. Introduction

A total of around 140 million X-ray examinations were estimated for Germany in 2014. About 60 million of them were dental examinations. The average effective dose per person and year caused by ionizing radiation from natural and artificial sources amounted to about 4 mSv in Germany (estimated in 2016). As much as 40 % of this amount, i.e. 1.6 mSv, originated from X-ray examinations [1]. These numbers make clear how important dosimetry is for quality assurance in X-ray imaging and how important it is, thus, to achieve an acceptable image quality with a minimum dose. For the collective effective dose, it is important to look to the contributions of the different types of X-ray examinations (see Figure 1). The collective dose is the product of the number of persons belonging to the exposed population group and the mean per capita dose. The unit of the collective dose is the "man sievert". What is particularly striking is that although only 11 % of the X-ray examinations are carried out by means of the dose intensive computed tomography (CT) and angiography (including intervention), these represent 81 % of the collective effective dose. In turn, the share of dental examinations amounts to 40 %, causing, however, only 0.4 % of the dose. Valuable conclusions can be drawn from these numbers in terms of particularly high-dose or low-dose examinations. Also, those examination types become obvious where special attention must be paid to quality assurance. While CT dosimetry is already being intensively worked on at PTB, the very dose-intensive interventional procedures [2] could not yet be adequately addressed. Because of the great importance of this area especially with respect to paediatric diagnostic radiology [3] , the PTB is planning a corresponding research program. In section 2 of this article it is briefly described how quality assurance in medical X-ray imaging is

[1] Dr. Ludwig Büermann, Department "Dosimetry for Radiation Therapy and Diagnostic Radiology", email: ludwig.bueermann@ptb.de

achieved. Dose measurements are key for quality assurance and patient dosimetry. Furthermore, such traceable and quality assured dosimetry systems provide reliable dose data such as shown in Figure 1. The underlying dose quantities will be discussed in section 3. Non-invasive X-ray multi meters are used for quality assurance measurements in X-ray imaging. The basic principles of those together with performance requirements on instruments defined in international standards is subject of section 4. Finally, in section 5 special emphasis is given to the steps towards personalised dosimetry in computed tomography.

2. Quality assurance in medical X-ray imaging

The basic components of the quality assurance in medical X-ray imaging are acceptance and constancy tests and the concept of diagnostic reference levels. An acceptance test is carried out after new equipment has been installed, or major modifications have been made to existing equipment, in order to verify compliance with manufacturer's specifications or requirements. A constancy test consists of a series of tests, carried out in order to ensure that the functional performance of the equipment meets established criteria or to enable the early recognition of changes in the properties of components of the equipment. Diagnostic reference levels are defined as dose values for typical examinations with X-rays, related to standard phantoms or to groups of patients with standard dimensions and using with X-ray equipment with suitable examination procedures. Acceptance and constancy tests are performed according to harmonized international standards. Many countries define additional test points and performance criteria according to national requirements which are not part of the international standards. Some typical test points in an acceptance test are patient positioning accuracy, check of dose indication, behaviour of the image detector, image quality (like noise, spatial, high- and low contrast resolution) and automatic exposure control. Acceptance criteria for each of these test points are fixed in the standard. Some of the acceptance test points are also used for constancy tests but with specially defined constancy criteria. The frequency of constancy tests is fixed in the standards with some tests are done daily, others monthly or yearly. In Germany, Austria and Switzerland it is mandatory that dosimeters used for acceptance tests are subject to legal control and require, therefore, an acceptance for verification. In Germany, this is task of the PTB (see section 4). An additional part of quality assurance are the diagnostic reference levels which in Germany are determined and published by the Federal Office for Radiation Protection (*Bundesamt für Strahlenschutz* – BfS). The dose quantities used for this purpose are explained in the next section. The main tasks of PTB in this context are to provide the traceability of the dose quantities, to standardize and realize reference X-radiation qualities, to standardize performance requirements on dosimetric equipment and to offer type testing of diagnostic dosimeters within the framework of the German verification law and verification ordinance.

3. Dose quantities used in medical X-ray imaging

3.1 Fundamental dose quantity air kerma

The fundamental dose quantity used in medical X-ray imaging is air kerma (kinetic energy released per mass) which is given in units of J/kg. The special name for the unit of kerma is gray (Gy). The air kerma equals the absorbed dose in air if conditions of secondary electronic

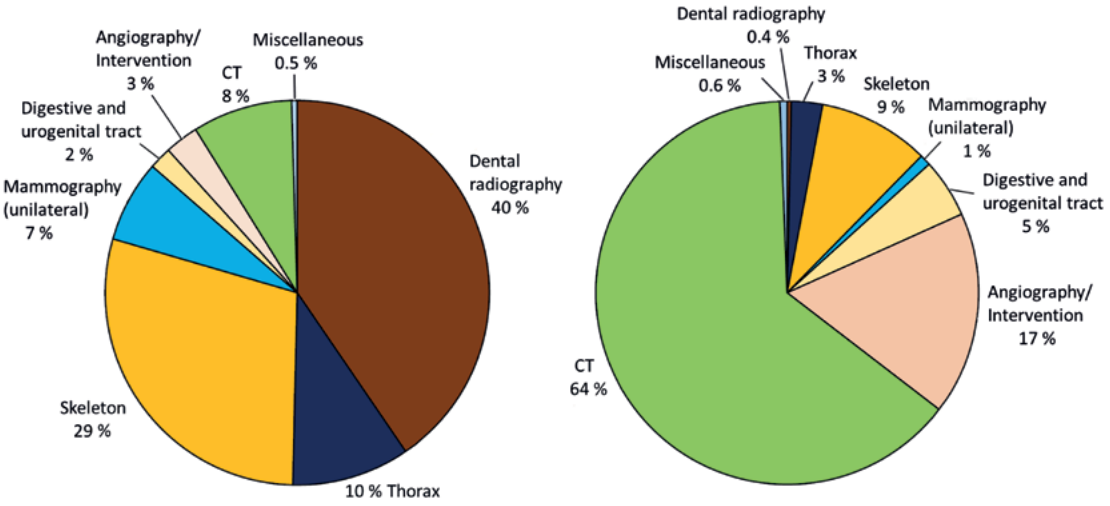

Figure 1: Percentage of the different types of examinations contributing to the overall frequency and to the collective effective dose in Germany in 2014 [1].

equilibrium (SEE) prevail. SEE is approximately present when the X-ray beam has passed a layer of air which dimensions are larger than the mean free path lengths of the secondary electrons released by the photons. Exact definitions of fundamental quantities and units for ionizing radiation are published in the ICRU Report 85 [4]. The unit of air kerma for X-rays is realized with free-air chambers. These measure the ionization current free in air under SEE conditions [5]. The air kerma rate is obtained from the measured ionization current by the conversion factor $W/e \approx 34$ J/C (=eV), where W is the average energy to create an ion pair in dry air (zero relative humidity) and e is the elementary charge. Note that the W-value is defined for electrons only. For photons, an effective W-value is obtained from the spectrum of secondary electrons liberated in air. Fortunately, W/e is constant for electrons with kinetic energies greater than 4 keV [4]. Therefore, the effective W-value is constant for X-rays used in diagnostic radiology.

3.2 Dose quantities used in radiography and fluoroscopy

Application-specific dose quantities are based on air kerma and defined in ICRU Report 74 [7]. Dose quantities used in radiography and fluoroscopy are illustrated in Figure 2.

The incident air kerma is the air kerma from the incident beam on the central X-ray beam axis at the skin entrance of the patient's body. Only the primary radiation incident on the patient or phantom and not the backscattered radiation is included. The entrance-surface air kerma is the incident air kerma with the backscattered radiation included. The air kerma-area product is the integral of the air kerma free-in-air over the area A of the X-ray beam in a plane perpendicular to the beam axis. Diagnostic reference levels in classical radiography and fluoroscopy are given in units of air kerma area product. In mammography, diagnostic reference levels are given in terms of average glandular dose normalized to the incident air kerma. The application-specific risk-related effective dose, E of patients in units of Sievert (Sv) is obtained from the air kerma area product, P_{KA} by multiplication of corresponding conversion factors $c = E / P_{KA}$. These values are used for the estimation of the patient dose values shown in Figure 1. These conversion factors cannot be measured directly. Instead, they are calculated by means of Monte-Carlo simulations using computational reference models of the human body. Alternatively, they can be determined by dose measurements in adequate physical (anthropomorphic) phantoms [7].

3.3 Dose quantities used in computed tomography

The fact that – compared to classical projection radiography – the dose in computed tomography (CT) is clearly higher can be explained as follows: a CT image corresponds to approx. 1000 projections which are recorded during the rotation of the X-ray tube assembly around the patient. Dosimetry in CT is somewhat more complex than in classical radiography. Here, the so-called "CT dose index" (CTDI) is used as the quantity. The CTDI is the line integral of the air kerma along the axis of rotation (z-axis) of the scanner for a single radiator rotation, divided by the total slice thickness in z-direction. The CTDI is indicated in the unit "mGy". The measurement is performed with a pencil-shaped ionization chamber, 100 mm in length, which is also referred to as the "CT chamber" (Figure 3). The CT chamber is calibrated in the quantity "air kerma length product" in the unit "Gy*m". The CTDI is measured both free in air and in cylindrical bodies on the central axis and at four peripheral positions. Cylindrical plexiglass bodies with diameters of 16 cm (head phantom) and 32 cm (body phantom) are in use (Figure 3). The head phantom is used for skull images and in pediatrics, whereas the body phantom is used for examinations on adults in the area of the trunk.

A suitably weighted mean value of the CTDI values measured at the periphery and on the central axis is representative of the mean phantom dose in a slice and is referred to as the "weighted

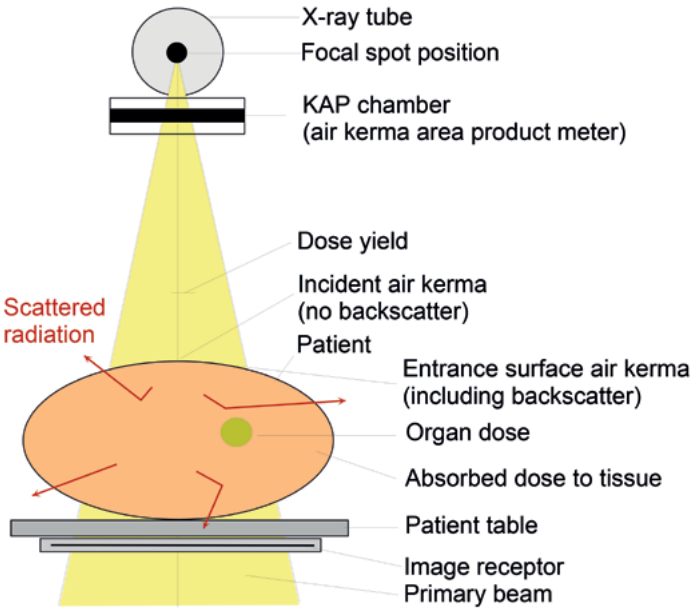

Figure 2: Schematic representation of classical projection radiography and the places where application-specific dose quantities are defined.

CTDI" (abbreviated to: "$CTDI_w$"). Usually, several slices are recorded either in series or spirally, whereby the patient table is moved while the tube is rotating. The ratio between the table's advance during a single radiator rotation and the total slice thickness in z-direction is referred to as the "pitch". Pitch values smaller than 1 thus indicate overlapping slices in CT images. Overlapping slices are associated with an increased dose per slice, which is taken into account by the pitch-corrected $CTDI_w$. This value is also called the "volume CTDI" (abbreviated to: "$CTDI_{vol}$"), or the "effective, weighted CTDI". A measure of the total dose of a scan series is the product of $CTDI_{vol}$ and the scan length L, which is also called the "dose length product" (DLP) of a scan series. For new CT devices, DIN EN 60601-2-44 prescribes the display of the $CTDI_{vol}$ and of the DLP. Common units are "mGy" for the $CTDI_{vol}$ and "mGy*cm" for the DLP. Diagnostic reference levels for CT examinations are given for both quantities, $CTDI_{vol}$ and DLP with relation to either the head or the body phantom [8]. The effective dose *E* of the patient is estimated by multiplication of the DLP with a suitable conversion factor $k = E / DLP$. These conversion factors are calculated by means of Monte Carlo simulations for standard CT scanners and reference patient models [8]. More advanced methods to obtain patient- and scanner-specific dose estimates are presented in section 5.

3.4 Determination of the organ-absorbed dose and of the effective patient dose

The absorbed dose (unit: J/kg = Gy) in tissue or organs is the relevant quantity for the estimation of biological radiation damage. A distinction must be made between deterministic radiation damage and stochastic radiation damage. In X-ray diagnostics, the threshold dose of 0.2 Gy – 0.5 Gy, which may lead to deterministic radiation damage, is usually not reached, except in interventional examinations. The probability of stochastic radiation damage such as, for example, cancer or genetic damage, depends not only on the absorbed dose, but also on the radiation type (e.g. photons, electrons, neutrons, protons or alpha particles) and their energy. To take this fact into account, the absorbed dose is multiplied by so-called "radiation weighting factors", and the equivalent dose is obtained, whose unit (J/kg) is given the special name of "sievert" (Sv) to distinguish it from the physical absorbed dose. As the radiation weighting factor for photons is 1, the equivalent dose in X-ray diagnostics corresponds to the absorbed dose. In addition to the equivalent dose, the probability of stochastic radiation damage also depends on the type of tissue or organ, which is taken into account by the so-called "tissue weighting factors". The effective dose in partial or full-body irradiations is, therefore, obtained as the weighted sum of the equivalent dose to a tissue or organ. Values of the weighting factors for tissue and organs can be found in the literature [9]. As in X-ray diagnostics, the organ-absorbed dose or the tissue-absorbed dose of a patient cannot be measured directly, they are calculated from application-specific dose quantities with the aid of conversion factors. Conversion factors are, in this context, the organ-absorbed dose or the tissue-absorbed dose of a standard patient, normalized (in classical radiography) to the incident dose or the dose area product or (in CT) to the CTDI and DLP [7].In mammography, the conversion factor is obtained as the mean glandular dose normalized to the incident dose [10]. Such conversion factors are calculated almost exclusively with Monte Carlo simulations, in connection with defined models of standard patients [7]. As the determination of the effective patient dose is ultimately based on measurable dose quantities, correct calibration and quality assurance of the dosimeters for radiodiagnostics is of great importance in order to obtain reliable and comparable data.

4. Non-invasive X-ray multi meters used in medical X-ray imaging

Non-invasive X-ray multimeters (NIXMs) are used for quality control measurements in the useful beams of diagnostic X-ray devices. They are designed to measure different X-ray beam

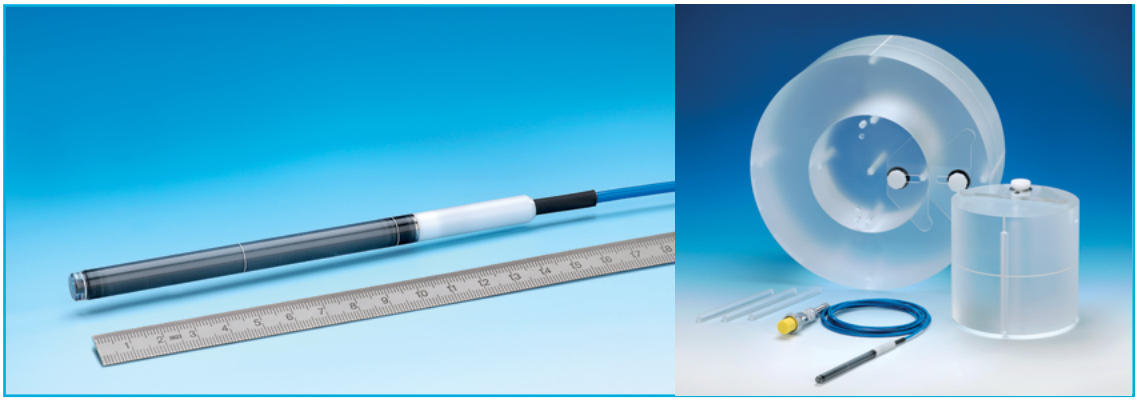

Figure 3:
CT measuring chamber (left) and CT standard phantoms (right). The phantoms are made of plexiglass; they are 14 cm in length and have the following diameters: 16 cm (head phantom) and 32 cm (body phantom).

parameters such as the X-ray tube voltage, the dose, the dose rate, the dose per pulse, the irradiation time, the tube current-time (mAs) product, the waveform, the half-value layer (Quick-HVL) and the total filtration (TF) in a single exposure. The waveform is defined as the tube voltage as a function of time. The HVL is the thickness of an absorber material (usually aluminium) which attenuates the dose rate by a factor of two. The total filtration is the equivalent aluminium thickness the primary X-ray beam must penetrate from the focal spot to the patient. NIXMs are mainly used in general radiography, fluoroscopy and mammography. Some instruments have been developed for applications in computed tomography (CT). This section includes brief descriptions of the basic principles, general components, calibrations, international standards and independent performance tests, as well as future challenges.

4.1 Basic principles

NIXMs are based on at least two semiconductor sensors covered with metal filters of different thicknesses. If irradiated with X-rays of a certain quality generated with conventional X-ray tubes, the sensor signals are proportional to the energy fluence rates ("beam intensities") transmitted. Thus, ratios of the different sensor signals are directly correlated to parameters that characterize the X-ray beam quality such as peak tube voltage (kVp) and total filtration. Knowledge of the X-ray quality makes it possible to correct the signal measured for the non-ideal energy dependence of the semiconductor sensors with respect to the quantity of air kerma. High signal sampling rates (kHz range) enable the system to record kVp as a function of time (waveform), from which the quantity practical peak voltage (ppV [11]) is deduced. The practical peak voltage is based on the concept that radiation generated by high voltage of any waveform produces the same contrast as radiation generated by an equivalent constant potential. Furthermore, it is possible to measure the exposure time as well as other quantities derived from it such as the dose per pulse and the mean pulse dose rate.

4.2 General components and calibration

A typical modern non-invasive X-ray multimeter is composed of one or more detector units, a signal processor unit, system software and an indicator unit. Either all these components form a single instrument or they are combined with other electronic devices (computers or tablet) to supplements to them. Furthermore, different devices (or detector units) may be offered for special applications in radiography, fluoroscopy, mammography and computed tomography. Calibrations are usually performed at the manufacturer site or at accredited calibration laboratories over periods of one or two years.

4.3 International performance standards

There is no general international performance standard for NIXMs. Instead, one standard defines requirements concerning the dose and dose rate measuring channels of a given NIXM (IEC 61674 [12]), while another standard defines requirements concerning the measuring channel for the non-invasive measurement of the tube voltage (IEC 61676 [11]). There are no performance standards for non-invasive measurements of TF, Quick HVL or exposure time. Standard X-ray qualities for testing NIXM devices are defined in IEC 61267 [13]. Increasing attention is being devoted to requirements concerning the system software where NIXMs are used to perform measurements that are subject to legal regulations (e.g. WELMEC Guide 7.2 of the European cooperation in legal metrology).

4.4 Independent performance tests

In most cases, manufacturers indicate the compliance of their NIXMs with two standards: IEC 61674 [12] (dose/dose rate) and IEC 61676 [11] (tube voltage). However, no international standards exist for the other quantities measured by these devices. Only a small number of publications exist, in which independent performance tests of NIXMs have been conducted; most of these publications deal with the performance of the dose/dose rate or tube-voltage indications as a function of different influence parameters [14]. In Germany, diagnostic dosimeters are covered by the Verification Act if used for legal dose measurements such as acceptance tests of medical X-ray devices. For this reason, such dosimeters need to be type tested by the Physikalisch-Technische Bundesanstalt (PTB). Such type tests are based on the requirements in the IEC 61674 [12] standard for the hardware components and the WELMEC Guide 7.2 [15] for the software components.

4.5 Future challenges

Within the field of future NIXM developments, one of the most potentially challenging issues is finding a way to adapt them to accommodate the continual improvements and occasional technical changes to X-ray imaging modalities

(e.g. digital breast tomosynthesis, contrast-enhanced dual energy mammography and cone beam CT). Adaptation to new radiation qualities and improvements in the angular response will be necessary. Real-time in-phantom dose probes based on semiconductors may also be a topic for future applications.

5. Procedure for personalized dosimetry in computed tomography

5.1 Patient dosimetry in computed tomography

Patient dosimetry in Computed Tomography (CT) is currently based on two quantities, obligatorily indicated by any CT Scanner: The volume computed tomography dose index ($CTDI_{vol}$) and the dose-length product (DLP)[8] (section 3). The estimation of stochastic radiation risk, expressed in terms of the effective dose (E), is obtained by $E = k \cdot DLP$, where k is a calculated region-specific normalized effective dose conversion coefficient. However, this way of CT-dose estimation has a lot of shortcomings and is not suitable for CT-scanner- and patient-specific dose estimates. Therefore, a procedure was developed, which opens the gate to personalized CT dosimetry.

The aim of this work was to lower the high uncertainties of the effective dose estimates for one organ from 20 % – 50 % to significantly lower levels of 10 % – 20 % and to establish and verify a general procedure for patient-specific dose estimates (PSDE) in computed tomography (Figure 4). The procedure is based on the calculation of the post-scan 3D dose distributions within the exposed parts of the patient's body using the commercially available software package "ImpactMC" [16]. This package enables the users to perform a fast Monte Carlo simulation of the complete scan. Inputs needed for such a simulation are the reconstructed CT-image (DICOM file) of the patient and anthropomorphic model extensions for scatter contribution, the scanner source model and the actual scan protocol parameters. Quick automatic organ segmentation in the 3D CT image is a challenge but seems to be solved by machine learning based approaches [17]. Scanner simulation with Monte Carlo methods need special input data like the CT-X-ray source model including the permanent and bow tie filtrations. The permanent filtration for modern CT scanners usually consists of 1 mm to 3 mm aluminium with an additional flat filter of 0.1 mm copper, giving a total filtration of between 6 mm and 9 mm of aluminium equivalent. The bow-tie filters are beam shaping filters which reduce unnecessary patient absorbed dose by matching the filter shape to the patient size and clinical application. These data are usually confident and not available. Therefore, it was necessary, to develop a non-invasive measurement procedure and equipment in order to obtain so-called "equivalent source models" (5.2). Next it was necessary to verify the obtained simulated 3D dose distributions by measured values (5.3). This work was done within the EMPIR programme 15HLT05, "Metrology for multi-modality imaging of impaired tissue perfusion". Following partners were involved: PTB, STUK (Säteilyturvakeskus, Radiation and Nuclear Safety Authority of Finland) and HUS (Helsingin Yliopisto, Helsinki University Central Hospital, Medical Imaging Center). PTB provided its research CT scanner (Optima 660, GE-Healthcare) and developed and tested a mobile equipment for equivalent source determinations. STUK was experienced in the use of the Monte Carlo simulation of CT-scans with the software package ImpactMC and CT chamber measurements. HUS had the clinical environment for real CT perfusion studies and provided different scanner types for measurements with the mobile equipment and anthropomorphic phantoms. Additional measurements were performed at the local hospital (*Städtisches Klinikum Braunschweig*).

5.2 Determination of equivalent CT source models in clinical environments

An essential part of the scanner needed for the simulation are the X-ray beam properties, i.e. the tube characteristics described by the emitted photon fluence spectrum, the fixed filtration and the beam shaping filter, usually called "bow tie" (BT) filter. Photon fluence spectra and the material and shape of the BT-filter are usually not known or proprietary information. However, non-invasive

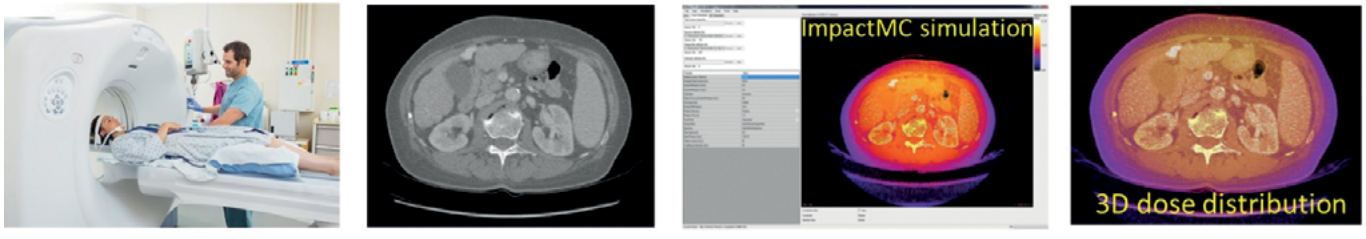

Figure 4:
General procedure to determine scanner- and patient specific dose estimates in CT (from left to right): CT-scan of the patient (1), organ segmentation in CT image (2), 3D dose map from CT-scan simulation (3), organ and effective dose determination (4).

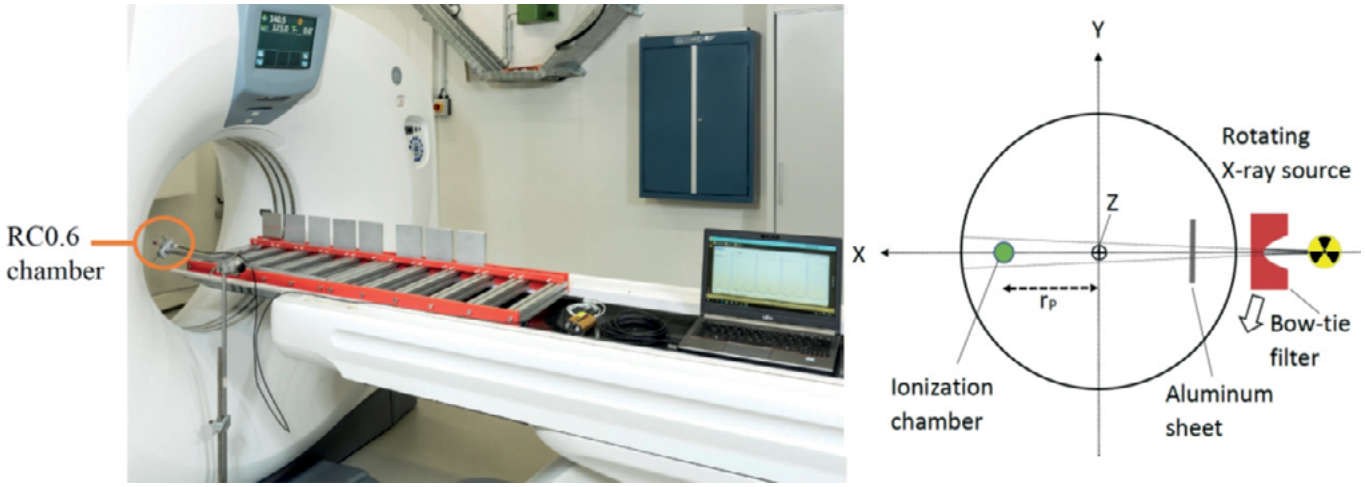

Figure 5: Mobile measurement setup. With this setup, aluminum attenuation curves and form filter characteristics can be investigated that allow the computation of equivalent CT source models. Aluminum sheets of increasing thickness are placed on the patient table, while the dose rate is measured with an ionization chamber and time-resolved readout. The schematic drawing on the right illustrates the attenuation measurement when the source, the aluminum sheet and the ionization chamber are aligned.

experimental methods are available to determine at least a good approximation to the X-ray spectra and material equivalent representations of the BT-filters. These data usually designated as "equivalent source models" can then be used as inputs to the MC simulation program. The task was to develop, construct and verify a mobile apparatus and the corresponding evaluation software for the non-invasive determination of equivalent source models that are well suited for on-site measurements at CT machines in a clinical environment. PTB developed such a mobile equipment as shown in Figure 5 and described in more detail in [18, 19]. The special set up and use of the hardware at a CT and a software guide is described in an internal technical report.

This mobile system allows application in clinical environments for fast measurement of aluminum half value layer thickness to calculate the X-ray spectra for different anode voltages. Short preparation and measurement times and the minimal amount of hardware that is needed are the big advantages of the system. Custom software has been developed which allows for fast analysis of the data within few minutes to obtain the spectra. In addition, the data is used for the construction of equivalent bow-tie geometries using the characterization of bow-tie relative attenuation [20] (COBRA) method. Within one measurement series both HVL measurements as well as COBRA data are collected without the need of rearranging the system. Results of equivalent source models measured with the mobile equipment at four different scanner types located at PTB, Städtisches Klinikum Braunschweig and HUS in Helsinki are shown in Figure 6. The reproducibility of the approach has been tested by comparing the estimated values for the equivalent aluminum thickness to be less than 4 %. Further, the implementation of the COBRA algorithm into the software is tested by comparing the attenuation curves with the ones obtained from static measurements [21].

5.3 *Experimental verification of calculated 3D dose distributions*

The next task was to verify calculated 3D dose

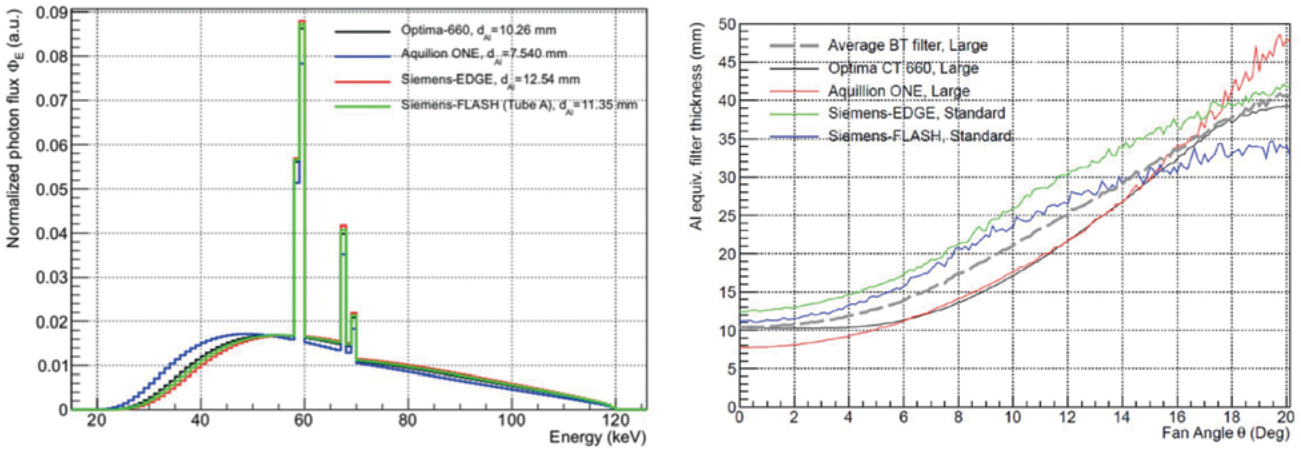

Figure 6:
Left: Photon fluence spectra of different CT scanner types. The photon fluence spectra of the clinical CT scanners is calculated using Al attenuation measurements with the mobile measurement system and the SpekCalc [22] software for determination of photon spectra for tungsten anode material. Right: Aluminum equivalent bow tie filters of four different CT machines.

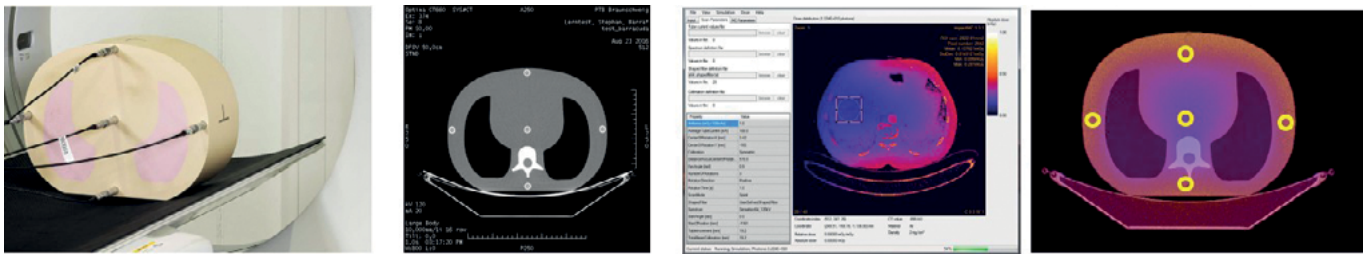

Figure 7:
Procedure to verify calculated 3D dose distributions in anthropomorphic phantoms after the CT-scan by in-phantom dose measurements (from left to right): CT-scan of the phantom equipped with five dose probes (1), region segmentation in CT image (2), 3D dose map from CT-scan simulation (3), dose determination at five positions and comparison with measurements(4).

distributions by measurements with dosimeters in anthropomorphic phantoms at different scanner types. The following steps were required (Figure 7): (1) Determine the equivalent source model of the used scanner type using the mobile equipment developed by PTB; (2) scan the phantom with the embedded dosimeters and measure the dose; (3) simulate the scan with ImpactMC [16] and determine the dose at the positions of the embedded dosimeters. Measurements were done at four different scanner types: GE Optima 660 (PTB), Toshiba (Canon) Aquilion ONE (Städtisches Klinikum Braunschweig), Siemens SOMATOM Definition Edge (HUS) and Siemens SOMATOM Definition Flash (HUS). The relative standard uncertainties of the dose measurements were in the range 1 % to 2 % and those of the calculations between 3 % for axial and 8 % for helical scans. A typical result is shown in Table 1 (taken from [19]). In general, measured and calculated dose values inside the phantoms were within the range of uncertainties of 5 % to 10 %. The procedures are applicable to any scanner type under clinical conditions. Results show that these are well suited for verifying CT x-ray source models needed for personalized CT dosimetry based on post-scan Monte Carlo calculations. The procedures could be part of a potential acceptance test if personalized CT dosimetry is integrated in future CT scanners.

6. Conclusion

In Germany, about 40 % of the average effective dose per person and year caused in total by ionizing radiation from natural and artificial sources amounts from X-ray imaging. This number makes clear how important a traceable dosimetry is for quality assurance and patient dose estimations in X-ray imaging. The main components of quality assurance are acceptance and constancy testing according to international standards as well as diagnostic reference levels published by national authorities. The underlying dose quantities can be divided in the fundamental quantity air kerma, the air kerma-based application-specific quantities used in general radiography and fluoroscopy, mammography and computed tomography, and the risk-related quantity effective dose. The latter is obtained from the application-specific quantities by multiplication of a usually calculated dose conversion factors. The most important measuring instruments for quality control measurements in the useful beams of diagnostic X-ray devices are non-invasive X-ray multimeters. Performance requirements on such devices are fixed in international standards as well as standard X-ray qualities for calibrating and testing. The PTB contributes significantly to the quality assurance in X-ray imaging by realization and dissemination

Table 1.
Results of measurements and simulations of the air kerma length product in an anthropomorphic phantom at the Toshiba Aquilion ONE using a spiral scan mode. The dose values at the five positions of the "Thorax-Medium Adult" anthropomorphic phantom are measured with a 100 mm pencil-type ionization chamber (PTW) and compared to simulated values from ImpactMC. The scan parameters have been set to spiral mode, covering 8 cm with 100 mA a rotation time of 0.5 s and a nominal collimation of 40 mm.

Voltage (kV)	Position	Measured (mGy cm / 100 mAs) σ_c = 3.3 %	Siumulated Dynamic method (mGy cm / 100 mAs)	Difference %
120	12 o'c	75.20	76.17	1.3
	3 o'c	61.49	63.03	2.5
	6 o'c	63.85	66.54	4.2
	9 o'c	61.02	60.14	–1.5
	center	46.00	49.42	7.4

of the fundamental dose units, definition and realization of standard X-ray qualities, definition and standardization of requirements on dosimetric instruments and drafting of international dosimetry protocols. Further, the PTB is responsible for type testing of diagnostic dosimeters. X-ray computed tomography and interventional procedures are by far the largest contributors to the radiation burden of patients. Therefore, these two modalities need special attention in research and development. The PTB has a research program for personalized dosimetry in computed tomography. Viable procedures were developed for the verification of personalized dosimetry in computed tomography using Monte Carlo-based simulations. Future research shall be devoted to the dosimetry for interventional procedures, digital breast tomosynthesis, contrast-enhanced dual energy mammography and cone beam CT.

Acknowledgement

The CT dosimetry project (section 5) has received funding from the EMPIR programme 15HLT05, "Metrology for multi-modality imaging of impaired tissue perfusion". The EMPIR initiative is co-funded by the European Union's Horizon 2020 research and innovation programme and the EMPIR Participating States.

References

[1] BMU/BfS. Umweltradioaktivität und Strahlenbelastung im Jahr 2016 (Parlamentsbericht). *Drucksache 19/5350*. 2018. https://www.bmu.de/DL2123.

[2] López PO, Dauer LT, Loose R, et al. ICRP Publication 139: Occupational Radiological Protection in Interventional Procedures. *Ann ICRP*. 2018;47(2):1–118. doi:10.1177/0146645317750356

[3] Khong P-L, Ringertz H, Donoghue V, et al. ICRP Publication 121: Radiological Protection in Paediatric Diagnostic and Interventional Radiology. *Ann ICRP*. 2013. doi:10.1016/j.icrp.2012.10.001

[4] ICRU report 85: fundamental quantities and units for ionizing radiation (Revised). *J ICRU*. 2011;11(1):33–33. doi:10.1093/jicru/ndr004

[5] Burns DT, Büermann L. Free-air ionization chambers. *Metrologia*. 2009;46(2). doi:10.1088/0026-1394/46/2/S02

[6] Büermann L, Grosswendt B, Kramer H-M, et al. Measurement of the x-ray mass energy-absorption coefficient of air using 3 keV to 10 keV synchrotron radiation. *Phys Med Biol*. 2006;51(20):5125-5150. doi:10.1088/0031-9155/51/20/004

[7] ICRU Report No. 74. Patient Dosimetry for X Rays Used in Medical Imaging. *J Int Comm Radiat Units Meas*. 2005;5(2):iv-vi. doi:10.1093/jicru/ndi018

[8] Boone JM, Brink JA, Edyvean S, et al. ICRU Report 87: Radiation dose and image-quality assessment in computed tomography. *J ICRU*. 2012;12(1):9-149. doi:10.1093/jicru/ndt006

[9] ICRP. The 2007 Recommendations of the International Commission on Radiological Protection. ICRP publication 103. *Ann ICRP*. 2007;37(2–4):1-332. doi:10.1016/j.icrp.2007.10.003

[10] DeLuca PM. ICRU Report No.82: Mammography – Assessment of Image Quality. *J ICRU*. 2009;9(2):NP.3-NP. doi:10.1093/jicru/ndp030

[11] International Electrotechnical Commission. IEC 61676: Medical Electrical Equipment—Dosimetric Instruments for Non-Invasive Measurements of X-ray Tube Voltage in Diagnostic Radiology.

[12] International Electrotechnical Commission. IEC 61674: Medical Electrical Equipment – Dosimeters with Ionization Chambers and/or Semiconductor Detectors as Used in X-ray Diagnostic Imaging.

[13] International Electrotechnical Commission. IEC 61267: Medical Diagnostic X-ray Equipment—Radiation Conditions for Use in the Determination of Characteristics.

[14] Büermann L, Böttcher R. Performance test of multi-parameter measuring devices used for quality assurance in diagnostic radiology. *Proc an Int Symp Stand Appl Qual Assur Med Radiat Dosim (IDOS 2010)*. 2010;2:33.

[15] WELMEC. WELMEC 7.2 Software Guide. 2015;2015:1-114.

[16] Chen W, Kolditz D, Beister M, Bohle R, Kalender WA. Fast on-site Monte Carlo tool for dose calculations in CT applications. *Med Phys*. 2012;39(6):2985–2996. doi:10.1118/1.4711748

[17] Sharma S, Kapadia A, Fu W, Abadi E, Segars WP, Samei E. A real-time Monte Carlo tool for individualized dose estimations in clinical CT. *Phys Med Biol*. 2019;64(21). doi:10.1088/1361-6560/ab467f

[18] Rosendahl S, Büermann L. Dynamic determination of equivalent CT source models for personalized dosimetry. *Curr Dir Biomed Eng*. 2017;3(2):791–794. doi:10.1515/cdbme-2017-0167

[19] Rosendahl S, Büermann L, Borowski M, et al. CT beam dosimetric characterization procedure for personalized dosimetry. *Phys Med Biol*. 2019;64(7). doi:10.1088/1361-6560/ab0e97

[20] Boone JM. Method for evaluating bow tie filter angle-dependent attenuation in CT: Theory and simulation results. *Med Phys*. 2010;37(1):40–48. doi:10.1118/1.3264616

[21] Alikhani B, Büermann L. Non-invasive experimental determination of a CT source model. *Phys Medica*. 2016;32(1):59–66. doi:10.1016/j.ejmp.2015.09.006

[22] Poludniowski G, Landry G, DeBlois F, Evans PM, Verhaegen F. SpekCalc: a program to calculate photon spectra from tungsten anode x-ray tubes. *Phys Med Biol*. 2009;54(19):N433–8. doi:10.1088/0031-9155/54/19/N01

Image Quality Assessment for CT and Mammography

Mathias Anton[1], Tobias Kretz[2], Marcel Reginatto[3], Clemens Elster[4]

Abstract

Mammography and computed tomography are modalities of medical imaging involving ionizing radiation. The choice of applied dose is determined by a tradeoff between the quality of the images and possible risks to the patient. Established measures of image quality assume linearity and shift-invariance of the imaging system, but the application of these measures is problematic due to the development of improved imaging systems that violate these assumptions.

Task-specific image quality assessment using model observers provides a promising alternative which has become increasingly popular. This approach assesses image quality based on the ability of a mathematical or human observer to successfully solve a clinically relevant task using images which can be obtained by means of technical phantoms. Current questions of research in this field include the design of appropriate technical phantoms, the development of efficient mathematical observers, and the evaluation of the uncertainty of the mathematical observers.

In 2016, PTB started research in this field, which may be viewed as being in between medical research and classical metrology. One of the goals is to include uncertainty evaluation in the mathematical model observers in line with current standards in metrology, and to foster current efforts in reaching standardized procedures for the application of task-based image quality assessment in computed tomography and mammography. Another aim of this research is to apply modern techniques of data analysis, including deep learning, to improve image quality assessments. This paper presents some of the results of this research.

1. Introduction

X-ray computed tomography (CT) and mammography using x-ray radiation are two important imaging techniques applied in clinical practice. While they provide valuable diagnostic information, these techniques result in health risk to the patient through the applied radiation dose. In Germany, for example, CT contributes a significant part of the overall radiation exposure to the population [1]. For CT or mammography, the higher the applied dose, the better the image quality and thus the higher the confidence of diagnosis; however, the potential risk to one's health also increases with increasing doses. The choice of dose thus poses a tradeoff, and reliable assessment of image quality is needed to optimally balance this tradeoff.

Established measures of image quality such as the modulation transfer function and noise power spectrum assume that the imaging system is linear and shift-invariant [2]. These strong assumptions are violated in modern CT imaging systems [3] and in mammography that uses nonlinear iterative reconstruction algorithms, image filters and sophisticated post-processing data analysis techniques [4]. Task-based image quality assessment [2] provides an alternative to these classical methods. In task-based image quality assessment, a clinically relevant task is considered, such as the detection of a lesion, and image quality is assessed through the ability to successfully solve this task either by a human observer or a mathematical model observer. Throughout the paper, we will restrict ourselves to mathematical model observers and will simply call them model observers. Technical phantoms such as the CDMAM phantom [5] for mammography or the Catphan® phantom for CT [6] are often used in the context of image quality assessment. In its simplest form, a binary classification task

[1] Dr. Mathias Anton, Department "Dosimetry for Radiation Therapy and Diagnostic Radiology", email: mathias.anton@ptb.de

[2] Tobias Kretz, Departments "Dosimetry for Radiation Therapy and Diagnostic Radiology" and "Mathematical Modelling and Data Analysis", email: tobias.kretz@ptb.de

[3] Dr. Marcel Reginatto, Department "Neutron Radiation", email: marcel.reginatto@ptb.de

[4] Dr. Clemens Elster, Department "Mathematical Modelling and Data Analysis", email: clemens.elster@ptb.de

is posed, e.g., absence or presence of a specific signal in an image. The widely used "channelized Hotelling observer" satisfies certain optimality properties for the binary classification task [2], and some of the results in this paper will refer to this popular observer. The performance of a model observer can be characterized through its receiver operating characteristic (ROC) curve, and the area under the ROC curve, AUC, is often taken as the single, final Figure of merit. A European guideline [7] makes a proposal for the assessment of image quality in mammography. The approach is based on so-called contrast-detail curves which determine how well small structures can be detected in the images of the CDMAM phantom. The data analysis involved in this procedure will be discussed in connection with recent results achieved at PTB.

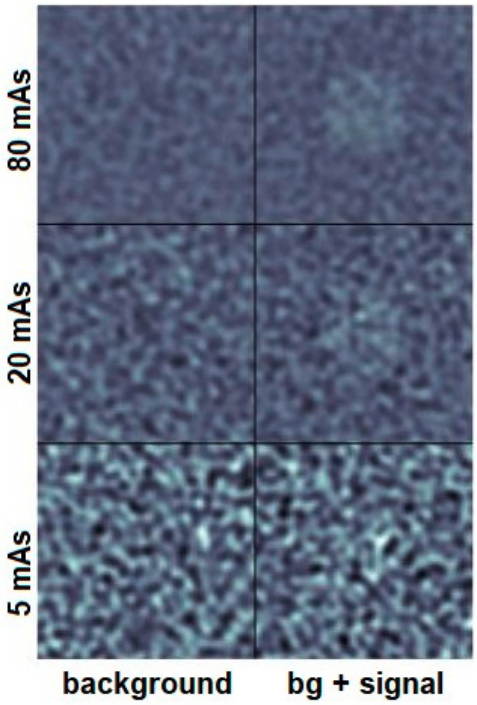

Figure 1:
Parts of CT images of a low-contrast PTB-phantom showing a region with (right) and without (left) a signal to be detected. The applied dose increases from bottom to top. Averages over 10 images are displayed.

Any Figure of merit for the quality of (phantom) images needs to be accompanied by an uncertainty quantification. This is essential to compare results of different imaging systems, or to reliably decide whether an imaging system meets required levels of image quality. So far, uncertainties have been calculated on the basis of classical statistics (e.g. [8]). However, in metrology, the basis for harmonized uncertainty evaluation (the GUM [9]) is closely related to a Bayesian view on measurement uncertainty (e.g. [10]).

Image quality assessment of CT and mammography requires the characterization of measurement devices, which is a typical task in metrology, and the application of model observers is closely related with computer-aided diagnosis, a field of medical research that is rapidly growing. Task-based image quality assessment can thus be viewed as lying on the interface between medical research and classical metrology. In 2016 PTB started a research collaboration in the field of image quality assessment in CT and mammography between the divisions "Ionizing Radiation" (Braunschweig) and "Medical Physics and Metrological Information Technology" (Berlin). PTB's engagement will contribute actively to the formation of generally accepted standards in this field, which is highly relevant given the potential risks of radiation dose. In its research, PTB has so far concentrated on uncertainty quantification using a Bayesian approach as well as on the design of novel model observers. Currently, PTB is engaged in an attempt to further develop novel model observers as well as in the application of deep learning to image quality assessment.

The paper is organized as follows. Section 2 introduces the task of binary classification, together with a brief discussion of the channelized Hotelling observer. The section then describes the Bayesian uncertainty analysis developed by the PTB [11, 12] for characterizing the results of

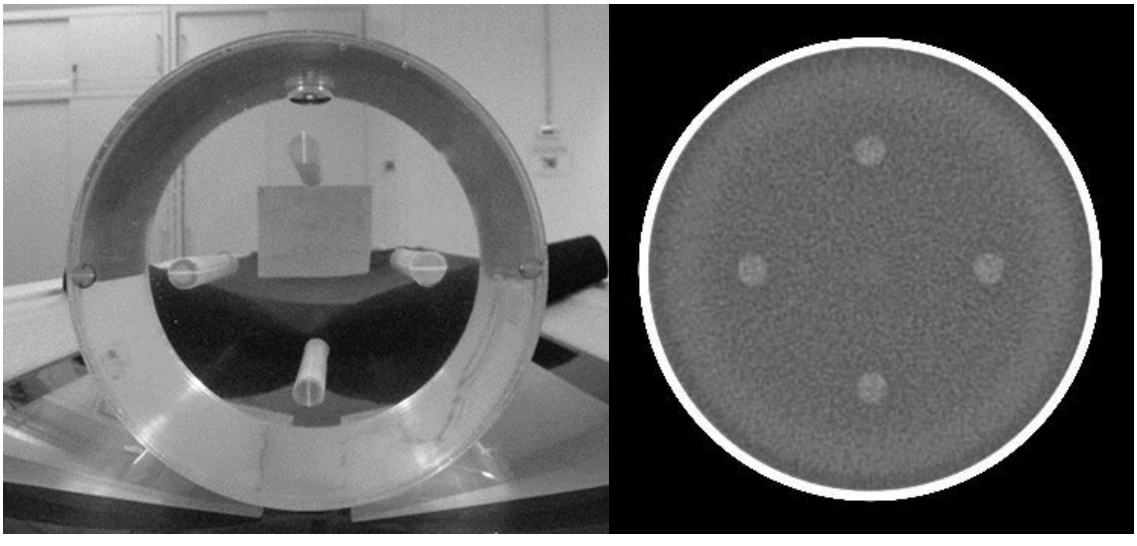

Figure 2:
PTB low-contrast phantom (left) and its CT image (right).

the channelized Hotelling observer. In Section 3, a parametric model observer developed at PTB [13] is presented and its gain in efficiency examined through comparing it with the channelized Hotelling observer. The parametric model observer is applied in the context of the EUREF guideline procedure for mammography quality assurance with the result that the number of required images can be reduced by about a factor of 3 with the parametric model observer [14]. Finally, Section 4 provides an outlook on current and forthcoming research at PTB in the field of image quality assessment for CT and mammography.

2. Bayesian uncertainty analysis for the channelized Hotelling observer

Figure 1 illustrates a simple exercise of task-based image quality assessment. The Figure shows parts of CT images of a low-contrast PTB-phantom (Figure 2) for varying dose. Images on the right include a signal in the center. While for large doses the signal is visible, one can hardly see a signal for the low doses. Through application of a binary model observer this difference in image quality can be quantified in an objective way.

The channelized Hotelling observer uses several (typically a few hundred) images with (class 1) and without (class 2) signal. These images are used to estimate the means of the two classes and the assumed common covariance matrix. The term "channelized" refers to the fact that the raw images are projected on pre-selected channels before carrying out the analysis. The channels are chosen in such a way that they reflect properties of the human visual system, see [2]. Typically, about 10 channels are used, with the result that the images are projected onto low-dimensional vectors. The Bayesian uncertainty analysis developed for the channelized Hotelling observer does not depend on the choice of channels, and it could in principle be applied likewise for the Hotelling observer itself. An assumption underlying the channelized Hotelling observer is that the images in the two classes can be modeled as multivariate normal with a common covariance matrix. The latter assumption is also referred to as the small signal assumption. The AUC of the ideal channelized Hotelling observer is given by

$$\mathrm{AUC} = \Phi(\mathrm{SNR}/\sqrt{2}) \qquad (1)$$

where

$$\mathrm{SNR}^2 = (\theta_1 - \theta_2)^T V^{-1} (\theta_1 - \theta_2) \qquad (2)$$

Φ denotes the distribution function of the standard normal distribution. The two vectors θ_1 and θ_2 denote the means of the assumed normal distributions in the two classes of images, i.e. θ_1 denotes the mean of all images with signal, and θ_2 the mean of all images without signal. The matrix denotes the covariance matrix V which is assumed to be the same for the class of images with and without signal. The AUC quantifies the ability of the observer to correctly distinguish between images with and without signals. It can be interpreted as the probability of correctly distinguishing between randomly selected images with and without signal. The AUC varies between 0.5 (pure guessing) and 1 (sure decision).

Since the parameters θ_1 and θ_2 and V are generally not known, equation (1) cannot be directly applied. The parameters θ_1 and θ_2 and V can be estimated using labeled training data of both classes. These estimates are then plugged into equation (1) to provide an estimate of AUC. In [8] this procedure has been analyzed and exact 95 % confidence intervals have been constructed. A 95 % confidence interval for AUC will cover the true value of AUC in 95 % of the cases when applied under repeated sampling. A single 95 % confidence interval, however, does not allow for any probabilistic statement about the true value of AUC.

In Bayesian inference, one combines the prior knowledge about all unknowns with the information contained in the data. Technically, one applies Bayes' theorem to derive the posterior distribution for all unknowns [15]. In our case, these unknowns constitute the parameters θ_1 and θ_2 and V. The final posterior distribution of the AUC can be calculated from the posterior of the parameters θ_1 and θ_2 and V using relation (1) and applying the change-of-variables transformation of probability calculus. Bayesian inference typically requires carrying out expensive calculations which are usually performed with Markov chain Monte Carlo (MCMC) methods [16].

PTB has developed a Bayesian inference of AUC given the data from a labeled training set. The approach makes use of a particular noninformative prior which leads to analytical results concerning the (conditional) posterior distribution. In using the analytical results, it is possible to sample the posterior for AUC in a simpler way than by applying conventional MCMC methods. Specifically, independent samples from the posterior can be obtained by a simple Monte Carlo procedure, see [12] for further details. Figure 3 shows the resulting posterior for AUC using 800 images for each of the cases illustrated in Figure 1. In all cases high mean values for AUC result. As expected, the larger the dose the higher the resulting mean of AUC, and the distributions also become narrower. The whole posterior distribution characterizes the state of knowledge about AUC, and hence the posterior can be viewed as the most comprehensive uncertainty characterization. While it is possible to derive

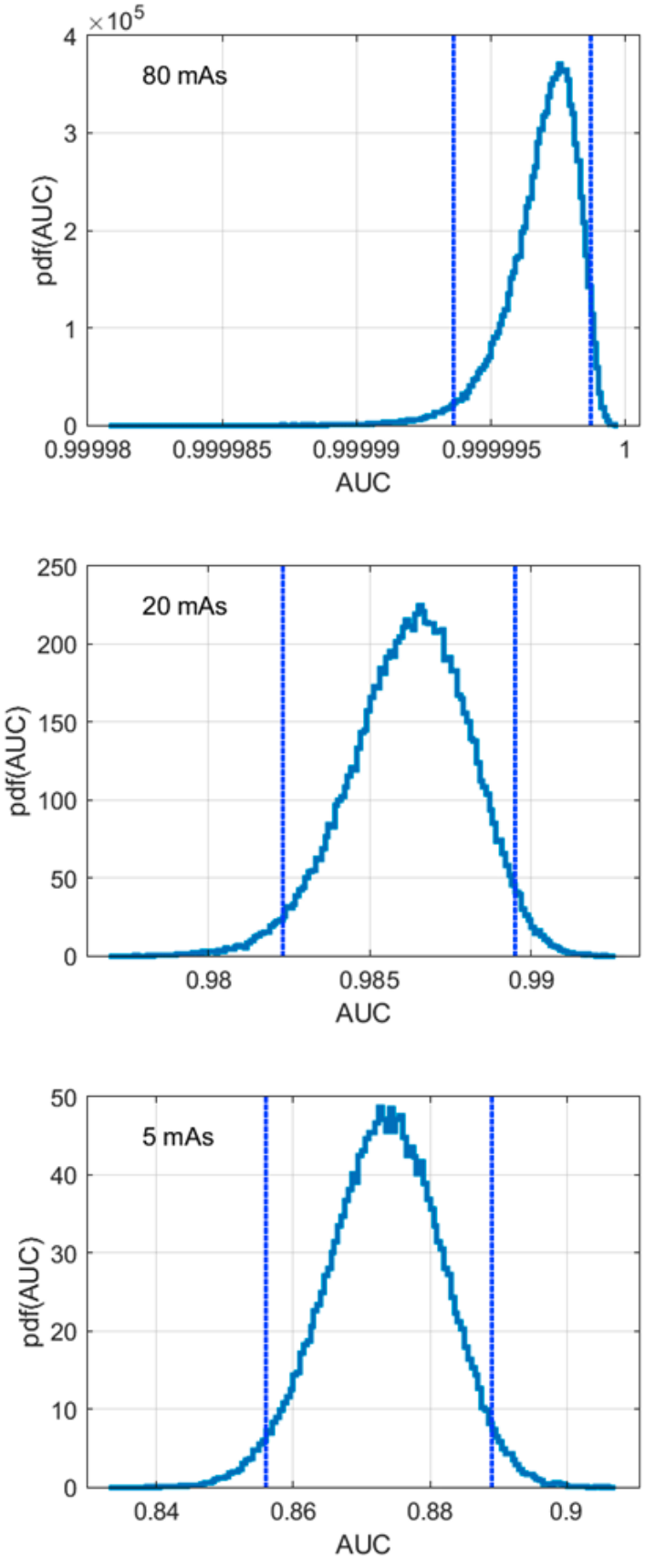

Figure 3:
Posterior distributions for AUC on the basis of 800 images for each of the cases illustrated in Figure 1.

summary statistics such as the posterior mean as an estimate, or the posterior standard deviation as the standard uncertainty associated with the posterior mean, note that the distributions in Figure 3 are generally not symmetric, in which case such simple summary statistics are not comprehensive enough. The posterior distribution can be used to calculate the probability that the AUC exceeds a certain threshold. In general, the number of training images will affect the width of the posterior distribution, i.e. the larger the training data set, the smaller the width. For example, if it is required that the AUC is above 0.92, and that such a requirement ought to be verified with at least 99 % probability, then the case presented in the top of Figure 3 would not satisfy these requirements. However, when increasing the training data, the width of the posterior will shrink and possibly the imaging system would then pass such a check. Note that distributions like those shown in Figure 3 would not result from a conventional uncertainty analysis based on classical statistics which does not allow probability statements to be made based on the observed training images.

3. Parametric model observer

3.1 Basics of approach

Technical phantoms such as the Catphan® phantom (The Phantom Laboratory, Salem, NY, USA) or the CDMAM phantom [5] consist of simple geometries. This information is not utilized by nonparametric observers like the Hotelling observer. PTB has started to develop parametric model observers that can be more efficient when used in combination with technical phantoms with simple geometries. Figure 4 illustrates the basic idea for a simplified situation. The observed image is modeled as a superposition of a known signal template and a known background template. A model observer based on this parametric model may be defined, with an AUC given by

$$\mathrm{AUC} = \Phi(\sqrt{n_1}\,|\,\theta_1 - \theta_2|/(\sigma\sqrt{2})) \qquad (3)$$

where θ_1 and θ_2 denote the (unknown) scaling of signal and background template, σ stands for the (unknown) standard deviation of the assumed white Gaussian noise, and n_1 is the number of pixels in the signal template, see [13] for details. In contrast to the AUC of the channelized Hotelling observer in (1), only three parameters need to be estimated. Recall that θ_1 and θ_2 in equation (1) refer to vectors, while in equation (3) they are scalars. It follows that (much) fewer images are needed to reliably estimate the AUC in (3) than for

the channelized Hotelling observer. Furthermore, the AUC in (3) can basically be estimated from the images containing a signal, thus two classes of images are no longer required. We refer to [13] for further details, including a Bayesian estimation procedure and the procedure of combining multiple images in the analysis.

3.2 Application to virtual mammography

Potential benefits of the parametric model observer have been explored for image quality assessment in mammography using x-ray radiation. The EUREF guideline [7] describes a procedure that is currently applied for routinely checking the quality of mammography devices. According to this procedure, at least 16 images of the CDMAM phantom need to be recorded and subsequently analyzed. The analysis consists of constructing so-called contrast-detail curves which quantify how well small structures on the CDMAM phantom can be detected. The estimation of the contrast-detail curves is based on a logistic regression of (the sum of) binary outcomes of an automated observer applied to a set of images. Each binary outcome refers to a successful / unsuccessful detection of a structure in a specific region of a single image. The uncertainty of the sum of the binary outcomes follows a binomial distribution, and the final uncertainty thus depends essentially on the number of images taken. Since the single structures show a simple geometry, the parametric model observer developed at PTB can be utilized to replace the model observer used by the EUREF guideline.

In order to explore the potential benefit of using the parametric observer, PTB has developed virtual mammography (cf. Figure 5 and [14]). The simulation tool produces synthetic mammography images which have been successfully compared with real mammograms of the CDMAM phantom [14]. Synthetic mammograms have the advantage of a known ground truth and can thus be used for exploring the potential benefit of the parametric model observer in the context of the EUREF guideline procedure. Figure 6 shows resulting contrast-detail curves when applying the EUREF guideline procedure and its proposed alternative using the parametric model observer. Repeating the virtual mammography image quality assessment several times for randomly varying images shows that both contrast-detail curves are consistent with each other. Furthermore, the observed accuracy is roughly the same for both procedures. However, 16 images were used for the EUREF guideline procedure, and only 5 for the proposed alternative [14]. The parametric model observer can thus help to significantly reduce the effort in standard mammography quality assurance.

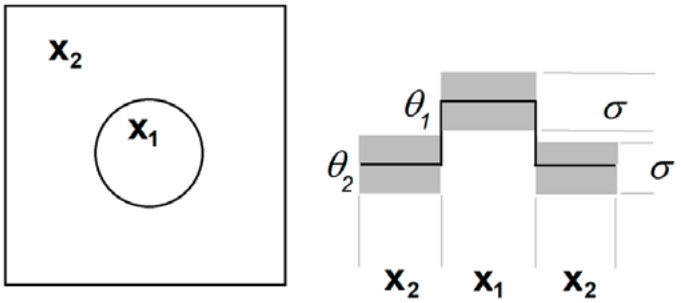

Figure 4:
Illustration of the concept used for the parametric model observer. The magnitudes of the signal region and of the background region are modeled by two parameters, assuming the same noise level of observations in the two areas.

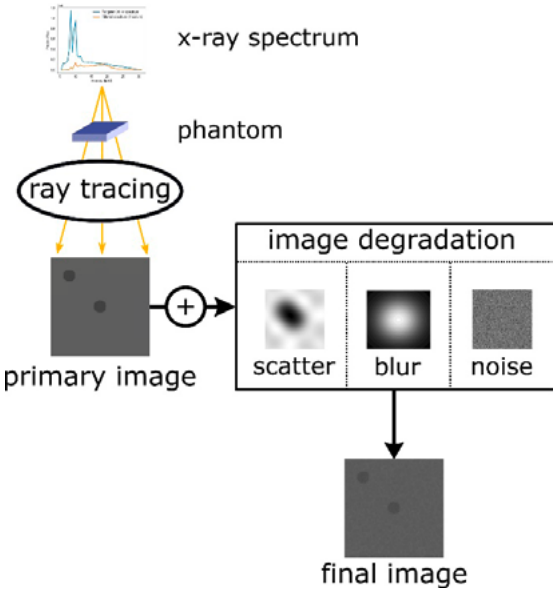

Figure 5:
Flow chart of virtual mammography.

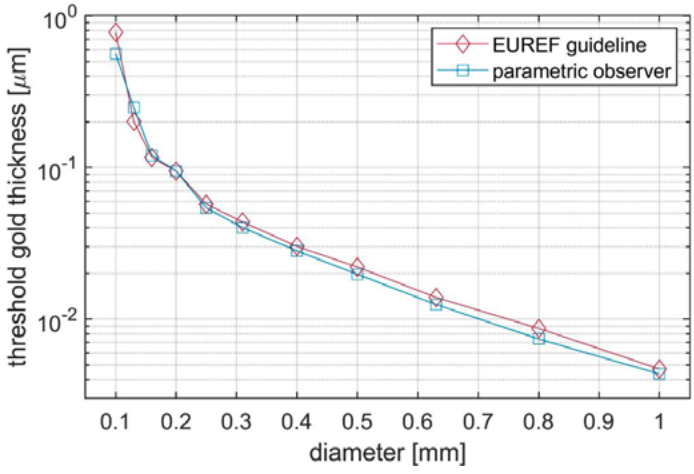

Figure 6:
Resulting contrast-detail curves obtained by the EUREF guideline procedure with 16 images (red), and by the proposed modification using the parametric observer with only 5 images (blue).

Outlook

The parametric model observer presented in this paper, when applied in conjunction with technical phantoms showing simple geometries, allows for a more efficient estimation of the image quality in terms of AUC than established non-parametric observers. For mammography image quality assessment this can yield savings in effort of up to a factor of three. In the context of CT image quality assessment, however, the parametric model observer needs to be refined to better correlate with results of human observers. First investigations showed that for CT data the white noise model underlying the parametric model observer as well as the clear distinction between signal and noise region need to be improved. Furthermore, the two parametric schemes can prove to be too simple for other technical phantoms. For these reasons PTB is currently extending the parametric model observer to a general regression observer. First results indicate that this development leads to results for CT that correlate well with those of human observers.

Another route of current research followed at PTB is the use of deep learning for image quality assessment in mammography. The idea is to train a convolutional neural network (CNN) to learn the mapping from the mammograms to the contrast-detail curve directly from the images. Ultimately, the mapping ought to be applied on a single-image basis, which would make it highly useful for daily routine quality assurance. The virtual mammography developed at PTB plays an important role in this context by providing a huge database of CDMAM images with known ground truth for training the CNN. First results in this direction look very promising.

In 2020 PTB will be launching another project to explore the potential of deep learning methods for quality assessment of CT and mammography with the aim to replace observers for CT with neural networks.

Starting in 2016, PTB has successfully established a network of experts from academia working in the fields of image quality assessment for CT / mammography and deep learning. Some of these experts will be involved in carrying out the forthcoming PTB project on assessing methods from deep learning for medical imaging. The established network also includes representatives of committees responsible for future guidelines and standards for image quality assessment. Through these experts, as well as through the membership of PTB in relevant committees of metrology such as the Consultative Committee for Photometry and Radiometry (CCPR), the long-time goal of establishing widely accepted standards and guidelines for image quality assessment in CT and mammography shall be reached.

References

[1] Bundesamt für Strahlenschutz (BfS) 2016 Umweltradioaktivität und Strahlenbelastung im Jahr 2014: Unterrichtung durch die Bundesregierung—Parlamentsbericht 2014 Technical Report Bundesministerium für Umwelt, Naturschutz, Bau und Reaktorsicherheit (BMUB).

[2] Barrett HH and Myers KJ. Foundations of Image Science. New York: Wiley, 2003.

[3] Vaishnav JY, Jung WC, Popescu M, Zeng R and Myers KJ. Objective assessment of image quality and dose reduction in CT iterative reconstruction Med. Phys. 41 071904, 2014.

[4] Rojas LJ, Fausto AM, Mol AW, Velasco FG, Abreu POS, Henriques G and Furquim TAC. Optimization of the exposure parameters in digital mammography using contrast-detail metrics. Physica Medica, 42, 13–18, 2017.

[5] Bijkerk K, Lindeijer J and Thijssen M. The CDMAM-Phantom: a contrast-detail phantom specifically for mammography. Radiology, 185, 395, 1993.

[6] Goodenough DJ, Levy JR and Kasales C. 1998. Development of phantoms for spiral CT-presented as a scientific paper and scientific exhibit at the 1996 Annual Meeting of the Radiological Society of North America Comput. Med. Imaging Graphics 22 247–55, 1998.

[7] Perry N and Puthaar E. European guidelines for quality assurance in breast cancer screening and diagnosis. Eur Commun, 2006.

[8] Wunderlich A, Noo F, Gallas BD and Heilbrun ME. Exact confidence intervals for channelized Hotelling observer performance in image quality studies IEEE Trans. Med. Imaging 34 453-64, 2015.

[9] BIPM, IEC, IFCC, ILAC, ISO, IUPAC, IUPAP, OIML. Evaluation of Measurement Data-Guide to the Expression of Uncertainty in Measurement. Joint Committee for Guides in Metrology, JCGM 2008;100:2008.

[10] Elster C. Bayesian uncertainty analysis compared with the application of the GUM and its supplements. Metrologia, 51, S159–S166, 2014.

[11] Reginatto M, Anton M and Elster C. Assessment of CT image quality using a Bayesian approach. Metrologia, 54, S74-S82, 2017

[12] Khanin A, Anton M, Reginatto M and Elster C. Assessment of CT image quality using a Bayesian framework. IEEE Transactions on Medical Imaging,37, 2687–2694, 2018, 2019

[13] Anton M, Khanin A, Kretz T, Reginatto M and Elster C. A simple parametric model observer for quality assurance in computer tomography. Phys. Med. Biol., 63,5011, 2018.

[14] Kretz T, Anton M, Schäffter T and Elster C. Determination of contrast-detail curves in mammography image quality assessment by a parametric model observer. Physica Medica, 62, 120–128, 2019.

[15] Gelman A, Carlin JB, Stern HS and Rubin DB. Bayesian Data Analysis. Chapman and Hall/CRC Texts in Statistical Science, London: Chapman and Hall, 2003.
[16] Robert C and Casella G. Monte Carlo statistical methods. Springer Science & Business Media, 2013.

Doping mit Wachstumshormon – zuverlässig nachgewiesen durch Massenspektrometrie

Höher, schneller, weiter … Dieses Motto ist Ansporn vieler Leistungssportler, um noch größere Höchstleistungen zu erbringen. Leider beschränken sich manche Athleten dabei nicht bloß auf präzise abgestimmtes Training und Ernährung, sondern greifen zu unerlaubten leistungssteigernden Substanzen. Die neue massenspektrometrische Analysemethode der PTB verspricht mehr Zuverlässigkeit im Nachweis von Doping mit Wachstumshormon.

Technische Beschreibung

Menschliches Wachstumshormon (hGH) ist eine körpereigene Substanz, die in natürlichem Rhythmus innerhalb weniger Stunden zwischen sehr niedrigen und höheren Werten (im Serum etwa 0,1–30 ng/mL) im Körper variiert. Eine erhöhte hGH-Konzentration allein eignet sich daher höchstens bedingt als Befund zum Doping-Nachweis. Vielmehr macht man sich die Tatsache zunutze, dass bei Einnahme der klassischen hGH-Doping-Variante (22-kDa-hGH), das natürliche Verhältnis der körpereigenen hGHs charakteristisch gestört wird. Die von der WADA zugelassenen Testverfahren werden von beschuldigten Athleten vor Gerichten angezweifelt.

Die Besonderheit des neuen PTB-Verfahrens besteht darin, dass die einzelnen Varianten des Wachstumshormons praktisch zweifelsfrei anhand ihrer massenspektrometrischen „Fingerabdrücke“ unterschieden und die Mengenverhältnisse auch an der Untergrenze der natürlichen Konzentration noch zuverlässig genug bestimmt werden können. Dazu werden spezifische Abschnitte ausgewählter anderer hGH-Formen ebenso vermessen und in das Verhältnis zu 22kDA hGH gesetzt. Eine „Verwechslung“ ähnlicher im Körper vorkommender Protein-Moleküle ist somit, nicht mehr möglich.

Das Verfahren besteht aus verschiedenen Nachweisroutinen und ermöglicht erstmals Massenspektrometer zum sicheren Nachweis von Doping mit hGH einzusetzen.

Wirtschaftliche Bedeutung

Derzeit werden international jährlich 250.000–300.000 Doping Kontrollen durchgeführt. In diesem Segment verspricht das vorgestellte Verfahren eine signifikant verbesserte Zuverlässigkeit im Nachweis von hGH-Doping.

Entwicklungsstand

Vorläufige Ergebnisse aktueller Versuchsreihen bestätigen die Wirksamkeit des Verfahrens. Ein Patent steht zur Lizenzierung zur Verfügung.

Doping mit Wachstumshormon-Massenspektrometrie verspricht mehr Zuverlässigkeit im Nachweis

Vorteile:

- signifikant verbesserter Nachweis von hGH im relevanten Konzentrationsbereich von 0,1–30 ng/mL
- Validierung unsicherer Ergebnisse anderer Untersuchungsmethoden

Ansprechpartner:

Andreas Barthel
Innovationsmanager
Telefon: +49 531 592-8307
Telefax: +49 531 592-69-8307
E-Mail: andreas.barthel@ptb.de

Dr. Cristian Arsene
Arbeitsgruppe Bio-organische Analytik

PTB-Nummer 0356

Generativ gefertigte Halterung (schwarz) der Flusskapillare mit spiralförmigem Aufbau beim Einsetzen in das MPS

Selektive Charakterisierung magnetischer Nanopartikel

Die Magnetpartikelspektroskopie (MPS) ist ein hochempfindliches und schnelles magnetisches Messverfahren zur Quantifizierung und Charakterisierung magnetischer Nanopartikel. Erstmals wurde die MPS mit einem chromatografischen Trennverfahren kombiniert, um MNP direkt während ihrer größenselektiven Fraktionierung magnetisch zu charakterisieren.

Technische Beschreibung

Zur Kopplung der MPS an chromatografische Trennverfahren wurde ein Konzept für eine Flusszelle erarbeitet. Diese besteht aus einer Kapillare, die den sensitiven Bereich der Empfängerspule des Spektrometers durch spiralförmige Windungen optimal ausnutzt. Bauartbedingt sind laminare Strömungsbedingungen über einen weiten Flussgeschwindigkeits-Bereich gewährleistet. Die technische Umsetzung erfolgte durch eine im 3D-Druck erstellte, leicht austauschbare Haltervorrichtung für Kunststoffkapillaren. Im Anwendungsfall befindet sich die Flusszelle im MPS und ist in eine Detektorkette (Konzentrations- und Größenbestimmungsdetektoren (DLS, MALS)) eingebunden. Diese Multidetektor-Plattform ist direkt einer Größenfraktionierung (A4F) nachgeschaltet. Durch diese geschickte Kombination aus empfindlicher magnetischer Messtechnik und etabliertem Größenbestimmungsverfahren während der größenselektiven Fraktionierung wird der Zusammenhang zwischen Partikelgröße und magnetischem Verhalten auf schnelle und effektive Weise erkennbar. Dies trägt letztlich zu einem besseren Verständnis der Wirkweise von MNP in biomedizinischen Anwendungen bei.

Vorteile:

- hochempfindliche magnetische Charakterisierung strömender Nanopartikelsuspensionen
- laminare Strömungsbedingungen, keine Durchmischung in der Flusszelle
- Zusammenhang zwischen Partikelgröße und Magnetismus direkt erkennbar
- einfache Integration in Multidetektor-Plattformen

Wirtschaftliche Bedeutung

Durch den neuartigen Ansatz ist die magnetische Analyse von MNP nach Trennparametern (z. B. Größe, Dichte, Leitfähigkeit) aufgeschlüsselt möglich. Das Verfahren besitzt großes wirtschaftliches Potential, da bestehende Multidetektor-Plattformen um einen hochsensitiven magnetischen Detektor erweitert werden können.

Entwicklungsstand

Eine Trennung nach hydrodynamischer Partikelgröße und gleichzeitiger Multidetektor-Charakterisierung (UV, DLS, MALLS und MPS) wurde erfolgreich an kommerziellen medizinischen Nanopartikelsystemen (Endorem®, Feraheme®, Resovist®) demonstriert. Das Verfahren wurde zum Patent angemeldet.

Ansprechpartner:

Dr. Bernhard Smandek
Technologietransfer
Telefon: +49 531 592-8303
Telefax: +49 531 592-69-8303
E-Mail: bernhard.smandek@ptb.de

Dipl.-Ing. Norbert Löwa
Arbeitsgruppe Biomagnetismus

PTB-Nummer 0408

Label- und hämolysefreie Vollblut-Differenzierung in mikrofluidischen Sensoren mittels AC-Impedanz

Die quantitative Untersuchung von Zellen im Blut mittels Durchflusszytometrie ist ein routinediagnostisches Verfahren in der Hämatologie. Durch die neue PTB-Technologie kann jetzt die zuverlässige Messung der Konzentration der Subpopulationen von Leukozyten mittels AC-Impedanz ohne Hämolyse durchgeführt werden. Somit ist erstmalig eine zuverlässige Vollblut-Differenzierung unter anderem auch bei Leukämiepatienten möglich.

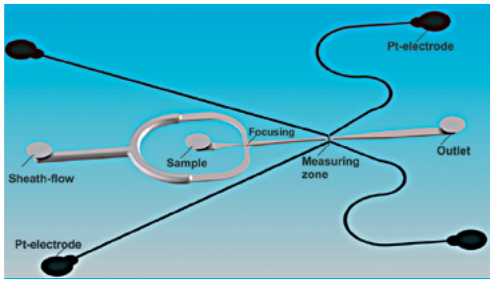

Das µFCM (micro flow cytometer) mit Durchflusskanal und für die AC-Messung erforderliche Elektroden

Technische Beschreibung

Die Neuigkeit der Erfindung besteht darin, die Differenzierung der drei Leukozyten-Untergruppen allein durch AC-Impedanzmessungen durchzuführen. Als Präparation der Probe ist ausschließlich eine geeignete Verdünnung notwendig, um die Zählraten der Zellen an die elektronischen Baugruppen und die Datenerfassung anzupassen. Die hämolysefreie Blutprobe wird über ein Mikrokanal-System in ein Wechselspannungsfeld eines Sensors zur Messung der elektrischen Impedanz durchgeleitet (typisch 1 bis 10 kHz).

Durch verschiedene Impedanz-Werte können auf diese Weise die darin enthaltenen Blutkörperchen (Erythrozyten, Thrombozyten und Leukozyten) bestimmt werden. Die Subpopulationen von Leukozyten (Lymphozyten (Ly), Monozyten (M) und Granulozyten (Gn)) können ebenfalls zuverlässig bestimmt werden.

Vorteile:

- Vollblut-Differenzierung ohne Hämolyse
- zuverlässige Konzentrationsbestimmung
- kostengünstiges Verfahren

Wirtschaftliche Bedeutung

In der Hämatologie ist die Konzentrationsbestimmung von Blutkörperchen ein wichtiges diagnostisches Hilfsmittel und wird auf labormedizinischer Ebene verwendet. Weitere potentielle Anwendungen betreffen die Differenzierung und Konzentrationsbestimmung von Zellen bei onkologischen und immunologischen Fragestellungen sowie die Untersuchung von Algen in Bioreaktoren.

Entwicklungsstand

Das System wurde ausführlich auf Laborebene getestet. Eine deutsche Patentanmeldung ist anhängig. Lizenzen für die Nutzung dieser neuen Methode sind verfügbar.

Ansprechpartner:

Dr. Bernhard Smandek
Technologietransfer
Telefon: +49 531 592-8303
Telefax: +49 531 592-69-8303
E-Mail: bernhard.smandek@ptb.de

Dr. Jörg Neukammer
Durchflusszytometrie und Partikel Analysis

PTB-Nummer 0422

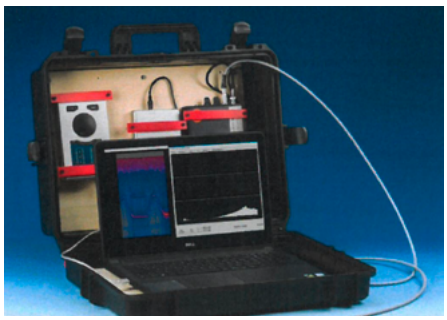

Funktionsmodell des Messkoffers mit handelsübli-chen Komponenten. Am Ende des grauen Kabels befindet sich der Ultra-schallmesswandler

Ultraschallpegelmesssystem

Die Zahl der deutschen Arbeitsplätze, an denen mit Ultraschall gearbeitet wird, ist durch den zunehmenden Einsatz von Ultraschall-reinigungsanlagen, Schweiß- und Schneidemaschinen stetig steigend. Um zu der gesetzlich geforderten Gefährdungsbeurteilung dieser Arbeitsplätze zu gelangen ist es erforderlich den Lärm an diesen Arbeitsplätzen zu messen und zu beurteilen. Derzeitige Messmetho-den sind hier ungenügend. Das Ultraschallpegelmesssystem ist für den mobilen Einsatz ausgelegt und entspricht den Bedingungen an den praktischen Einsatz an Arbeitsplätzen und ermöglicht gleichzei-tig eine rückführbare Messung.

Vorteile:

- Rückführbare Messung von Ultraschall
- Mobil einsetzbar
- Steigender Arbeitsschutz
- Bessere Gefährdungs-beurteilung

Technische Beschreibung

Das für den mobilen Einsatz ausgelegte Messsystem wird den Lärm an ultraschallbelasteten Arbeitsplätzen mit spezifizierter Unsicherheit messen können. Das Messsystem basiert aus einer Kombination von Einzelkomponenten (Hardware) wie z. B. Mikrofon, AD-Wandler, Vor-verstärker und Computer und einer zugehörigen Spezial-Software. Die Software kann die geforderten Messgrößen unter Berücksichtigung der belegten Messunsicherheit und dem Zeitverhalten zuverlässig erfassen. Darüber hinaus können Spektrogramme, Fouriertransformationen und Fraktionierungen in Oktavintervallen grafisch dargestellt werden.

Wirtschaftliche Bedeutung

Das neue Messsystem bietet neuartige Möglichkeiten für eine exakte mobile Messung von Ultraschallpegeln am Arbeitsplatz. Aufgrund der im industriellen Bereich steigenden Nutzung von Ultraschallgeräten wird eine zuverlässige Kontrolle der Ultraschallpegel immer wichtiger. Gerade die Möglichkeit Ultraschall mobil messen zu können eröffnet ein weites Spektrum an Nutzungsmöglichkeiten der neuen Technologie. Berufsgenossenschaften und Unfallversicherung haben ein großes Inte-resse an einer Verwendung des Messsystems, um eine bessere Gefähr-dungsbeurteilung betroffener Arbeitsplätze gewährleisten zu können.

Entwicklungsstand

Das Verfahren wurde bereits getestet und ein erstes Funktionsmuster für den Messeinsatz wurde entworfen.

Ansprechpartner:

Andreas Barthel
Innovationsmanager
und Patentreferent
Telefon: +49 531 592-8307
Telefax: +49 531 592-69-8307
E-Mail: andreas.barthel@ptb.de

Dr. Christoph Kling
Arbeitsgruppe Geräuschmesstechnik

PTB-Nummer 0462

Mobiler Messstand für Röntgenstrahlerprüfungen

Röntgenstrahler müssen während der Entwicklung, der Zertifizierung und zur Qualitätskontrolle auf ihre Gehäusedurchlassstrahlung überprüft werden, wobei der unerwünschte Austritt von Strahlung (bei abgedecktem Nutzstrahl) der entscheidende Parameter ist. Für ihre eigene, gesetzliche Aufgabe der Bauartprüfung hat die PTB einen mobilen Messstand für die Prüfung von Röntgenstrahlern aufgebaut. Mit diesem Messstand können vor Ort zuverlässige Dosisleistungsmessungen in einem festen Abstand von 1 m vom Brennfleck einer Röntgenröhre durchgeführt werden.

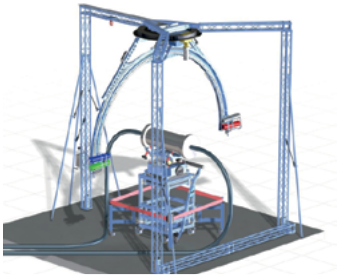

Schematische Darstellung des mobilen PTB- Messstandes für Röntgenstrahlerprüfungen

Technische Beschreibung

Der Messstand kann demontiert und in einem normalen Kleinbus transportiert werden. Errichtet auf den drei Pfeilern (siehe Bild), besteht der Messstand aus einem Messtisch für die präzise Positionierung des Röntgenstrahlers sowie einem „C-Bogen“, der um den Fokus der Röntgenröhre rotiert. Auf diesem C-Bogen bewegen sich vier Dosimeter in vertikaler Richtung auf einem Halbkreis, vertikale und horizontale Abtastungen (Scans) werden durch einen eingebetteten Mikroprozessor gesteuert. Die Spursegmente sind mit hochgenauen mechanischen Schnittstellen verbunden, wodurch kleine Messunsicherheiten gewährleistet werden.

Mit diesem Aufbau ist ein Raumwinkel von mehr als 2 π in einem Scan zugänglich. Die Drehung des zu prüfenden Röntgenstrahlers um 180° führt zu einer vollständigen und überlappenden Prüfung des zu untersuchenden Strahlers.

Mit diesem Messstand können geometrische Konstruktionsfehler von Röntgenstrahlern nachgewiesen und lokalisiert werden.

Die PTB hat diesen Messstand für Röntgenstrahlerprüfungen für ihre eigenen gesetzlichen Aufgaben konstruiert und setzt ihn für mobile und stationäre Dosisleistungsmessungen der Gehäusedurchlassstrahlung (Leckstrahlung) von Röntgenstrahlern ein.

Wirtschaftliche Bedeutung

Die Untersuchung von Röntgenstrahlern sowie der Nachweis möglicher Strahlungsaustrittsstellen ist für Anwendungen in der Medizin, der Industrie und der Forschung von hoher Relevanz.

Entwicklungsstand

Zwei mobile Messstände für Röntgenstrahlerprüfungen sind in der PTB im Einsatz. Lizenzen für mechanische und elektronische Komponenten sind verfügbar.

Vorteile:

- Vor-Ort-Messung von Dosisleistungsprofilen von Röntgenstrahlern
- Raumwinkel: 4 π
- Dosisleistung: µSv/h bis Sv/h
- durch modularen Aufbau einfach transportierbar

Ansprechpartner:

Dr. Bernhard Smandek
Technologietransfer
Telefon: +49 531 592-8303
Telefax: +49 531 592-69-8303
E-Mail: bernhard.smandek@ptb.de

Dr. Stefan Neumaier
Dosimetrie bei niedrigen Dosisleistungen

PTB-Nummer 7025

PTB mitteilungen

Imprint

The PTB-Mitteilungen are the metrological specialist journal and the official information bulletin of the Physikalisch-Technische Bundesanstalt. As a specialist journal the PTB-Mitteilungen publish original scientific contributions and general articles on metrological subjects from the areas of activities of the PTB. The Mitteilungen have a long tradition dating back to the beginnings of the Physikalisch-Technische Reichsanstalt (founded in 1887).

Publisher
Physikalisch-Technische Bundesanstalt (PTB)
ISNI: 0000 0001 2186 1887
Postal address:
P.O. Box 33 45,
38023 Braunschweig
Delivery address:
Bundesallee 100,
38116 Braunschweig

Editorial Staff / Layout
Press- and Information Office, PTB
Prof. Dr. Tobias Schaeffter (Scientific Editor)
Dr. Dr. Jens Simon (Editor in Chief)
Sabine Siems (Layout / Editing)
Phone: (05 31) 592-82 02
Fax: (05 31) 592-30 08
Email: sabine.siems@ptb.de

Printed in Germany ISSN 0030-834X

The technical articles from this issue of the PTB-Mitteilungen are also available online at:
doi: 10.7795/310.20200299

Bundesministerium für Wirtschaft und Energie

The Physikalisch-Technische Bundesanstalt, Germany's national metrology institute, is a scientific and technical higher federal authority falling within the competence of the Federal Ministry for Economic Affairs and Energy.

The Physikalisch-Technische Bundesanstalt, Germany's national metrology institute, is a scientific and technical higher federal authority falling within the competence of the Federal Ministry for Economic Affairs and Energy.

Physikalisch-Technische Bundesanstalt
National Metrology Institute

Bundesallee 100
38116 Braunschweig

Press and Information Office

Phone: 0531 592-3006
Fax: 0531 592-3008
Email: presse@ptb.de
www.ptb.de